



UNIVERSITY OF NAIROBI

**ARDUINO BASED PROGRAMABLE LEAD ACID BATTERY MONITORING
SYSTEM FOR AUTOMOBILES**

BY

IGNATIUS NAKHOYWA BARASA

I56/69786/2011

**A Thesis Submitted for Examination in Partial
Fulfillment of the Requirements for Award of the
Degree of Master of Science in Physics of the University of Nairobi**

October, 2017

Declaration

I declare that this thesis is my original work and has not been submitted elsewhere for examination, award of a degree or publication. Where other people's work or my own work has been used, this has properly been acknowledged and referenced in accordance with the University of Nairobi's requirements.

Signature Date:

IGNATIUS NAKHOYWA BARASA

I56/69786/2011

Department of Physics

University of Nairobi

This thesis is submitted for examination with our approval as university research supervisors:

Signature

Date

Dr. Justus Simiyu

.....

.....

Department of Physics

University of Nairobi

P.O box 30197-00100 Nairobi Kenya

simiyuj@uonbi.ac.ke

Dr. Sebastian M. Waita

.....

.....

Department of Physics

University of Nairobi

P.O box 30197-00100 Nairobi Kenya

swaita@uonbi.ac.ke

Dedication

This thesis is dedicated to my parents, Maurice and Alice Nafula (1941 – 2012) Barasa.

Acknowledgements

I acknowledge the Almighty God for bequeathing me with the strength and will power to commence my research work and to continue steadfastly to the end. Many hurdles came up along the way, the worst of them being the loss of my laptop bearing all my data and complete thesis, phone and all my identification documents to a thief who broke into my house on 7/3/2016. By God's grace, I managed to pull myself together and proceeded with my research.

I am very thankful to my supervisors Dr. Justus Simiyu and Dr. Sebastian Waita who walked alongside me and guided me in carrying out this research. Without them, this work could not have been correctly and successfully accomplished and to them I say, "thanks and God bless".

Many thanks go to my dad who used to call me weekly without fail in 2015, 2016 and 2017 to enquire about and cheer me on with my research work. My wife Jecinta, sons Lemuel Wanyama and Douglas Osborne Simiyu saw and felt to the full both the positive and negative impact of my research work and to them I say, "thanks a lot for your endurance and motivation".

I finally thank everyone else who helped me either directly or indirectly in accomplishing my research work.

Abstract

The most prevalent battery used for cranking the car engine is the lead acid battery. With each engine cranking event, during which time the alternator halts recharging the battery, there is an associated voltage loss in the battery. The battery monitoring system in this research used the voltage loss associated with each car cranking event to compute the state of health of the car's battery. The battery monitoring system showed that a state of charge of 71 %, down from the recommended 75 %, can be used in carrying out a battery load test. The state of health of 64.3%, down from 80 %, can be used as a battery state of health threshold for some automobiles. The state of charge and state of health threshold values depend on the application in which a battery is put. Of the 5 batteries used in this research three of them needed to be replaced since their state of health fell below the threshold. Two of the batteries were brand new and so they performed well throughout the research. The battery monitoring system displays the real-time state of health of the battery to the motorist thus providing around the clock assurance of the actual health status of the car's battery, saves time as well as unplanned expenses and keeps at bay the inconvenience of abrupt battery failure.

Key words: State of health, state of charge, cranking, lead acid battery, battery monitoring system

Table of contents

Declaration	ii
Acknowledgements	iv
Abstract	v
List tables	ix
List of figures	xi
List of Abbreviations	xiv
List of symbols.....	xvi
CHAPTER ONE	1
INTRODUCTION	1
1.1 Introduction	1
1.2 Problem Statement	3
1.3 Objectives.....	3
1.4 Justification and Significance of the Study	3
CHAPTER TWO	5
LITERATURE REVIEW	5
2.1 Introduction	5
2.2 Definition and Background of a Battery Monitoring System	5
2.3 Advances in Battery Monitoring.....	8
2.4 Typical Battery Monitoring Methods.....	15
2.5 Present day Commercial Battery Monitors in the Market.....	18
CHAPTER THREE	24
THEORETICAL BACKGROUND.....	24
3.1 Battery Charging and Discharging Process.....	24
3.2 Standard Tests for Rating Starting Lighting and Ignition Batteries.....	25
3.3 The Car Starting System	26
3.3.1 Engine cranking signals (V, I and T).....	29
3.4 The BMS Block Diagram.....	30
CHAPTER FOUR.....	32

METHODOLOGY	32
4.1 Introduction	32
4.2 The BMS Circuit Design.....	32
4.2.1 The Voltage Sensor Design	34
4.2.2 The Current Sensor Design.....	35
4.2.3 Temperature Sensor Design.....	36
4.2.4 Voltage Regulator Design.....	37
4.2.5 The User Interactive Interface Design	37
4.2.6 The Display Module Design	38
4.2.7 Processing Unit and Data Logging and Retrieval System Design.....	39
4.3 Effects of Voltage, Current and Temperature on State of Health	40
4.4 Fabrication of the Battery Monitoring System.....	42
4.5 The SoH Display Algorithm	44
4.5.1 Laboratory BMS Test	46
4.5.2 Field Setup of the Battery Monitoring System	48
CHAPTER FIVE	51
RESULTS AND DISCUSSION	51
5.1 Laboratory Testing of the Sensors using the BLT, BMS and DMM.....	51
5.1.1 Voltage sensor test output.....	51
5.1.2 Current sensor output.....	53
5.1.3 Temperature sensor output.....	56
5.1.4 Combined V, I and T Analysis	59
5.2 Field Test using the BMS and the car	68
5.2.1 Voltage, current and temperature display	68
5.2.2 Combined V, I and T Analysis	68
5.3 Laboratory V, I and T Test Analysis for the BMS.....	73
5.3.1 The 110 Ah Land Rover Varta battery	73
5.3.2 The 75 Ah Chloride Exide Battery	77
5.3.3 The 110 Ah Yuasa battery	80
5.3.4 The 100 Ah Unistar Battery	82
5.3.5 The 75 Ah moll m3 plus K2 battery	86
5.4 Field results from the BMS in the car	87
5.4.1 The 80 Hp engine.....	87
5.4.2 The 115 Hp engine.....	97

5.4.3	The 100 Hp engine.....	104
5.4.4	The 125 Hp engine.....	106
5.4.5	The 250 Hp engine.....	108
5.5	Performance of the batteries in the field.....	116
5.6	The BMS	118
CHAPTER SIX.....		120
CONCLUSION AND RECOMMENDATIONS		120
6.1	Conclusions	120
6.2	Recommendations	122
REFERENCES		123
Internet links		129
APPENDICES		132
Appendix A: ELECTRONIC COMPONENTS DIAGRAMS AND THEIR SPECIFICATIONS.....		132
A-1	The Arduino microcontroller	132
A-2	The temperature sensor DS18B20	133
A-3	The current sensor integrated circuit ACS758XCB-200U	134
A-4	The power regulator LM7805.....	135
Appendix B: THE BMS CIRCUIT SCHEMATIC.....		136

List tables

Table 2.1: The history of battery development	8
Table 2.2: The summary of the history of battery monitoring systems	15
Table 2.3: The relationship between Open circuit voltage, specific gravity and SoC.....	16
Table 2.4: Types of battery load testers and their technical specifications compiled from their respective operation manuals	19
Table 3.1: Typical parameters of the lead acid battery	25
Table 4.1: The specifications of the 12 V lead acid battery samples used in this research	33
Table 4.2: The specifications of the five cars used in this research.....	33
Table 5.1: The calibration data for the voltage sensor obtained from the voltage sensor of the BMS and the DMM.....	51
Table 5.2: The calibration data for the current sensor obtained using the BMS and the MX 355 clamp meter.....	54
Table 5.3: The calibration data for the temperature sensor of the BMS and the IR thermometer	56
Table 5.4: The combined calibrated BMS voltage, current and temperature output readings	59
Table 5.5: The computed data for 18 cranking events using the 100 Ah Unistar battery	60
Table 5.6: The V - I logs for the 100 Ah Unistar battery obtained for C# 11 using the BLT	61
Table 5.7: The combined V, I and T logs for a single cranking event in the 125 Hp engine	69
Table 5.8: A sample of the data for 21 cranking events in the 125 Hp engine.....	70
Table 5.9: The summary of the SoH and SoC of the 110 Ah Land Rover Varta battery	76
Table 5.10: The summary of the SoH and SoC of the 75 Ah Chloride Exide battery.....	79
Table 5.11: The summary of the SoH and SoC of the 110 Ah Yuasa battery	81
Table 5.12: The summary of the SoH and SoC of the 100 Ah Unistar battery	85
Table 5.13: Summary of the SoH and SoC of the 75 Ah moll m3 plus K2 plus battery	87
Table 5.14: The summary of the SoH and SoC for the 75 Ah moll m3 plus K2 plus battery	90
Table 5.15: The summary of the SoH and SoC for the 110 Ah Yuasa battery in the 80 Hp engine	93
Table 5.16: The summary of the SoH and SoC for the 100 Ah Unistar battery in the 80 Hp engine	96
Table 5.17: The summary of the SoH and SoC indication for the 75 Ah moll m3 plus k2 battery in the 115 Hp car.....	98

Table 5.18: The summary of the SoH and SoC indication for the 100 Ah Unistar battery in the 115 Hp engine	101
Table 5.19: The summary of the SoH and SoC indication for the 110 Ah Yuasa battery in the 115 Hp engine	104
Table 5.20: The summary of the SoH and SoC indication for the 110 Ah Yuasa battery in the 100 Hp engine	106
Table 5.21: The summary of the SoH and SoC indication for the 100 Ah Unistar battery in the 250 Hp engine	109
Table 5.22: The summary of the SoH and SoC indication for 110 Ah Yuasa battery.....	112
Table 5.23: The summary of the SoH and SoC indication for the 75 Ah moll m3 plus k2.....	116

List of figures

Figure 2.1: The structural design of a typical lead acid battery	7
Figure 2.3: Sample result from the Autometer BVA 2100.....	20
Figure 2.4: Sensors embedded in a battery to monitor individual cells.....	23
Figure 3.1: A simplified car starting system.....	27
Figure 3.2: A car starter motor.....	28
Figure 3.3: Voltage – Current relationship of a battery during a car cranking event	30
Figure 3.4: The block diagram of the BMS	31
Figure 4.1: The voltage divider circuit designed for the BMS to measure the battery voltage	34
Figure 4.2: The current sensor circuit designed for the BMS for measuring the battery current .	35
Figure 4.3: The temperature sensing circuit designed for the BMS for measuring the battery temperature	36
Figure 4.4: The circuit for supplying 5 V to the temperature sensor, microcontroller and current sensor	37
Figure 4.5: The user interactive interface design for the BMS.....	38
Figure 4.6: The PG160128A thin film transistor display of the BMS in standby mode	39
Figure 4.7: The Arduino Uno R3 board and the stackable SD card data logger for the BMS	40
Figure 4.8: The data logger bearing the SD card mounted on the Arduino Uno R3 board	40
Figure 4.9: The flow chart showing steps for battery monitoring	41
Figure 4.10: The digital multimeters for calibrating the voltage and current scales of the BMS.	42
Figure 4.11: The IR Raytek thermometer for calibrating the temperature scale of the BMS.....	43
Figure 4.12: The pictorial setup of the 12 V SLI battery, the BMS and the 500 A BLT for simulating the car engine cranking event in the laboratory.	47
Figure 4.13: The battery monitoring system installed in the 250 Hp engine car.....	49
Figure 4.14: The battery monitoring system installed in the 115 Hp engine car.....	49
Figure 4.15: The battery monitoring system display, the green box, in the 250 Hp engine car ...	50
Figure 5.1: The calibration graph for the voltage sensor of the BMS	52
Figure 5.2: The calibration graph for the current sensor of the BMS.....	55
Figure 5.3: The calibration curve for the temperature sensor of the BMS	57
Figure 5.4: The battery current-voltage characteristics for C# 11 for the 100 Ah Unistar battery	65
Figure 5.5: The TFT display for the C# 11 for the 100 Ah Unistar battery.....	66
Figure 5.6: The current - voltage characteristics of the 100 Ah Unistar battery for C# 11	67

Figure 5.7: TFT display of C# 10 for the 125 Hp engine car using the 100 Ah Unistar battery ..	71
Figure 5.8: The current - voltage characteristics of the 100Ah Unistar battery in the 125 Hp engine for C# 10	72
Figure 5.9: The 78 cranking events at sequential intervals of 10 cranks in 40 minutes for the brand new 110 Ah Land Rover Varta battery in the laboratory.....	73
Figure 5.10: The TFT display for C# 9 for the brand new 110 Ah Land Rover Varta battery.....	75
Figure 5.11: The TFT display for C# 73 for the brand new 110 Ah Land Rover Varta battery... ..	75
Figure 5.12: The SoC and SoH for the brand-new Chloride Exide battery in the laboratory	77
Figure 5.13: The TFT display for C# 48 for the brand new 75 Ah Chloride Exide battery	78
Figure 5.14: The TFT display for C# 114 for the brand new 75 Ah Chloride Exide battery	79
Figure 5.15: The SoH and SoC against crank number for the 110 Ah Yuasa battery in the laboratory	80
Figure 5.16: The TFT display for C# 54 for the 110 Ah Yuasa battery	81
Figure 5.17: The cranking data for the 110 Ah Unistar battery in the laboratory	82
Figure 5.18: The TFT display for C# 2 for the 100 Ah Unistar battery	83
Figure 5.19: The TFT display for C# 31 for the 100 Ah Unistar battery	84
Figure 5.20: The TFT display for C# 45 for the 100 Ah Unistar battery	84
Figure 5.21: The cranking data for the 75 Ah moll m3 plus k2 battery in the laboratory	86
Figure 5.22: The SoC and SoH against crank number for the 75 Ah moll m3 plus K2 plus battery	88
Figure 5.23: The TFT display for C# 35 for the 75 Ah moll m3 plus k2 battery in the 80 Hp engine	90
Figure 5.24: The SoC and SoH against crank number for the 110 Ah Yuasa battery in the 80 Hp car.....	91
Figure 5.25: The TFT display for C# 1 for the 110 Ah Yuasa battery	92
Figure 5.26: The TFT display for C# 47 for the 110 Ah Yuasa battery	93
Figure 5.27: The SoC and SoH against crank number for the 100 Ah Unistar battery in the 80 Hp car.....	94
Figure 5.28: The TFT display for C# 26 for the 100 Ah Unistar battery	95
Figure 5.29: The TFT display for C# 32 for the 100 Ah Unistar battery	96
Figure 5.30: SoC and SoH against crank number for the 75 Ah moll m3 plus k2 battery in the 115 Hp car.....	97

Figure 5.31: The TFT display for C# 9 for the 75 Ah moll m3 plus k2 battery in the 115 Hp engine	98
Figure 5.32: The SoC and SoH against Crank number for the 100 Ah Unistar battery in the 115 Hp car	100
Figure 5.33: The SoC and SoH against crank number for the 110 Ah Yuasa battery in the 115 Hp engine	102
Figure 5.34: The TFT display for C# 64 for the 110 Ah Yuasa battery in the 115 Hp engine...	104
Figure 5.35: The SoH and SoC against crank number for the 110 Ah Yuasa battery in 100 Hp car	105
Figure 5.36: The SoH and SoC against crank number for the brand new 75 Ah Chloride Exide battery in the 125 Hp car	107
Figure 5.37: The SoH and SoC against crank number for the 100 Ah Unistar battery in the 250 Hp engine	108
Figure 5.38: The SoH and SoC against crank number for the 110 Ah Yuasa battery in the 250 Hp engine	110
Figure 5.39: The TFT display of C# 32 of the 110 Ah Yuasa battery in the 250 Hp engine	111
Figure 5.40: The TFT display of C# 61 of the 110 Ah Yuasa battery in the 250 Hp engine	111
Figure 5.41: The SoH and SoC against crank number for the 110 Ah Land Rover Varta battery in the 250 Hp engine	113
Figure 5.42: SoH and SoC against crank number for the 75 Ah moll m3 plus k2 battery in the 250 Hp engine	114
Figure 5.43: The TFT display for C# 38 for the 75 Ah moll m3 plus k2 battery in the 250 Hp engine	115
Figure 5.44: The TFT display for C# 58 for the 75 Ah moll m3 plus k2 battery in the 250 Hp engine	115
Figure A-1: The Arduino UNO R3 physical computing platform.....	132
Figure A-2: The digital temperature sensor DS18B20	133
Figure A-3: The current sensor IC ACS755SCB-200U	134
Figure B-1: The complete schematic circuit of the battery monitoring system generated using Proteuse Design Suite 8.1 sheet 1	137
Figure B-2: The complete schematic circuit of the battery monitoring system generated using Proteuse Design Suite 8.1 sheet 2	137

List of Abbreviations

ac	alternating current
ADC	Analogue to digital conversion
Ah	Ampere hour
BLT	Battery load tester
BMD	Battery monitoring device
BMS	Battery monitoring system
CA	Cranking amps
C#	Crank number
cc	cubic centimeters
CCA	Cold cranking amps
CrankCheck™	Crank check trade mark
CSM	Current Sensing Module
CSOH	Cranking state of health
dc	direct current
DH	data hold
DMM	Digital multi meter
EIS	Electrochemical impedance spectroscopy
EMF	Electro motive force
EVs	Electric vehicles
HEVs	Hybrid electric vehicles
Hp	Horse power
IC	Integrated circuit
IEC	International electrotechnical commission
IEEE	Institute of electrical and electronics engineers
IR	Infra-red
JIS	Japan industrial standard
LAB	Lead acid battery
LED	Light emitting diode
rpm	revolutions per minute
RSOH	Reserve state of health

SD	Secure data
SG	Specific gravity
SLI	Starting lighting and ignition
SoC	State of Charge
SoH	State of Health
SRAM	Static random- access memory
TFT	Thin film transistor
TSM	Temperature sensing module
USB	Universal serial bus
VSM	Voltage sensing module

List of symbols

a	y-intercept in the regression formula
b	the regression coefficient of v on c
C, C++	programming languages
C_{diff}	electrolyte diffusion capacitance
C_u	Used capacity
C_t	Total capacity
C_{cap}	Instantaneous capacity
C_n	Nominal capacity at full charge
eV	Electron volt
H^+	Hydrogen ion
H_2O	Water
HSO_4^-	Hydrogen sulphate ion
H_2SO_4	Sulphuric acid
I	Current
I_{out}	Output current
K	Kelvin
kA	Kilo amperes
kb	Kilo byte
kHz	Kilo Hertz
kW	kilo watt
$k\Omega$	Kilo ohm
Li-ion	Lithium ion
$LiSO_2$	Lithium sulphate
n	number of terms
nF	nano Farad
η	current efficiency
η_{diff}	electrolyte diffusion overpotential
Ni-Cd	Nickel cadmium
O_2	Oxygen
Pb	Lead

PbO_2	Lead dioxide
$PbSO_4$	Lead sulphate
$R_1 - R_{14}$	Resistor 1 to resistor 14
R_{batt}	Battery resistance
R_{diff}	electrolyte diffusion resistance
SoC_{th}	State of Charge Threshold
SoH_{th}	State of health threshold
S_a	standard deviation in y-intercept
S_b	standard deviation of the slope
$S_{y/x}$	standard deviation in y-values
T	Temperature
T_0	Time at zero second
T_1	Time at 1 second
T_2	Time at 2 seconds
$U1, U2, U3$	integrated circuit 1, 2 and 3
VCC	Positive power supply
VSS	Negative power supply
V_d	digital voltage
V_{batt}	Battery voltage
V_o	y-intercept value on V-I graph
V_{out}	output voltage
V_{loss}	voltage loss
$V_{loss_{th}}$	voltage loss threshold
$V_{loss_{new}}$	voltage loss of a new battery
V_{in}	voltage in
V_{ocv}	Open circuit voltage
Wh	Watt hour
Wh/kg	Watt-hour per kilogram
Wh/L	Watt-hour per litre
$y_{BMSVcal}$	calibrated BMS voltage value
$y_{BMSIcal}$	calibrated BMS current value

$y_{BMSTcal}$	calibrated BMS temperature value
Z_i	Impedance
Σ	sigma

CHAPTER ONE

INTRODUCTION

1.1 Introduction

The global energy demand for industrial and domestic consumption keep rising hence the need for finding alternative sources and innovative ways of production, storage and monitoring among other issues. Since the well-known industrial revolution, the main sources of energy have been from fossil fuels and nuclear. The energy has been used in different forms with the most common one being electrical. Conversion to electricity further facilitated efficient means of transporting energy as well as distribution. There arose need for storage of electrical energy for areas where the user was not connected directly to the distribution grid. The need for storage further escalated due to the development of new sources of electricity as well as appliances ranging from communication, transport to industrial. The main form of storage of electrical energy has been by conversion into chemical energy via a battery.

The most prevalent battery technology, due to low internal resistance and low price is the lead acid battery (LAB). This battery technology has found wide range of applications in automotive industry mainly starting, lighting and ignition. For this application, cold cranking amps (CCA) and reserve capacity are some of the key battery parameters that affect its performance. Government estimates in China showed that there were about 80 million electric bikes in China in 2010 with close to 95 % of them being powered by a LAB (Joey *et al.*, 2016).

Another reason for the prevalence of the LAB is that 97 % of it is recyclable thereby placing the LAB at the top of the list of the most highly recycled consumer products in the world (Trojan, 2013). Lithium-ion (Li-ion) batteries are mostly used in portable electronic applications like laptops as well as in powering electric vehicles (EVs) (Sathiya *et al.*, 2015). Since Li-ion batteries have light weight, small size and high energy density, their introduction into the starting lighting and ignition (SLI) battery market will reduce the need for battery replacement and lower the risk of lead-based environmental pollution (Ceraolo *et al.*, 2011). A battery's deliverable capacity is directly related to the amount of active materials that it contains (Maria *et al.*, 2011).

The battery's temperature, voltage, current and state of charge (SoC) are the most common parameters that are normally monitored among others as recommended by the Institute of Electrical and Electronics Engineering (IEEE) (IEEE, 2012). The management at the Energy Storage Research Program at the Department of Energy in the USA, said that "every year roughly one million usable Li-ion batteries are sent in for recycling with most having a capacity of up to 80 percent," (Buchman, 2011). In the healthcare sector as well, the professionals of medical equipment, battery management is one of the top 10 medical devices challenge (Buchman, 2011).

Battery monitors are used in other applications like laptops, mobile phones and marine equipment among others. Most laptops come with pre-installed battery monitoring hardware and software and can be customized by the user depending on the algorithms used in them. The BMS in the laptop monitors the charging and discharging of the battery and displays the real time status of battery's capacity in percentage. Some laptops show the number of cycles, i.e the number of times the battery was discharged completely and recharged to full capacity, and use them to predict the end of the battery's life. When the charge drops to a preset value, a warning is given to the user about it and the laptop will request what action the user wants it carry out at this point. The laptop can go into power saving mode by turning of some of the applications installed in the laptop, reducing the brightness of the screen or shutting down completely. In this way, the BMS also manages the rate at which power is drawn from battery. The BMS also checks the temperature of the battery such that when it exceeds a certain value, the laptop goes into sleep mode to protect electronic parts of the laptop from damage.

In mobile phones, the embedded BMS indicates the real time capacity of the battery and the remaining run time of the battery based on the rate at which the battery discharges. The user can, depending on the type of phone, set the value of charge at which the phone should give a warning when the pre-set value is reached. When the charge drops down to the pre-set value, a warning is given as a beep, flickering light or a text message depending on the type of phone. The BMS may display the applications that are discharging the battery at a high rate and suggest to the user the actions that can be taken to reduce the discharge rate. The BSM can either switch of the phone at that point or go into power saving mode by lowering the brightness of the screen, turning off several phone applications and going into silent mode.

1.2 Problem Statement

The number of electrical appliances in the modern car keep increasing and consequently demand for more power from the battery and the charging system which can easily and abruptly lead to battery failure. In the 1970s, estimations showed that the vehicle's electrical power demand would rise from about 0.5 kilo watts (kW) to about 4 kW in the year 2000 and reach 10 kW a decade thereafter, in 2015 (Hollemeak, 2011). There is need therefore, for a battery monitoring system to monitor and relay to the user, the real time operational status of the car's battery by providing reliable information and notification of its working condition and the appropriate action to be taken thereafter.

1.3 Objectives

The main objective of this research was to fabricate a battery monitoring system (BMS) whose targeted use is in an automobile and it uses the voltage (V), current (I), temperature (T) and state of charge (SoC) signals drawn from the battery to compute its state of health (SoH). The specific objectives were:

- i. To design a BMS, circuitry, power supply and voltage regulators for a SLI lead acid battery to measure V, I, T and SoC.
- ii. To assess the behavior of the changes in V and I signal of the LAB during engine cranking and develop a program to compute the SoH of the battery.
- iii. To fabricate Arduino based SoH battery monitoring system from the points (i) and (ii) above.

1.4 Justification and Significance of the Study

The BMS uses a programmable Arduino Uno R3 computing board whose flexibility allows the user to customize its performance by uploading onto the computing board one's own preferred battery monitoring algorithm or re-programming the embedded code. The analyzed battery data will be displayed on a thin film transistor (TFT) screen placed on the car's dashboard to provide real time and around the clock assurance of the battery condition to the motorist and

simultaneously be saved into a secure digital (SD) memory card mounted onto the data logger of the BMS.

With the BMS installed in a commercial fleet of cars, battery maintenance costs will be cut down and hence motorists will not have to call for a technician's help when battery failure occurs further afield. The risk of abrupt battery failure will be managed in time by providing early warning about the status of the battery and provision of better data interpretation thereby reducing incorrect battery status diagnosis by the motorists. Currently without the BMS, many good batteries are erroneously replaced thereby increasing operational costs and degrading the environment.

The battery performance data can be sent to ThingSpeak, an open source online data platform, so that it can be retrieved later and used by other researchers. From the acquired battery data stored in the SD card or ThingSpeak, customized analysis can be carried out by BMS manufacturers to improve its functionality. The primary function of a BMS is ensuring that the use of the energy stored inside the battery for powering a given device is fully maximized and the risk of battery damage is minimized. Very few cars on Kenyan roads, both public and private, have a basic BMS installed in them beside the common red battery indicator on their car's dashboards.

CHAPTER TWO

LITERATURE REVIEW

2.1 Introduction

This chapter presents the background of the research topic and the advances made in battery monitoring. The present-day battery monitoring methods and commercially available battery monitors are then discussed. Thereafter, the process of charging and discharging of the LAB and its general characteristics are presented.

2.2 Definition and Background of a Battery Monitoring System

A BMS is an electronic device that measures pre-specified battery parameters, analyzes them according to pre-programmed instructions and relays the output to the end user most often over a screen. SoC is the amount of charge available in a battery in percentage form at any given time in comparison to the same battery's charge when it was brand-new and fully charged (Andrea, 2010). The SoH of a battery is a qualitative parameter that indicates the ability of the battery to deliver the charge that is stored in it at any given time in comparison to the same ability when the battery was brand new (Florez *et al.*, 2015). The definition of SoH can be based on the capacity or internal resistance of the battery depending on the application to which the battery is put (Weng *et al.*, 2013). There is no standard reference for SoH and so battery manufacturers calibrate their own SoH (Sayed *et al.*, 2014). There is lack of consensus among scholars on how SoH should be defined since it does not a measure of a specific physical quality and due to lack of consensus on how it should be defined, the formulae for SoH calibration is most often a trade secret (Yinjao *et al.*, 2011).

Battery monitoring systems are in use in most electronics such as laptops, cellphones and music systems but are rarely used in automobiles partly due to the higher power requirements in automobile applications (Canbing *et al.*, 2016). The monitoring of the SoH for SLI batteries is still a major challenge since there are no sensors for monitoring electrochemical reactions inside the battery cells (Jurgen *et al.*, 2014). Besides, manufacturing of stretchable wearable photo-voltaic, epidermal health monitors and sensitive robotics skins, soft surgical tools are emerging and so,

monitoring their status will be of great importance (Sheng *et al.*, 2013). A battery usually converts the chemical energy stored in its active materials to electrical energy through an electrochemical reaction (Joey *et al.*, 2016). The active materials for the LAB are the lead oxide (PbO_2) and lead (Pb) terminal plates and the solution of sulfuric acid (H_2SO_4) (Djamila and Ernest, 2012). It is made up of cells, electrodes, separators, electrolyte, terminals and an outer casing. The separator used is normally porous to electrical ions and electronically non-conductive to avoid the occurrence of short circuits that may eventually lead to unwanted voltage loss within the battery (Djamila and Ernest, 2012, 2012). The connection of the individual cells in the battery can either be in parallel or in series to produce the desired voltage and current output (David and Thomas, 2011). The ratio of a battery's Watthour (Wh), to its mass in kilogram is called the specific energy while energy density is the ratio of its Wh to its volume (Jha, 2012).

Lead acid batteries are divided into maintenance free, sealed lead acid and the valve-regulate-lead acid battery which have immobilized acid electrolyte (Force, 2015). Lead acid batteries are further classified into deep and shallow cycle batteries. Deep cycle batteries are used for supplying a specific current to certain loads for long periods of time while shallow cycle ones supply a burst of high current for a short period of time as used in starting a car engine (David and Thomas, 2011). The LAB has extremely low internal resistance of 0.022Ω per cell and so the voltage drop whenever current is drawn from the battery is remarkably small (Pistoia, 2008). Figure 2.1 shows the typical structure of a rechargeable battery.

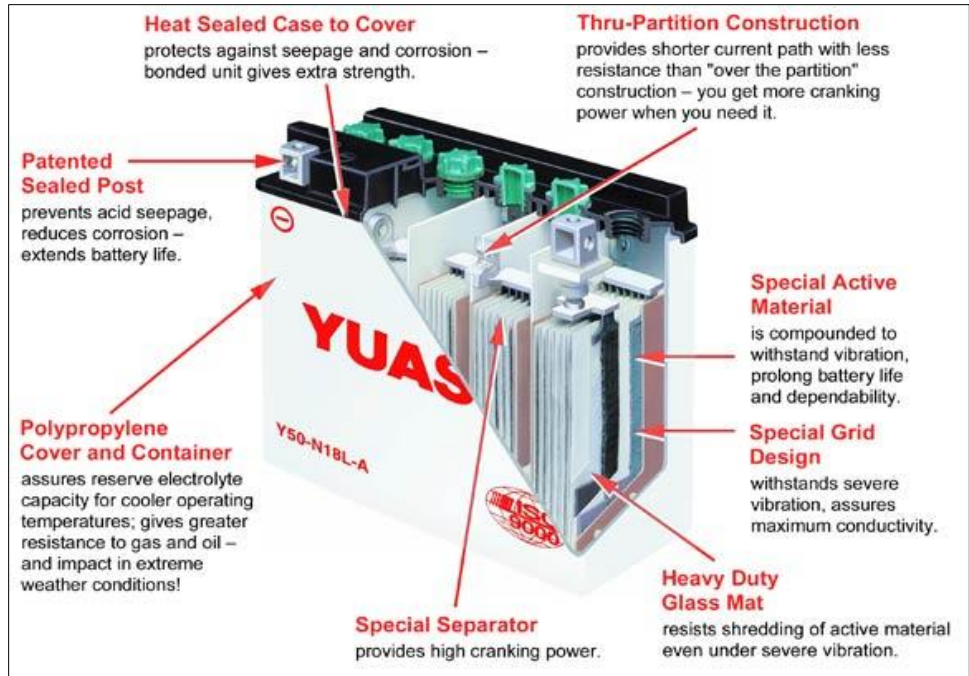


Figure 2.1: The structural design of a typical lead acid battery (Yuasa, 2016)

Batteries that cannot be recharged after use are called primary batteries while those that can be recharged after use are called secondary batteries (Brodd, 2013). Secondary batteries can be used either by being connected to a primary energy source and charged by the same in order to deliver their energy to the load like in automobiles, uninterruptible power supply and hybrid electric vehicles (HEVs) or recharged after use as used in portable consumer electronics like power tools and electric vehicles (EVs) (Pistoia, 2008).

Fuels cells, a type of electrochemical cell on the other hand, convert the chemical energy in their active materials, normally gases and liquids, directly into electrical energy (Sørensen, 2012). Space vehicles have used hydrogen-oxygen fuel since the nineteen sixties and in the recent years, research is under way for use in other applications like utility power, on-site electric generators and EVs (Barbir, 2013). The first rechargeable LAB was invented by a French physicist, Gaston Plante, in 1859 (Detchko, 2011).

For over two centuries, battery technology has developed and spread its use in various sections one among them being the automobile industry. The chronological development of the battery is summarized in Table 2.1.

Table 2.1: The history of battery development (Buchman, 2011)

Year	Researcher/country	Method
1600	Gilbert (England)	Establishment electrochemistry study
1791	Galvani (Italy)	Discovery of ‘animal electricity’
1800	Volta	Invention of the voltaic cell
1802	Cruikshank (England)	First electric battery capable of mass production
1820	Ampère (France)	Electricity through magnetism
1833	Faraday (England)	Announcement of Faraday’s Law
1836	Daniell (England)	Invention of the Daniell cell
1859	Plante (France)	Invention of the lead acid battery
1868	Leclanché (France)	Invention of the Leclanché cell
1888	Gassner (USA)	Completion of the dry cell
1899	Jungner (Sweden)	Invention of the nickle-cadmium battery
1901	Edison (USA)	Invention of the nickle-iron battery
1932	Schlect and ckermann (German)	Invention of the sintered pole plate
1947	Neumann (France)	Successful sealing of the nickle-cadmium Battery
1960	Union Carbide (USA)	Development of primary alkaline battery
1970	McClelland and Devit	Development of valve regulated lead acid battery
1990	Sanyo (Japan)	Commercialization of the nickel-metal hydrid battery
1991	Sony (Japan)	First introduction of Li-Ion battery
1992	Kordesch (Canada)	Commercialization reusable alkaline battery
1999	Bellcore (USA)	Commercialization lithium-ion polymer
2002	University of Montreal, Quebec Hydro, MIT, others	Improvement of Li-phosphate, nanotechnology, commercialization

2.3 Advances in Battery Monitoring

In 1940, Heyer developed an analog capacity indicator for the storage battery which could indicate the V and I readings based on the battery’s voltage drop upon applying a load to draw an equivalent current required to operate various starter motors. The battery to be tested had 3 cells each having a full charge of 1.8 V hence providing a total of 5.4 V. If the battery was in good condition there would be very little or no voltage drop otherwise, the battery was replaced when the SoC fell below 70 % (Heyer, 1940).

This invention was used on a 5.4 V battery whereas the modern automobile uses a 12 V battery. Since a hand-held carbon pile tester was used as a load to simulate engine cranking, this invention could not be installed in a car to monitor the battery in real time. Another setback of this invention was that there was power loss associated with the use of a current shunt thereby leading to errors in I and SoC measurements.

In 1963, Curtis instruments developed SoC gauges for EVs batteries whose function was to predict battery capacity. This was achieved by invoking an algorithm that used the time taken since the voltage fell below a certain value, to predict the capacity of the battery (Valer *et al.*, 2010). The current from the battery was passed through an integrator module that registered the depletion of the current and thereby displayed the SoC and regulated the charging rate (Valer *et al.*, 2010). Curtis gauges were the most sophisticated battery monitors at that time such that they were even used by astronauts on the moon. They were used for determining the battery's SoC and regulating the charging of the battery while in use and so could not be used to show the SoH of the battery.

In 1972, Gerard's group (Gerard *et al.*, 1972) developed a of modeling the battery monitor's parameters by using artificial neural networks. The aim of this invention was to provide the users of portable equipment with an estimation of the remaining working time. It had a SoC monitor, a logic circuitry and a storage battery recharging control circuit. A short current pulse was sent through the battery and the resulting difference in voltage between the battery's terminals was monitored by a comparator circuit that received the signal and compared it to a reference signal to give the SoC (Gerard *et al.*, 1972). This method offered only the SoC of the battery and charging control and so could not be used to determine the SoH of the battery.

In 1976, Christianson and Bourke developed a method in which a battery's SoC was indicated based on the open circuit voltage (V_{oc}) by using a function generator to simulate the characteristic curve of the battery (Clinton and Christianson, 1976). The function generator was used to produce a signal that correlated with the actual internal resistance of the battery. The V_{ocv} was directly proportional to the battery's SoC and could be found using Equation 2.1 (Clinton and Christianson, 1976):

$$V_{oc} = V_{batt} + IR \quad (2.1)$$

in which V_{batt} is the battery's terminal voltage, I the battery's current which is assumed as being positive while in charging mode and negative while in discharge mode and R is the internal resistance of the battery (Clinton and Christianson, 1976).

This battery monitor was used to indicate the difference between the current that goes into and out of the battery but was not able to respond to other factors such as the rate of discharge which is known to affect the residual energy in a battery. It was hard to measure the V_{oc} because the battery's current had to be zero for the measurement to be taken and a wider scale voltmeter was required for capturing the relatively small changes that occurred in the terminal voltage.

In 1979, Eby used V_{oc} and the load voltage for determining the SoC of a LAB while the battery discharges (Eby,1979). The values of the V_{oc} of the battery while in discharge mode were found by measuring the loaded voltages which were then referenced to a stored V_{oc} value to detect the charging and discharging rates. The acquired rates were used to reset the stored values of the initial V_{oc} measurements hence, producing a moving reference with the output representing the capacity of the battery (Eby,1979). This invention was aimed at providing a display of the capacity of the battery as being stable and linear and optionally provided a warning of the battery's capacity. The invention was used to manage the charging and discharging cycle of the LAB in EVs but couldn't show the SoH of the same battery.

Kikuoka and his group (Takao *et al.*,1983) developed a monitoring system for precisely measuring the SoC for a storage battery. The system controlled the charging and discharging of electrical quantities depending on temperature and charging efficiency of the battery. As the battery capacity gradually decreased with age, its number of discharge cycles increased and it was considered dead when the discharge capacity reduced by 50 % (Takao *et al.*,1983).

It is not possible to precisely determine the SoC of a battery by measuring only the rate of its charging and discharging and its efficiency. A method of correction of the capacity variation of a storage battery due to the life variation or self-discharge is needed for this method to work with precision. The 50 % limit for battery replacement is very low for the current automobile as batteries would be replaced too soon and so, this invention was best suited for EVs.

In 1987 Muramatsu developed a battery monitor for the Nissan motor company in Japan that used the relationship between the battery impedance measured at different frequencies and the remaining charge in the battery to determine the battery's SoC and SoH while the battery was installed in the car (Muramatsu, 1987). The battery monitor had a voltage sensor, a current sensor, an impedance calculator, and a calculator for determining the remaining capacity and the service life of the battery (Muramatsu, 1987). The battery used had to be an automotive 12 V LAB at a temperature of about 20 °C. Predetermined relationships between the battery impedance, remaining capacity and the remaining service life of the battery at different frequencies were used for continuous battery monitoring (Muramatsu, 1987). Since the rate depended on the remaining service life of the battery, the battery condition monitor could not be used to get the remaining capacity of the battery precisely. The invention by Muramatsu did not include the use of temperature compensation for the battery's internal impedance, an inclusion that could have provided a more precise value of the service life of the battery and the remaining capacity.

In 1988, Peled's group developed an algorithm for determining the SoC of Li-ion batteries using predetermined voltage and temperature measurements which were then used as input parameters for look-up tables in which were fixed values of certain measured parameters (Emanuel *et al.*,1988). The measured values were compared to predetermined values stored in the look-up table to indicate the SoC of the battery. The invention was suitable for lithium batteries, although it could also be used for other batteries having constant discharge curves as well. Lithium batteries have very constant or flat discharge curves which give no information with respect to the battery SoC with the V_{oc} being independent of the SoC in the range of 60 % - 100 % capacity (Emanuel *et al.*,1988). The temperature of the battery was measured then a load placed on the battery to cause a high discharge for a short period of time and after a short rest period, typically 16 minutes also known as recovery time, the V_{oc} of the battery was computed by comparing the measured temperature and V_{oc} with reference tables showing the SoC at different temperatures and V_{oc} for the respective battery (Emanuel *et al.*,1988). The use of this method therefore required calibration curves pre-prepared according to the type and size of the battery, the temperature, the load, the load time and the battery's recovery time (Emanuel *et al.*,1988).

A setback for this method is that different sets of parameters were bound to produce different calibration curves for certain predetermined temperatures. The 16-minute recovery time meant that

this method could not be used continuously to monitor the SoC of the battery. This invention cannot be used on the LAB that is used in automobiles because the LAB does not have a constant discharge curve.

In 2002, Crouch Jr. and Strickland invented a new way of finding the SoH of an automotive battery by using two registers. In the first register, there was stored a first numeric value that was obtained by looking at the number of engine cranks performed by the battery. The value was compared with a specific number of engine cranks to get the battery's first SoH which was then designated as SoH1 (Dell and Strickland, 2002). The value was found by getting the slope, a , of Equation 2.2 which represented the line of best fit of the graph of the remaining number of cranks in the battery against the battery's SoH (Dell and Strickland, 2002). The second numeric value was obtained by finding the deteriorated battery life following exposure to high temperature and low SoC and this was designated as SoH2 (Dell and Strickland, 2002). The ultimate SoH was found using Equation 2.2 (Dell and Strickland, 2002);

$$\text{SoH} = a \text{ minimum}(\text{SoH1}, \text{SoH2}) \quad (2.2)$$

The SoH1 was the SoH of the battery following the normal battery wearing out while SoH2 was the SoH of the battery based the high battery temperature and the low SoC values of the battery together with the usual battery's internal resistance (Dell and Strickland, 2002).

To determine SoH1, an assumption was made that the battery performed a certain number of engine cranking events during its lifetime and based on the actual number of cranking events that occurred, SoH 1 was then calculated. The assumption about the number of cranks could be misleading since this depends on the use to which the car is put. Consequently, the SoH of the battery is bound to be inaccurate.

Singh's group, (Harmohan *et al.*, 2002) developed a method for monitoring and displaying the SoH of a battery on a real-time basis to the motorist or on a system. This was accomplished by measuring the battery's current and voltage with and with no load on the battery and thereafter, the internal resistance was calculated. The CCA was then calculated from the computed battery internal resistance and polarization resistance and the result displayed to the user (Harmohan *et*

al., 2002). The display showed the voltage, current, temperature, SoC and CCA. Battery polarization resistance arising from non-uniformity in the electrolyte concentration in the battery electrodes to the electrolyte also affects the battery power output (Harmohan *et al.*, 2002).

In 2003, Hans *et al.*, developed a method for estimating the SoC of a rechargeable Li-ion battery by measuring the voltage, current, and temperature during the charge or discharge states (Hans, 2003). During the charge and discharge states, the SoC was determined by computing the value of charge drawn from or supplied to the battery using current integration method (Hans, 2003). If the battery was in equilibrium state, the voltage across the battery was measured and converted into an equilibrium SoC value. If the battery was not in equilibrium state, the charge drawn from or supplied into the battery was calculated by coulomb counting (Hans, 2003). The remaining battery capacity was then determined using Equation 2.3 below (Hans, 2003);

$$\eta_{\text{diff}}(T,I,t) = I(t)R_{\text{diff}}(T) \left[1 - \exp\left(\frac{-t}{R_{\text{diff}}(T)C_{\text{diff}}(T)}\right) \right] \quad (2.3)$$

where η_{diff} is the electrolyte diffusion overpotential, R_{diff} is the electrolyte diffusion resistance and C_{diff} the electrolyte diffusion capacitance.

Automobile manufactures currently provide only the real-time state of the car's charging system for warning the motorist when there is a problem with the charging system by using a dashboard mounted voltmeter, ammeter or a warning lamp which is often referred to as the "idiot light" (Lonnie *et al.*,2013). Driving a car for a short distance in which high power is drawn from the battery does not allow the battery to attain full charge which is so crucial for a long-life span of a LAB. A manufacturer of German luxury cars revealed that in every 400 car batteries from such cars returned under warranty, half of them were in good working condition (Lonnie *et al.*,2013). The apparent failure observed was traced to acid stratification in the batteries due to short charging period. Car manufacturers say that this problem is common to large luxury cars which have high powered auxiliary options than the basic car models (Lonnie *et al.*,2013). In some situations, this information could be life-saving such as when operating in combat zones or under severe weather conditions. It would also be important to know that by merely changing the usage pattern of a vehicle such as combining multiple shopping trips into a single extended trip or by knowing when

to apply an external battery charger that the life of the battery would be extended and impending failures avoided (Lonnie *et al.*,2013).

In 2014, Bertness developed an in-vehicle SoH monitoring system by using the linear relationship that exists between the conductance of the battery and it's working condition (Bertness, 2014). In this system, a microprocessor in the system provides an output that recommends replacement when the SoH drops by 15 % or more below its rated capacity. A cranking state of health (CSOH) which was a relative indicator of the battery's ability to crank the starter motor of the vehicle, was determined (Bertness, 2014). Then a reserve state of health (RSOH), a relative indicator of the battery's reserve capacity, was then determined (Bertness, 2014) by assuming about a given battery parameter and modifying the assumed parameter depending on actual measurements taken from the battery during charging, discharging and idle states (Bertness, 2014). The CSOH and RSOH values were thereafter permanently embedded in the vehicles' memory during it's manufacture. The measurements taken from the past could either be from the entire period it was used in the past or from several measured parameters for a specific time of use. A more recent measurement was then taken and compared with that past measurement and if the percentage change was found to be more than a predetermined value, the BMS interpreted it as a new battery having been installed into the vehicle. Once it was determined that the battery was new, the microprocessor in the BMS began the learning process of getting CSOH and RSOH for this battery and thereafter updated the stored parameter of the battery in the look up table of the BMS (Bertness, 2014). Table 2.2 shows a summary of the developments in battery monitoring systems.

Table 2.2: The summary of the history of battery monitoring systems (Valer *et al.*, 2010)

Year	Researcher/company	Method
1940	Heyer	Voltage measurements
1963	Curtis	Voltage measurements and their threshold levels
1975	Christianson	V_{oc}
1979	Eby	V_{oc} and voltage under load
1983	Kikuoka	Book-keeping
1987	Muramatsu	Impedance spectroscopy
1988	Peled	Book keeping
2002	Crouch Jr.	Look-up tables based on V, I and T measurements
2002	Singh	Internal and polarization resistance measurements
2003	Feil	Book-keeping, over-potential, EMF and capacity
2012	Gerad	Artificial Neural Networks
2014	Bartness	Dynamic inductance

2.4 Typical Battery Monitoring Methods

The most common method of determining the SoC of a battery is the coulomb counting method in which the current in amperes (A) drawn from the battery while the battery is charging or discharging is measured (Zhongyue *et al.*, 2014). The measured current is then used in the Equation 2.4 below to compute the SoC of the battery (Zhongyue *et al.*, 2014):

$$SoC_t = SoC_{t_0} + \int_{t_0}^t \frac{\eta I}{C_n} dt \quad (2.4)$$

where;

SoC_t is an estimate of SoC at time t

SoC_{t_0} the initial SoC when at the start of the estimation process

η is the current efficiency

I the value of the current and

C_n the nominal capacity of the battery.

The current is usually assumed to be positive and negative during charging and discharging modes respectively (Zhongyue *et al.*, 2014).

The coulomb counting method assumes that the overall battery capacity is fixed and so does not vary with the temperature, age or the discharge current (Vepa, 2013). Large SoC errors can occur during the estimation process due to the use of inaccurate initial SoC and cumulative errors occur if the estimation process took a longer time (Vepa, 2013). Due to coulombic efficiency and battery aging, the SoC reference will keep changing and so there is need for it to be compensated for before being used in computing SoH (Vepa, 2013).

A second method of monitoring the SoC of a battery is by use of the V_{oc} method whereby the V_{oc} is measured using a meter connected across the battery terminals. A 30-minute rest period is required in case the battery had just been charged to allow diffusion inside the battery to come to an end before the voltage readings are taken (Huggins,2014). The voltage obtained is then compared to the corresponding SoC value in the standard SoC chart shown in Table 2.3.

Table 2.3: The relationship between V_{oc} , specific gravity and SoC (Owen and Gus, 2015).

V_{oc} (V)	Specific gravity	SoC (%)
12.70	1.265	100
12.64	1.257	95
12.58	1.249	90
12.52	1.241	85
12.46	1.233	80
12.40	1.225	75
12.36	1.218	70
12.32	1.211	65
12.28	1.204	60
12.24	1.197	55
12.20	1.190	50
12.16	1.183	45
12.12	1.176	40
12.08	1.169	35
12.04	1.162	30
12.00	1.155	25
11.98	1.148	20
11.96	1.141	15
11.94	1.134	10
11.92	1.127	5
11.90	1.120	Discharged

Another method of determining SoC is by using a hydrometer to get the specific gravity (SG) of the electrolyte used in the battery. SG is the ratio of the weight of the electrolyte to that of the weight of an equal volume of water at a specific temperature. The SG shows how concentrated the acid in the electrolyte is and it correlates directly with the battery's SoC (Jurgen *et al.*, 2009). For a fully charged battery, the SG lies between 1.230 and 1.330 depending on the chemical technology used (Jurgen *et al.*, 2009). The chemical technology of distinct batteries has unique characteristics like nominal voltage, maximum and minimum voltage and charging and discharging curves (Texas, 2012).

Any battery parameter that changes considerably and at times irreversibly with usage, such as internal resistance, capacity, water loss and grid corrosion can be used for indicating the battery's SoH (Thyagarajan *et al.*, 2014). Changes in such parameters cause significant deviation in the performance of the battery such as sudden rise in temperature, increased power loss, gassing, passivation of the electrodes and grid corrosion (Sayeed *et al.*, 2014).

One of the methods of computing the SoH of a battery is by use of its temperature fluctuation while the battery is in use. Manufacturers recommend a temperature of 25 °C, (Acton, 2013), for normal operation of a 12 V car battery. A temperature rise above 25 °C increases the chemical activities in the cells by a factor of 2 for every 5.5 °C temperature increase (Jurgen *et al.*, 2014). The battery also experiences a leakage of its current which is exponentially dependent on temperature such that it doubles for every 10 °C increase in temperature (David and Paul, 2012). The rate of self-discharge reactions and chemical degradation double following temperature increases (Jurgen *et al.*, 2009).

Another method used for SoH determination is electrochemical impedance spectroscopy (EIS). An alternating current is applied to the battery using a current injector such that an identifiable current of a specified frequency and magnitude flows and causes a resultant voltage drop across the battery under test (Bergveld *et al.*, 2013). The output voltage (V_{out}), is then divided by the output current (I_{out}), to give the battery's impedance Z_i , as shown in Equation 2.5 (Yevgen and Jinrong, 2013):

$$Z_i = \frac{V_{out}}{I_{out}} \quad (2.5)$$

An impedance threshold value is then selected by the manufacturer to which the measured impedance will be compared. The acquired battery's impedance spectra are then used to predict the SoH of the battery (Zhongyue *et al.*, 2014). The EIS method is expensive, time consuming and requires expertise and so, it is mostly reserved to research laboratories (Buchmann, 2012).

Both scholars and manufacturers regard the percentage of nominal capacity as being the threshold of the health of the battery and generally use the expression shown in Equation 2.6 for getting the SoH (Patrick and Jurgen, 2015):

$$\text{SoH} = \frac{C_{\text{cap}}}{C_{\text{nominal}}} \times 100\% \quad (2.6)$$

Where C_{cap} is the battery's real-time capacity while C_{nominal} is the capacity of the battery at full charge (Patrick and Jurgen, 2015). Generally, when the capacity drops to 80 % after full charging and discharging cycles, replacement of the battery is recommended (Yinjao *et al.*, 2011). Different indicators have, however, been defined to quantify the SoH based on the battery characteristics, equipment, test and applications to which the battery is put (Yinjao *et al.*, 2011).

The Coulomb counting methods cannot account for battery ageing since they are based on fixed battery models in which it is assumed that the capacity of the battery is fixed regardless of the discharge current, age and temperature. The rest period needed when using V_{oc} method compromises the measurement accuracy because of voltage fluctuations and is unreliable for continuous battery monitoring (Koray *et al.*, 2005).

2.5 Present day Commercial Battery Monitors in the Market

A variety of stationary and handheld portable battery load tester (BLT) equipment from different manufacturers are used in car garages to diagnose the automotive SLI battery. Listed in Table 2.4

are some of the BLTs and their technical specifications from Argus analyzers, Autometer, Bosch, Cadex, Midtronics and Projector companies.

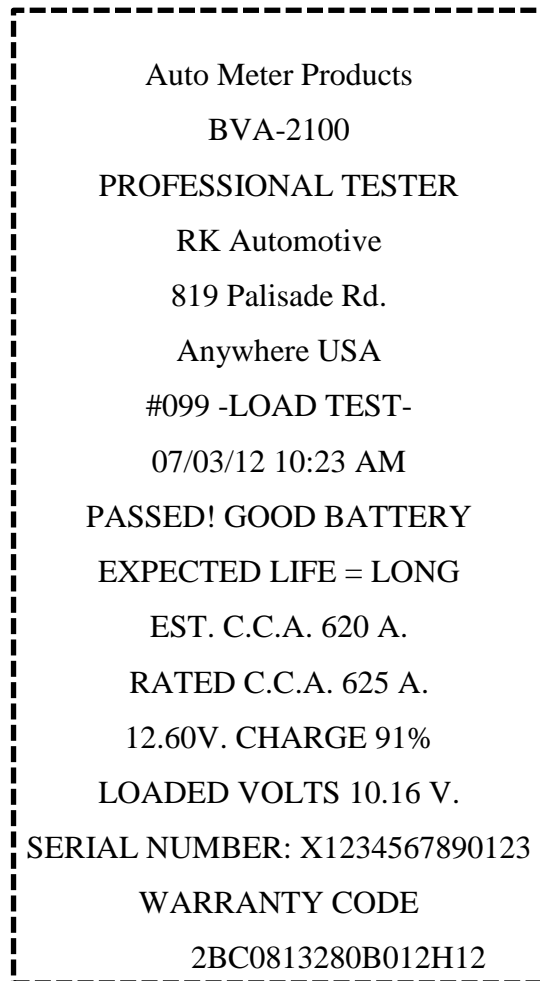
Table 2.4: Types of battery load testers and their technical specifications compiled from their respective operation manuals

BLT type	Test voltage (V)	Range CCA/Ah	Load (A)	Test time (Sec)
Argus analyzers AA500P	5 - 16	30 - 2000	0 - 1000	1
Autometer BVA 2100	- 40 - 40	200 - 1600	-1200 - 1200	15
Autometer BVA 350	0 - 30	200 - 1600	0 - 1000	15
Bosch BLT 301	0 - 12	20 - 1000 (32Ah - 180Ah)	0 - 450	5
Bosch BAT 110	0 - 20	200 - 850	0 - 500	1
Bosch BAT 131	0 - 24	100 - 2000	0 - 600	1
Cadex Spectro CA-12	0 - 30	50 - 1250	0 - 800	15
Delphi BMD	6 - 18	-1200 - 300	-300 - 1500	Full time
Midtronics GRX-3000	0 - 30	100 - 1700	0 - 1000	1
Midtronics EXP - 1000	0 - 60	100 - 3000	0 - 1000	1
Projector BLT 200	0 - 16	1000/160	0 - 500	15
Projector BLT 300	0 - 30	2000/320	0-1000	15

The Argus AA500P is a hand-held out of the car battery analyzer that uses the CrankCheck™ and the Large Pulse Resistance™ to measure the battery's capacity and the cranking ability. The Large Pulse Resistance technology works by drawing a high current pulse from the battery for a very short time and simultaneously measuring the voltage of the battery (www.argusanalyzers, 2016). The analyzer then measures the dc internal resistance of the battery which correlates to a CCA value for the battery and the SoC. A pulse load of 100 A is sent into the battery to enhance detection of mechanical defects and for testing batteries that have discharged down to as low as 20 % SoC.

The user needs not to know beforehand the battery's specification, size, rating or the motor details because the CrankCheck™ technology uses the actual engine cranking sequence to diagnose the battery performance (www.argusanalyzers, 2016).

The Autometer BVA 2100 is a BLT with an optional J1708 hookup port, which is usually located just below the dash board under the driver's side for interfacing with the vehicle under test (www.autometer.com, 2016). The BVA-2100 is automated and is used to immediately recognize a bad battery once connected across it, perform a voltage drop test analysis on 12 V and 24 V battery systems and print the results after each test, a sample of which is shown in Figure 2.3 (www.autometer.com, 2016):



Auto Meter Products
BVA-2100
PROFESSIONAL TESTER
RK Automotive
819 Palisade Rd.
Anywhere USA
#099 -LOAD TEST-
07/03/12 10:23 AM
PASSED! GOOD BATTERY
EXPECTED LIFE = LONG
EST. C.C.A. 620 A.
RATED C.C.A. 625 A.
12.60V. CHARGE 91%
LOADED VOLTS 10.16 V.
SERIAL NUMBER: X1234567890123
WARRANTY CODE
2BC0813280B012H12

Figure 2.3: Sample result from the Autometer BVA 2100 (Autometer, 2016)

The BVA-350 is a portable BLT and system analyzer that uses a pulsed load sent into the battery under test to determine that battery's SoC as well as to perform a complete starting and charging system analysis (www.autometer.com, 2016).

Bosch BLT 301 is a hand-held BLT used to test 12 V, 32 Ah – 180 Ah, lead-acid type automotive batteries using a fixed load. The test takes 5 seconds to determine the condition of the battery and displays the result as 'Good', 'Weak' or 'Bad' (de-ww.bosch-automotive.com, 2016).

BAT 110 uses conductance technology and a temperature compensation feature to test standard and maintenance free secondary batteries (de-ww.bosch-automotive.com, 2016). It has a large four-digit LED screen that displays the voltage and CCA with three illuminated LED indicators to show green, yellow and red for good battery, marginal battery and replace battery states respectively.

The BAT 131 is a hand-held clamp battery tester for testing 6 V and 12 V starter batteries in which the CCA can be set between 100 A – 2000 A according to the standards CCA, Japan industrial standard (JIS), Society of Automotive Engineers (SAE), German industrial standard (DIN) and International electro-technical commission (IEC) (de-ww.bosch-automotive.com, 2016).

The Spectro™ CA-12 from Cadex Inc. is a hand-held tester based on multi-model EIS that reads the internal resistance of the battery and uses other algorithms to compute a lengthy test of close to 40 million transactions in 15 seconds (Buchman, 2016). The Spectro™ CA-12 can read SoC of a battery having parasitic load currents measuring as high as 30 A and is unaffected by the surface charge of the battery under test (Buchman, 2016).

The GRX 3000 from Midtronics uses a combination of charge acceptance and conductance to diagnose the automotive battery before and while it is charging (www.midtronics.com, 2016) and has built-in temperature sensors in both the positive and negative terminal clamps.

The EXP 1000 is a portable hand-held BLT that uses conductance battery testing technology. It uses a combination of direct temperature measurement and deep scan technology to improve the accuracy of the measured quantities (www.ja.midtronics.com, 2016).

The Delphi Battery Monitoring Device (BMD) accurately calculates the SoC and SoH through specialized software algorithms to control the charging of battery and manage the vehicle's electrical loads. The device has a Local Interconnect Network interface for data and diagnostic communication which can be mounted on the battery's negative terminal in the car or embedded into the battery's electrical system. High currents of about 1500 A are measured using a 100 $\mu\Omega$ shunt. The Delphi BMD is designed for passenger vehicles, off-road vehicles, micro-hybrids, commercial vehicles and marine industry applications (www.delphi.com, 2016).

The Projector BLT 200 is normally installed in the car such that it draws its power from the cigarette lighter on the car's dashboard and can monitor 12 V and 24 V automotive battery system (www.projecta.com, 2016).

The BLT 300 has four temperature calibrations of 21°C, 10 °C, -1°C and -18 °C from which the battery can be monitored. The ambient battery temperature is approximated to the closest scale from these four and thereafter the battery V and I signals are taken and used to compute the SoC and SoH (www.projecta.com, 2016).

Currently, some mechanical and electronic systems in automobiles have electronic control units that contain self-diagnosis circuits. However, in earlier systems, a blink code was used to access the fault codes from a scanner stored in the memory (Denton, 2011). The accuracy of battery monitoring systems has been a point of discussion since they generally have an error of 10 % when all the parameters in question are considered (Patil *et al.*, 2011).

A method of placing sensors inside the battery to monitor individual cells, as shown in Figure 2.4, is under review (Matthias *et al.*, 2015).

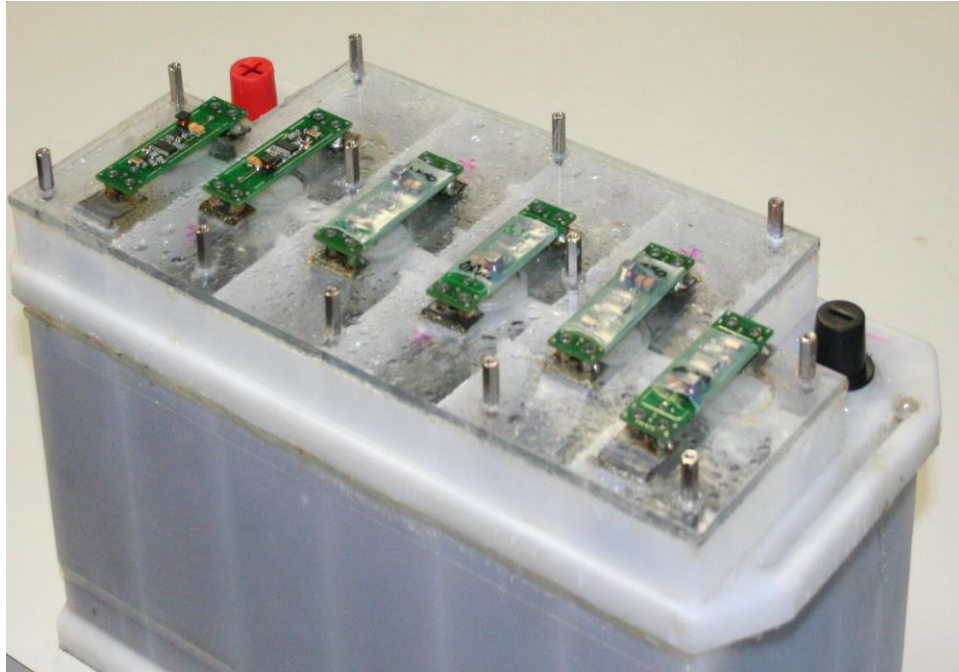


Figure 2.4: Sensors embedded in a battery to monitor individual cells (Matthias *et al.*, 2015)

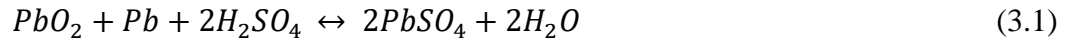
In this research, an algorithm that compensates for the voltage fluctuation based on the battery temperature changes was used alongside its SoC to compute the SoH of the battery. The BMS provided continuous monitoring of the SoC and SoH of the battery and the acquired computed data is stored in the SD memory card.

CHAPTER THREE

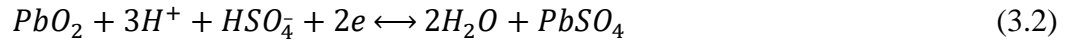
THEORETICAL BACKGROUND

3.1 Battery Charging and Discharging Process

During charging or discharging of the LAB, a chemical reaction takes place between the positive lead oxide (PbO₂) electrode, the negative lead (Pb) electrode and the sulphuric acid electrolyte. When the battery is in discharge mode, the positive and negative electrodes convert to lead sulphate (PbSO₄) and water. The chemical reactions that take place inside the battery are shown in Equations 3.1 to 3.4 (Djamila and Ernest, 2012);



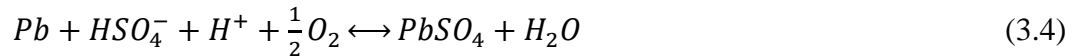
During discharge, the reaction takes place from the left-hand side of the Equation 3.1 towards the right while during charging, it moves from the right towards the left-hand side. The reaction taking place at the positive electrode is;



while the reaction at the negative electrode is represented by Equation 3.3;



At the negative electrode, oxygen recombines to lead sulphate in the presence sulphuric acid as;



The quantity of charge stored in a LAB depends on the dimensions of the battery plates and the quantity of electrolyte present in the battery (Owen and Guss, 2015). The characteristics of a battery, like discharge and self-discharge profiles, are influenced by the battery's chemistry (Texas, 2012).

The failure modes of the LAB are dependent upon the type of application and the specific battery design for that application. Some cells inside the battery may deteriorate faster than others due to increase in resistance and accumulation of discharge products leading to reduced output voltage (Chen *et al.*, 2012). Higher temperatures hasten the rate of degradation such that the cell having the highest rate determines the lifetime of the battery (Yalian *et al.*, 2013). Internal short circuits in the battery formed by dendrites growth across the separators between the positive and the

negative electrode during each battery cycle may lead to exothermic reactions and decreased capacity (Hui *et al.*, 2014). The properties of the LAB are shown in Table 3.1.

Table 3.1: Typical parameters of the lead acid battery (James and John, 2012)

Specific energy	20 - 35 Wh.Kg ⁻¹ which depends on usage
Energy density	54 - 95 Wh.L ⁻¹
Specific power	~250 W.Kg ⁻¹ before efficiency falls
Nominal cell voltage	2V
Amphour efficiency	~ 80%, varies with rate of discharge and temperature
Internal resistance	Extremely low, ~ 0.022 Ω per cell for 1 Amphour (Ah)
Commercially available	Readily available from several manufacturers
Operating temperature	Ambient, poor performance in extreme cold
Self-discharge	~ 2 % per day
Number of cycles	Up to 800 to 80 %
Recharge time	8 hours (but 90 % recharge in 1 hour)

SLI batteries are designed with battery grids having minimum electrical resistance, thin plates and higher concentrations of electrolyte to maximize the cranking ability. Heavy-duty SLI batteries used in construction equipment, trucks and buses have heavier and thicker plates that have high-density paste, premium separators and rubber cases so as to enhance their life. Since thicker plates provide less cranking current as compared to thinner ones, series and or series-parallel connections are used in these batteries (David and Thomas, 2002).

3.2 Standard Tests for Rating Starting Lighting and Ignition Batteries

Battery capacity ratings are usually established by the Battery Council International in conjunction with the Society of Automotive Engineers. The automotive SLI battery supplies power to all the electrical accessories of the vehicle when the engine is not running or the vehicle's charging system is faulty. It supplies float current whenever electrical demands of the vehicle exceed the charging system's output current, stabilizes the voltage of the entire automotive electrical system by absorbing abnormal transient voltages in the vehicles electrical system to protect certain electrical or electronic components from damage due to high voltages from the charging system and stores electrical energy for the vehicle for an extended period (Pistoia, 2009). The transient voltages are generated when the line between battery and alternator is open-circuited with the engine running

as is the case when an outside battery is used as a starting aid or when high-power consumers are switched off (Bosch, 2016). These transient voltage peaks last for milliseconds and can be as high as 350 V (Bosch, 2016).

Given the important functions played by the SLI battery, real time electronic monitoring of its functionality as presented in this research is of utmost importance to the motorist. SLI batteries are normally tested by briefly discharging them at high currents ranging between 200 A to 1500 A to ascertain their ability to crank the car engine (David and Thomas, 2002). The batteries are also tested for cold cranking amperes (CCA), which is the current in amperes that a battery can deliver for 30 seconds at a temperature of -17.7 °C without the terminal voltage falling below 7.2V (Hassan *et al.*, 2006). The CCA test is done to evaluate the battery's ability to provide power to crank the car's engine in cold temperatures. A manufacturer can use any standard to define the CCA using customized critical control parameters and values (Hassan *et al.*, 2006).

Other SLI battery tests that are normally done are charge rate acceptance, overcharge life and vibration resistance. The batteries are also subjected to accelerated life testing methods using high stressors like heat, humidity, temperature, vibration, load and the time under load so as to determine their performance under these conditions. After performing the tests, batteries are then produced in mass for use in cars and for other applications.

3.3 The Car Starting System

The car starting system comprises the battery, high current carrying cables and connecting wires, ignition key or switch, starter solenoid and or relay, starter motor, flywheel ring gear, starter drive and stator safety switch for automatic drive cars (Hollemeak, 2011). The ignition system circuit has a set of sparks plugs which offer high resistance to electron flow via the small gap of air between the center and ground electrodes (Denton, 2016). The stator motor, shown in Figure 3.1 among other components, changes the electrical energy from the battery into mechanical energy.

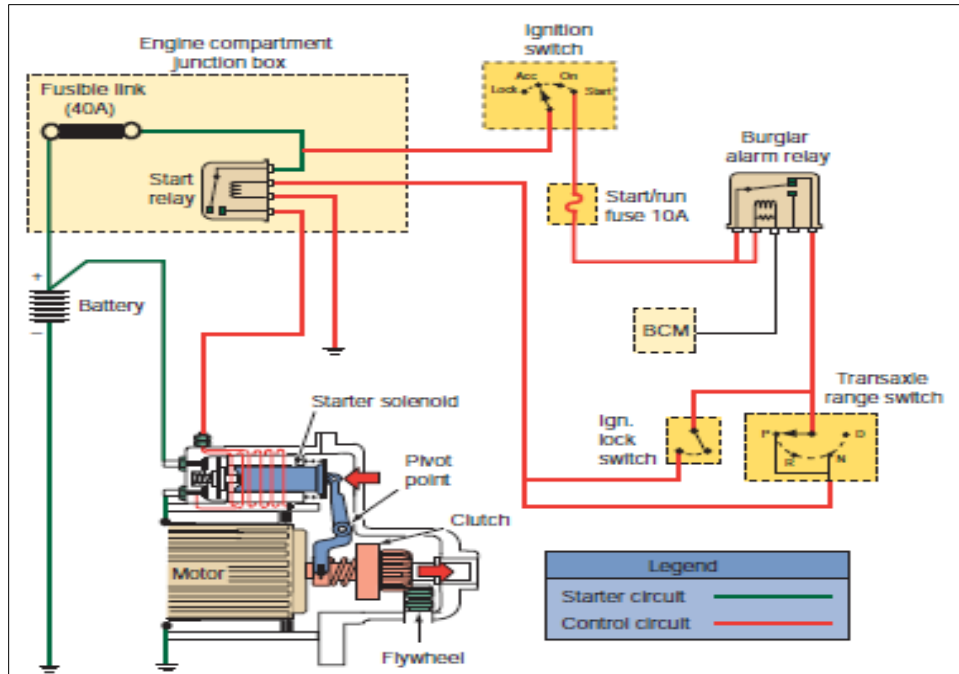


Figure 3.1: A simplified car starting system (Jack and Rob, 2014)

The starter motor draws a large amount of current required to generate enough torque to turn the flywheel which in turn runs the engine (Gilles, 2012). The current drawn can be as high as 1500A on some light duty vehicles and 3500 A on certain heavy commercial vehicles (Murugesan *et al.*, 2012). The high voltage from the ignition system ionizes the air gap in the spark plug and sets up a spark into the cylinder at near end of the compression stroke to ignite the compressed air and fuel vapor (Denton, 2014). For a spark to be able to jump across an air gap that is 0.6 mm wide, a voltage between 2 kV to 3 kV is required. Ignition systems transform the normal 12 V of the battery to around 8 kV to 50 kV or even 100 kV in the modern car versions and delivers the high voltage to the correct cylinder and at the right time (Denton, 2006).

Starting systems have a magnetic switch in form of either a solenoid or a relay for controlling the large current drawn during engine cranking. Figure 3.2 shows a typical stator motor commonly used in vehicles.

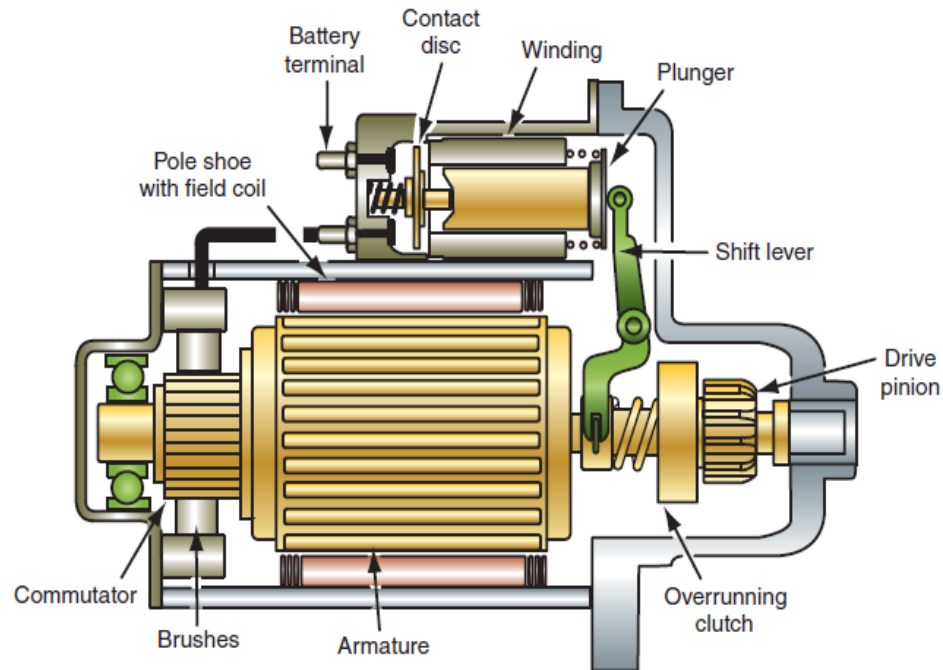


Figure 3.2: A car starter motor (Erjavec and Thompson, 2014)

The charging system of a car consists of the battery, the ac or dc generator, voltage regulator, drive belt, charge indicator, cables and wiring harness, ignition switch, starter relay and a fusible link (Hollembek, 2011). The ignition key passes through the five points of the switch during cranking. With the key at the (Hollembek, 2011);

- i. **accessories** position, **Acc**, the current from the battery is supplied to the electrical accessory circuits of the car.
- ii. **lock** position, electrical contacts in the ignition switch are open and the steering wheel and transmission gear selector are locked mechanically.
- iii. **Off** position, opens all the circuits controlled by the ignition switch and steering wheel and transmission gear selector are unlocked.
- iv. **On/Run** position, the current flows to the ignition, engine controls and any other circuits that are controlled by the switch. Some starting systems power an antitheft alarm upon removal of the key and turn it off whenever the key is inserted.
- v. **Start** position, current flows to the starter control circuit and cranks the engine.

The current fluctuations of the starter motor determine the number of times the current drawn reaches its peak value due to the compressions in each individual cylinder (Murugesan *et al.*, 2012). The value of the current drawn by the starter motor can be found from measuring the engine's compressions, which is critical for the smooth running of the engine, in the individual cylinders. With usage, the compressions in each cylinder deteriorate differently and so a check of the variations in compressions between the cylinders is necessary (Halderman *et al.*, 2014). If there is no compression in one cylinder, there will follow a current increase in the next cylinder, since part of the energy that is in the compressed air of the previous cylinder will be missing. The missing energy needs to be supplied by the starter motor and this manifests as the current increase just mentioned above (Murugesan *et al.*, 2012).

3.3.1 Engine cranking signals (V, I and T)

The high currents drawn during engine cranking are controlled by a power relay which gets actuated by a lower current of about 30 A and 80 A for light and heavy commercial vehicles respectively during engine cranking.

When the engine is cranked, the battery's voltage and corresponding current, ($V - I$), logs drop during the cranking period. After the cranking event, the V_{oc} of the battery does not normally go back to the value it was just before cranking which implies that there is always a voltage loss (V_{loss}) associated with each engine cranking event. The V_{loss} during engine cranking is illustrated in Figure 3.3. When the battery is charging, the current is normally taken to be positive while during discharge, it is taken to be negative hence the negative values of current shown on the x-axis.

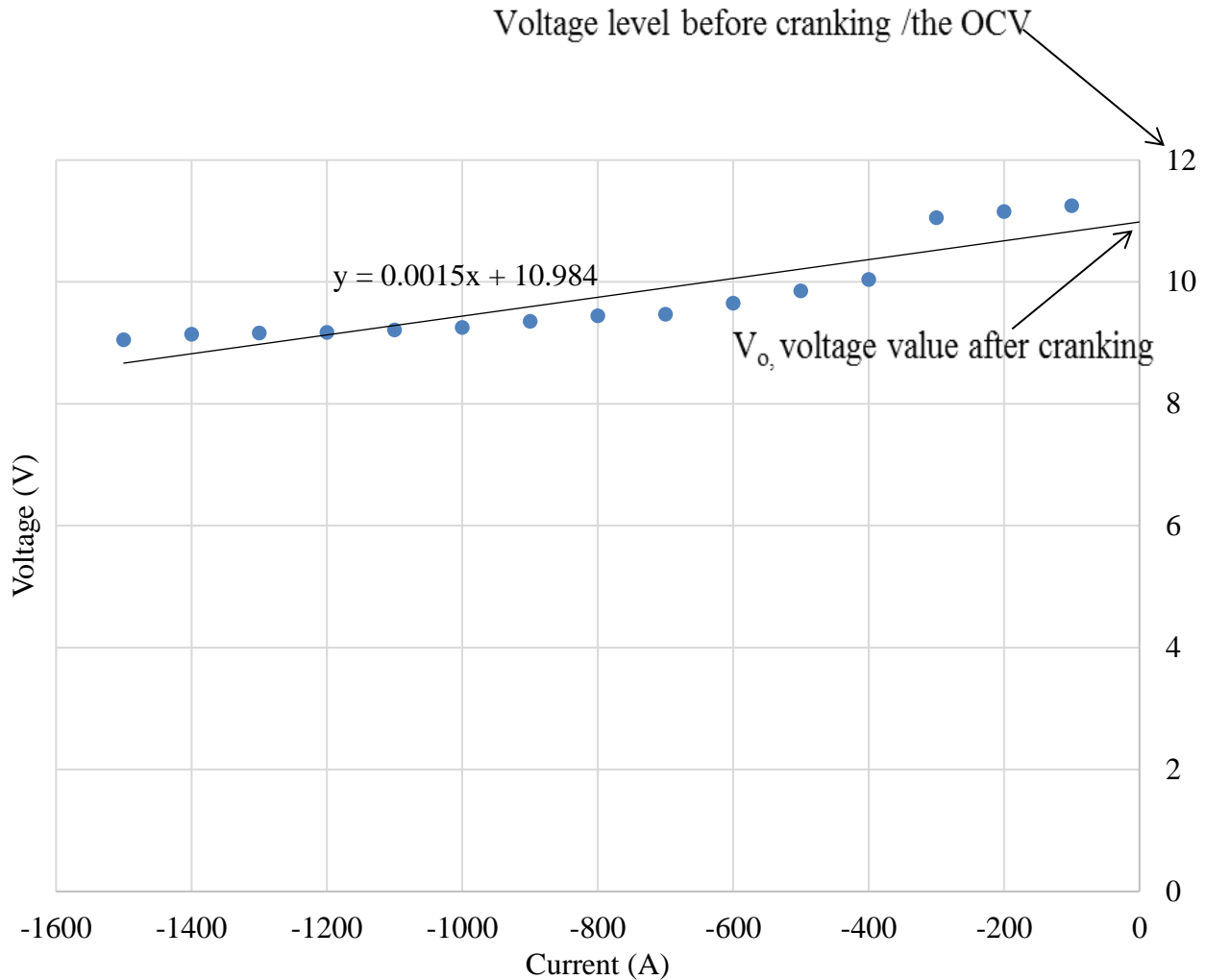


Figure 3.3: Voltage – Current relationship of a battery during a car cranking event (Zhang, 2012)

Based on the graph in Figure 3.3, the V_{oc} of the battery was 12 V but after the cranking event, the voltage did not get back to its initial value of 12 V but instead reached 10.984 V shown as the y-intercept voltage value at which the current is zero. The difference between the V_{oc} and the y-intercept voltage value, (V_o), gives the V_{loss} associated with this cranking event as 1.06V.

3.4 The BMS Block Diagram

The flowchart in Figure 3.4 showing the overview of the system components and their functional relationship was used to design the BMS. The direction of signals flowing in the system through

the constituent components is shown by the connecting arrows and with the specific function represented by each block written inside that block.

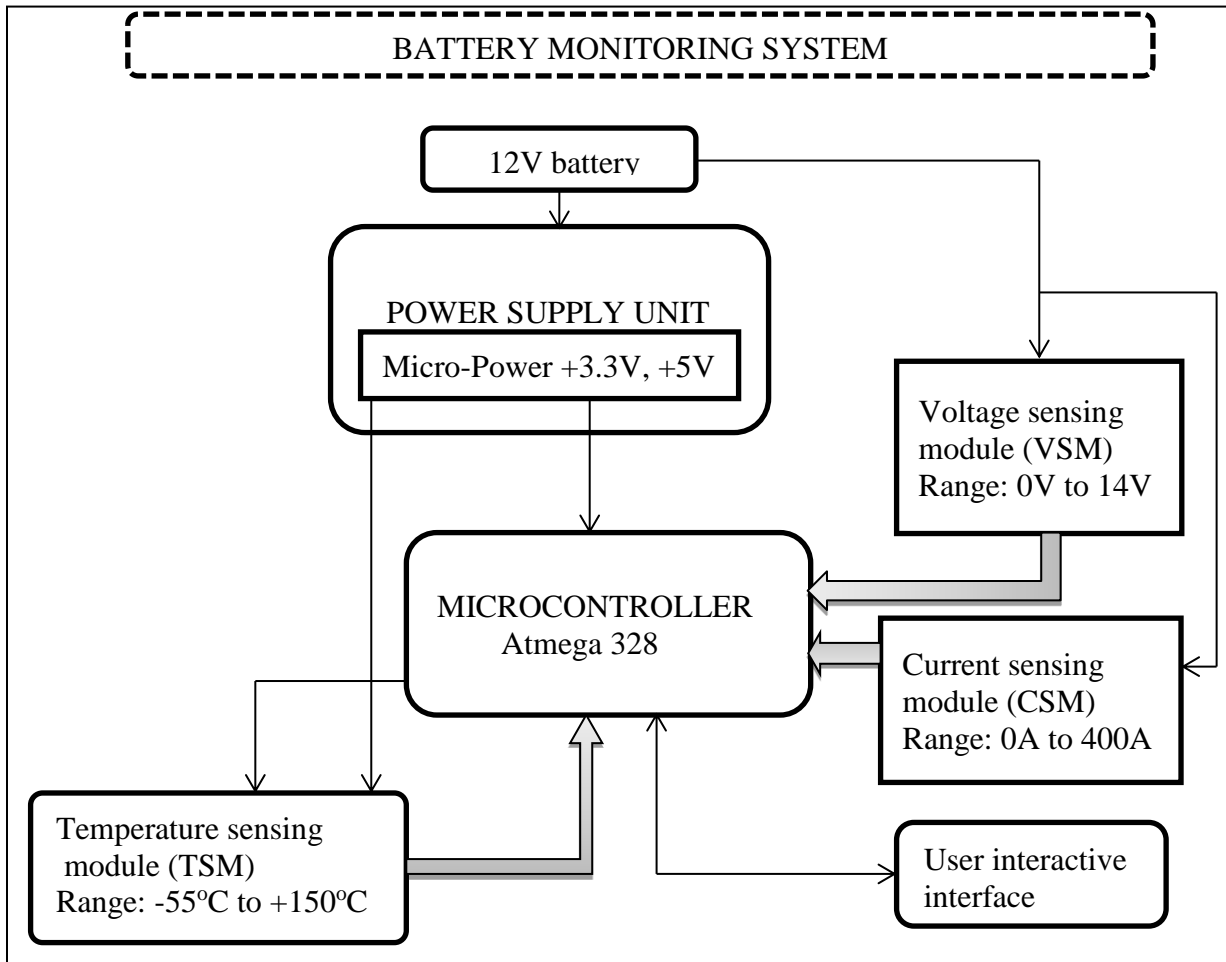


Figure 3.4: The block diagram of the BMS

CHAPTER FOUR

METHODOLOGY

4.1 Introduction

In this chapter, the components of the block diagram shown in Figure 3.4 in Chapter 3 on page 31 are described in detail. The processing unit, the Arduino Uno R3, the temperature sensor and voltage divider for measuring the battery temperature and voltage respectively are discussed. The current sensor IC, the voltage regulator, interactive user interface, the TFT screen and the data logger are also presented in this chapter. The specifications of the electronic components used are listed in Appendix A. The electronic circuit developer software, Proteuse Design Suite 8.5 from Labcenter Electronics Limited was used to generate Figures 4.1 to 4.7 as well as the complete schematic circuit of the BMS shown in Appendix B. The components below were sourced and used in the designs;

1. Current sensor IC part number ACS755SCB-200U from Allegro Microsystem, USA
2. Resistors, diodes, push buttons and capacitors from Fairchild Semiconductors, USA
3. The digital temperature sensor, DS18B20 from Maxim Integrated, USA
4. LM 7805 voltage regulator from Texas Instruments, USA
5. Arduino Uno R3 microcontroller board from Arduinocc™, Italy
6. The display screen PG160128A from Deek-Robot™ in Shenzhen, China
7. The data logging and retrieval board model Data logging shield V1.0 from Deek-Robot™ in Shenzhen, China.

4.2 The BMS Circuit Design

The apparatus used in this research were a 500 A BLT, the fabricated BMS and five functioning automobiles rated 250 Hp, 125 Hp, 115 Hp, 100 Hp and 80 Hp. The power output of the engine in Hp is directly proportional to the engine capacity. A high capacity engine draws in more air into it's cylinders prompting the fuel system to proportionately increase the fuel intake to the engine for combustion. The rated engine Hp can only be reached at specific engine rpm and not during cranking. Based on the objectives of this research, circuits were designed specifically for measuring the voltage, current and temperature. Since a magnetic field is normally created around

a current carrying conductor, a hall effect current sensor was used to measure the magnitude of the generated magnetic flux and convert it into a proportionate voltage. For measuring temperature, a DS18B20 digital thermal probe was used. A microcontroller unit (MCU) board, Arduino Uno R3, was used for acquiring the V, I and T signals and computing them to get the desired outputs. The power required by the current and temperature sensors was 5 V which was lower than the 12 V supplied by the car battery and so a voltage regulator was used to stabilize the dc voltage to the required value of 5 V. The specifications of the five batteries used are shown in Table 4.1.

Table 4.1: The specifications of the 12 V lead acid battery samples used in this research

Battery sample	Name	Capacity (Ah)	Type	Age (Years)	Reserve capacity (Minutes)	CCA (Amps)
1	Chloride Exide	75	Flooded	0	205	650
2	moll m3 plus K2	75	Maintenance free	2	200	660
3	Unistar	100	Flooded	2	200	650
4	Land Rover Varta	110	Maintenance free	0	205	850
5	Yuasa N70	110	Maintenance free	1	180	700

The models and specifications of the five cars used are shown in Table 4.2.

Table 4.2: The specifications of the five cars used in this research

Horse power (Hp)	@ revolutions per minute (rpm)
250	6000
125	6000
115	5600
100	6400
80	5600

4.2.1 The Voltage Sensor Design

The voltage sensing circuit was based on voltage-divider theorem configuration. The voltage divider with two resistors, resistor 14 (R14) rated 100 k Ω and resistor 15 (R15) rated 10 k Ω connected in series as shown in Figure 4.1 was designed to measure the battery's voltage. The voltage input (V_{in}) from the battery is applied across the two series resistors. Based on Equation 4.1, the resistor values were chosen to give an output voltage of 1.09 V. The analog input pin into Arduino board is pre-set by the manufacturer to take voltage values ranging between 0 V to a maximum of 5 V and so the 1.09 V from the BMS resistor network falls within this required voltage limit otherwise, the Arduino board can be damaged.

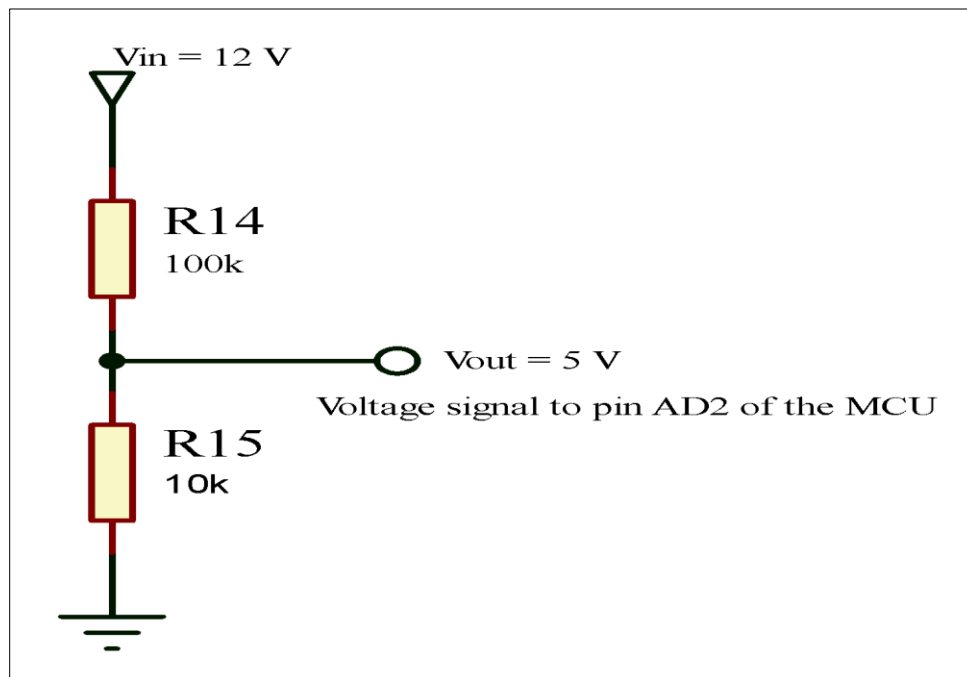


Figure 4.1: The voltage divider circuit designed for the BMS to measure the battery voltage

The output voltage (V_{out}) across R_{15} is given by Equation 4.1 below (Ronald *et al.*, 2009):

$$V_{out} = \frac{V_{in} \times R_{15}}{(R_{14} + R_{15})} \quad (4.1)$$

The analogRead command on the Arduino MCU converts the input voltage, which is the V_{out} from the voltage divider ranging between 0 V to 5 V, to a digital value ranging between 0 and 1023. The digital voltage (V_d) output is obtained based on Equation 4.2 below (Bayle, 2013):

$$V_d = \frac{5 \times V_{out}}{1023} \quad (4.2)$$

where V_{out} is the analog voltage reading from the voltage divider using Equation 4.2. The measured BMS voltage and the corresponding voltage logs from the HT326 CAT IV Professional Digital Multimeter (DMM) were plotted against each other and a linear regression equation relating them was deduced and used for calibrating the BMS voltage sensor.

4.2.2 The Current Sensor Design

The 5 pin ACS755SCB-200U current sensor from the Allegro family of current sensors was used for measuring the current drawn during engine cranking. Since one of this type of current sensors measures a maximum of 200 A, two of them were connected in parallel to be able to measure a current of up to 400 A.

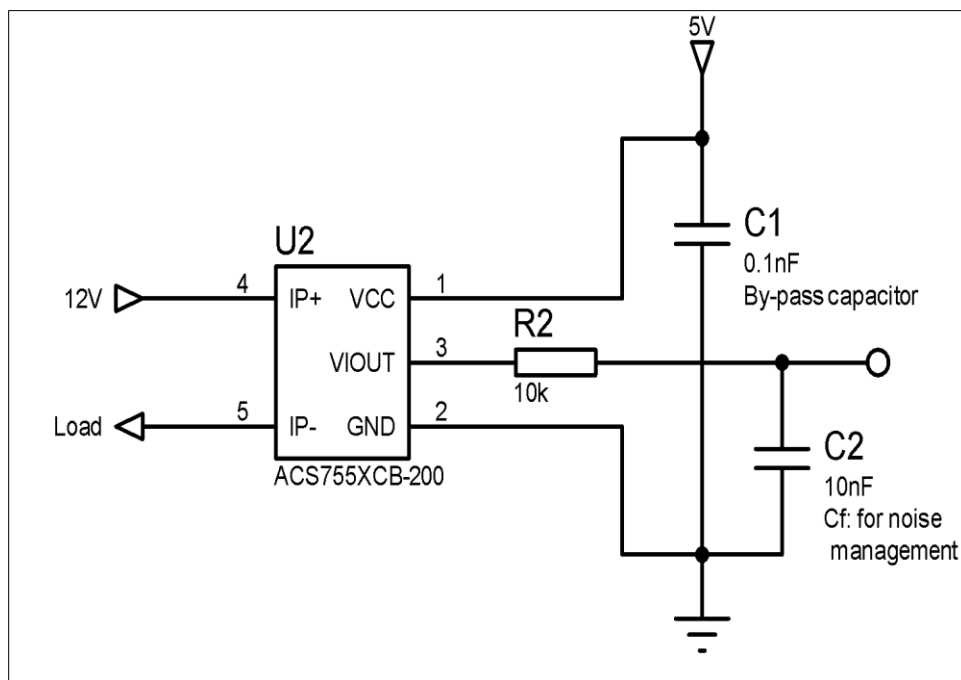


Figure 4.2: The current sensor circuit designed for the BMS for measuring the battery current

When the current flows through the copper conductor which is in the current sensor IC shown in Figure 4.2 as pin 4 and pin 5, a magnetic field is generated in the conductor which is then converted into a proportionate voltage (Microsystem, 2016). The BMS current sensor logs and the corresponding current logs from the Metrix MX 355 clamp meter were plotted against each other then a linear regression equation relating them was deduced and used for calibrating the BMS current sensor. The current sensor was then tested individually before the temperature and voltage sensors were incorporated into the BMS design.

4.2.3 Temperature Sensor Design

The battery's temperature measurements were done using a digital thermal probe, DS18B20, which was attached to the side of the battery under test. The temperature sensor uses two voltage signals derived from bipolar transistors inside the digital temperature probe to generate a proportionate temperature measurement based on its voltage output (Maxim, 2016). The circuit connection of the DS18B20 temperature sensor is shown in Figure 4.3.

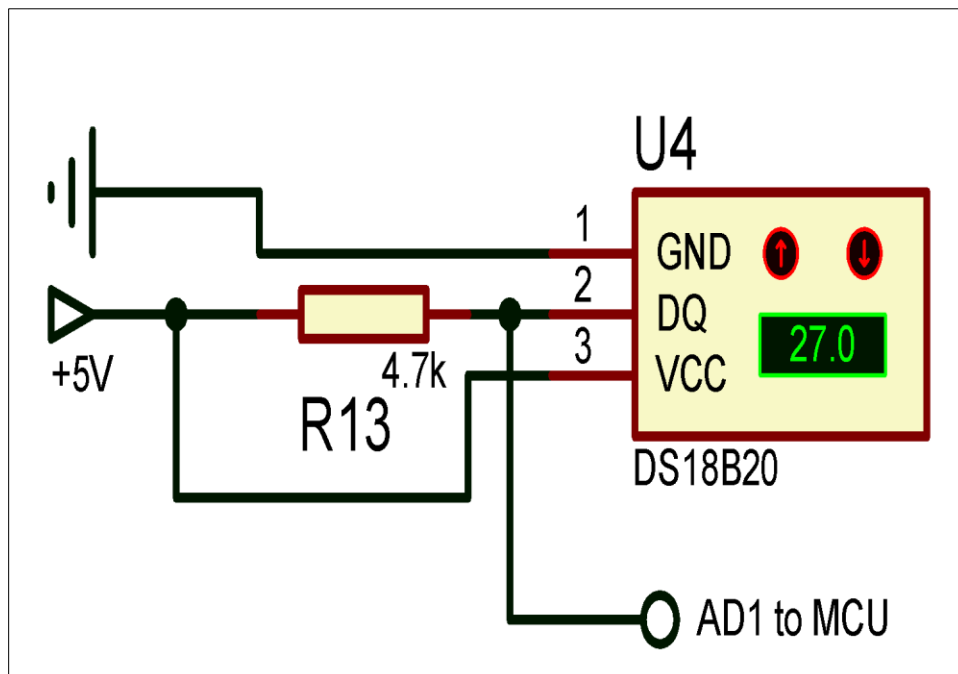


Figure 4.3: The temperature sensing circuit designed for the BMS for measuring the battery temperature

The BMS temperature sensor logs and the corresponding temperature logs of the Raytek non-contact thermometer were plotted against each other and a linear regression equation relating them was deduced and used for calibrating the BMS temperature sensor. The temperature sensor was then tested individually before the current and voltage sensors were incorporated into the BMS design.

4.2.4 Voltage Regulator Design

The LM 7805 IC was used as shown in Figure 4.4 to regulate the voltage supply to 5 V to be used by the temperature sensor, current sensor and the Arduino Uno R3 microcontroller.

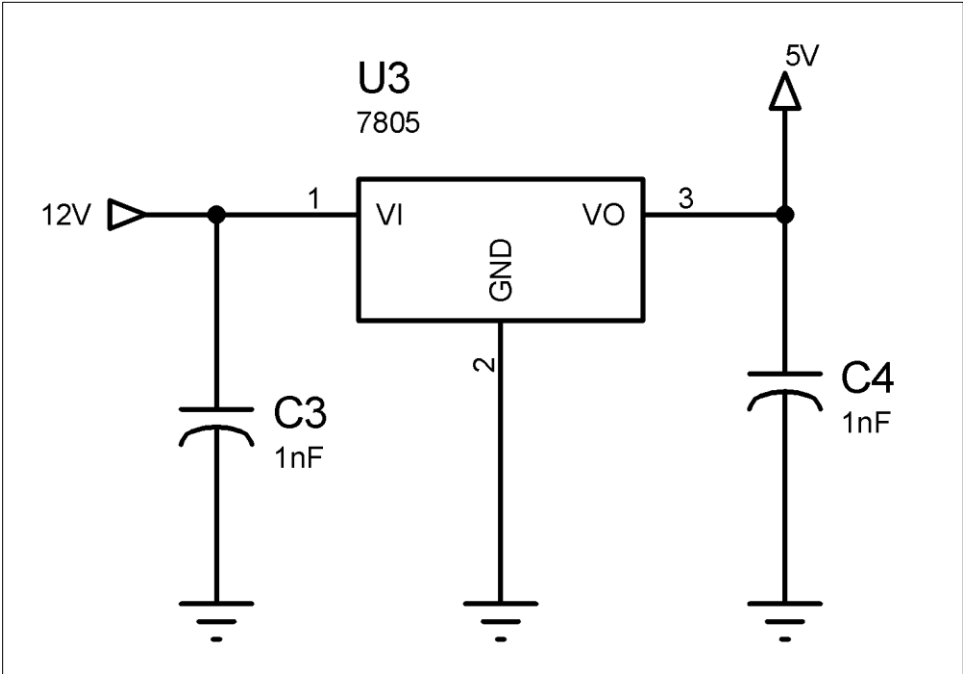


Figure 4.4: The circuit for supplying 5 V to the temperature sensor, microcontroller and current sensor

The 1 nano Farad capacitor between the input pin and the ground is used to get the required output of 5V (Fairchild, 2014).

4.2.5 The User Interactive Interface Design

The user interactive interface shown in Figure 4.5 has three button switches whose functions are;

- i. Power button: used for turning the BMS on or off.

- ii. Reset button: used for resetting the BMS.
- iii. Data hold button: used for prolonging the display time for the measured signals on the TFT.

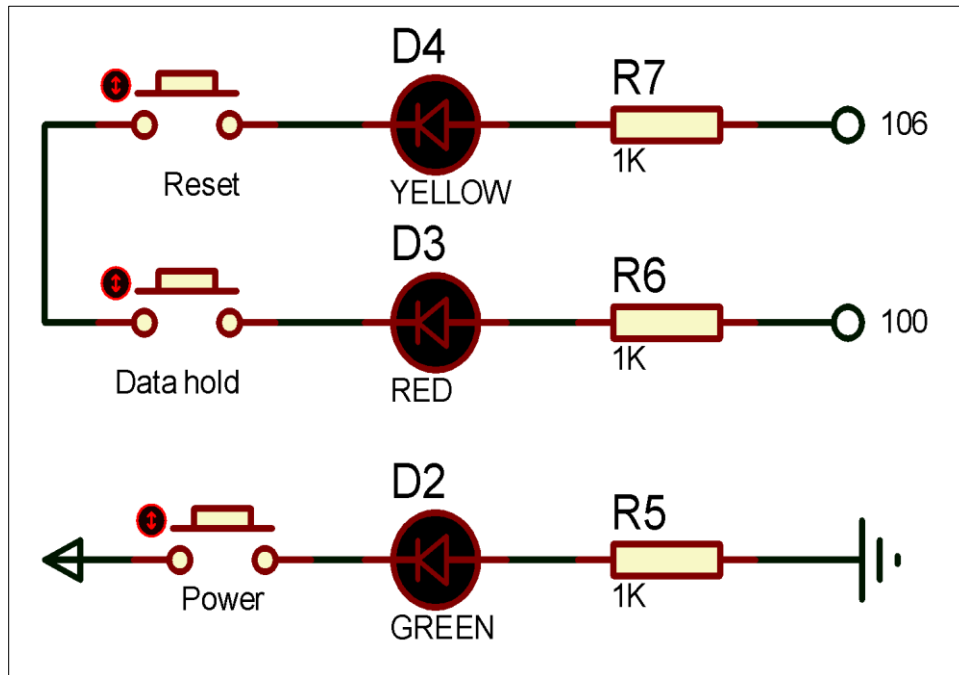


Figure 4.5: The user interactive interface design for the BMS

4.2.6 The Display Module Design

The output visual display was via a 160 x 128, 160 columns and 128 rows, arrays of the TFT screen PG160128A shown in Figure 4.6.

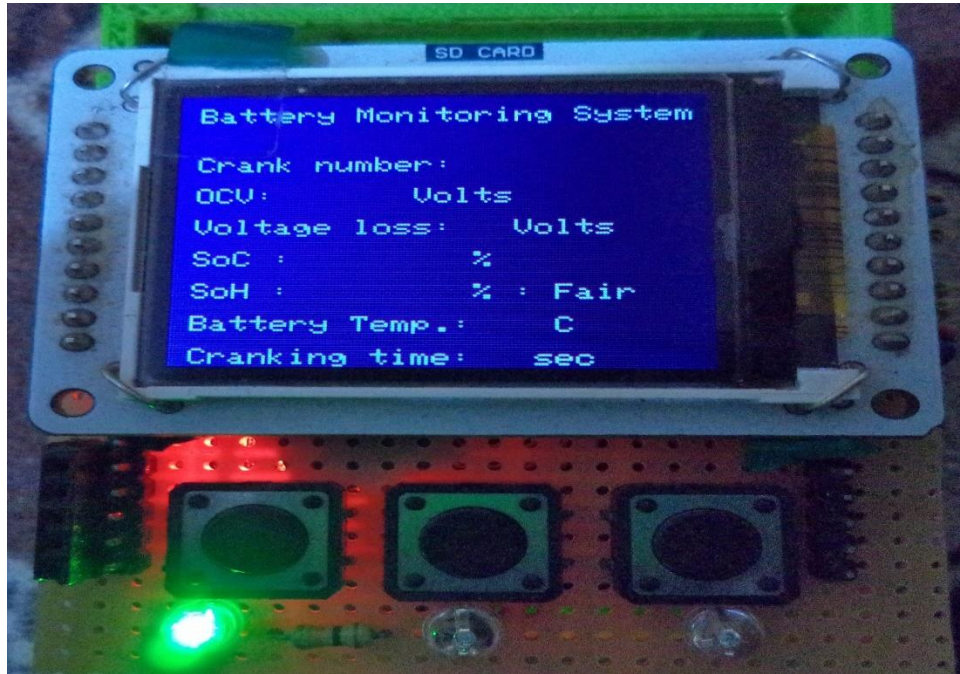


Figure 4.6: The PG160128A thin film transistor display of the BMS in standby mode

4.2.7 Processing Unit and Data Logging and Retrieval System Design

The processing unit of the BMS is the open source Arduino Uno R3 MCU board which has ATmega 328 microcontroller. It is based on Atmel AVR processor and contains the important parts as those of a common computer like the processor, peripherals, memories and inputs and outputs (Bayle, 2013). The Arduino MCU was programmed using Arduino programming language which is a combination of C and C++ programming languages (Evans, 2011). The Arduino MCU board and the data logger shield bearing an SD card are shown in Figure 4.7.

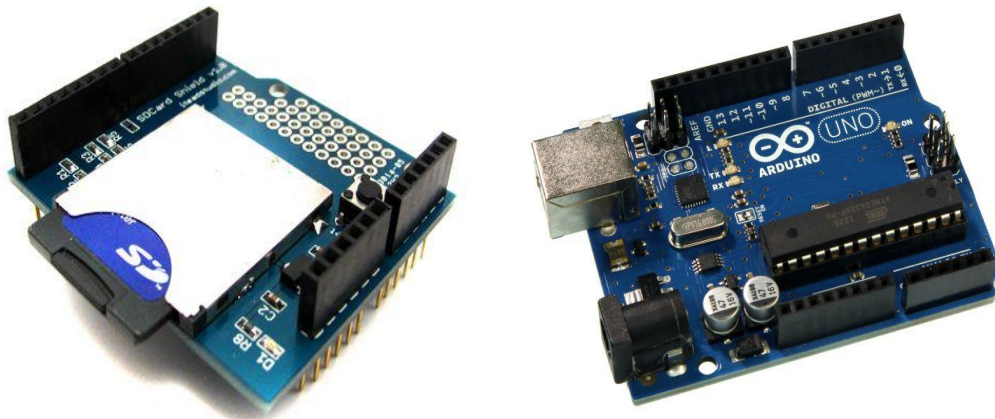


Figure 4.7: The Arduino Uno R3 board and the stackable SD card data logger for the BMS
The data logger was mounted on to the Arduino board as shown in Figure 4.8;



Figure 4.8: The data logger bearing the SD card mounted on the Arduino Uno R3 board

4.3 Effects of Voltage, Current and Temperature on State of Health

The voltage sensing circuit, current sensor circuit and the temperature sensor circuit described in section 4.2.1, 4.2.2 and 4.2.3 respectively were jointly used to get the voltage, current and temperature signals of the battery during every cranking event. The acquired signals were stored in an excel tabular form and were used in computing the SoH of the battery for each of the cranking event undertaken. The flow diagram of the BMS is shown in Figure 4.9.

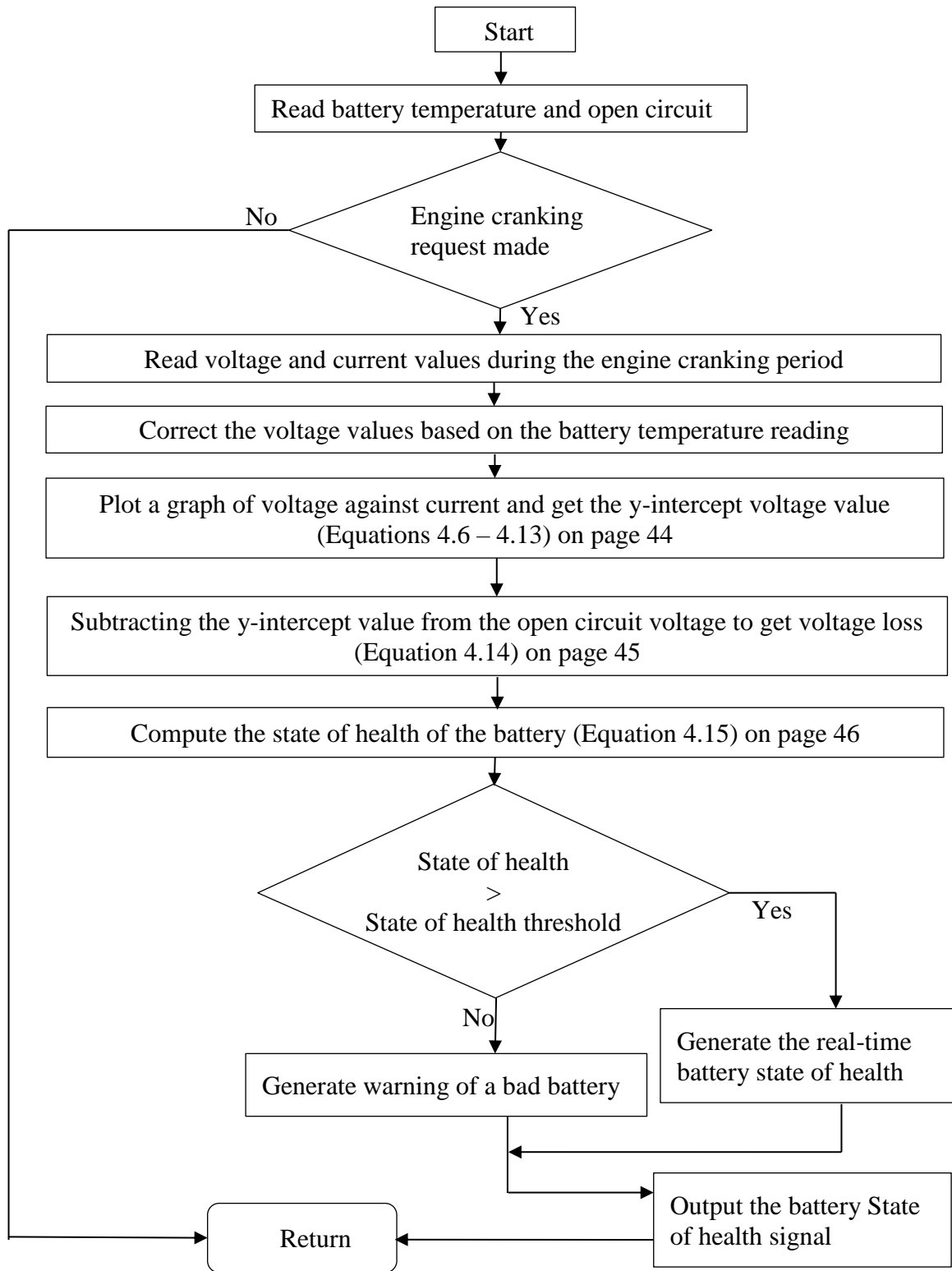


Figure 4.9: The flow chart showing steps for battery monitoring

4.4 Fabrication of the Battery Monitoring System

The voltage scale of the BMS was calibrated using a HT326 CAT IV Professional DMM capable of measuring 600 V dc/ac voltage. The current scale of the BMS was calibrated using a Metrix MX 355 clamp meter model number 900431MEF from German that can measure 400 A dc/ac current. The voltage and current digital meters used in calibrating the BMS are shown in Figure 4.10.



Figure 4.10: The digital multimeters for calibrating the voltage and current scales of the BMS

The temperature scale was calibrated using a portable IR thermometer, PM30 Standard Model (Raytech Corporation in the United Kingdom) capable of measuring temperature ranging between $-18\text{ }^{\circ}\text{C}$ to $870\text{ }^{\circ}\text{C}$. The IR thermometer is shown in Figure 4.11.



Figure 4.11: The IR Raytek thermometer for calibrating the temperature scale of the BMS

A calibration curve was obtained by fitting a linear equation to a set of calibration data. The calibration data were experimental values comprising measured responses corresponding to given voltage reference values. The errors in the slope and the y-intercept were found using Equations 4.13, 4.14 and 4.15

The Equation 4.3 was used for standard deviation in the y-direction to estimate the errors in the BMS measured values was (Devore, 2009):

$$S_{\frac{y}{x}} = \sqrt{\frac{\sum(y_i - \hat{y}_i)^2}{n-2}} \quad (4.3)$$

Where; y_i is the measured y- value using the BMS,

\hat{y}_i is the y-value calculated from the calibration equation

n is the number of terms and

$S_{\frac{y}{x}}$ is the standard deviation

The standard deviation of the slope was calculated using Equation 4.4 (Devore, 2009):

$$S_b = \frac{S_{\frac{y}{x}}}{\sqrt{\sum_i(x_i - \bar{x})^2}} \quad (4.4)$$

Where;

S_b is the standard deviation of the slope,
 x_i are the x-values from the reference voltage and
 \bar{x} is the mean of the x-values.

The standard deviation of the y-intercept, S_a , was calculated using Equation 4.5 (Devore, 2009).

$$S_a = S_y \frac{1}{x} \sqrt{\frac{\sum_i x_i^2}{n \sum_i (x_i - \bar{x})^2}} \quad (4.5)$$

After calibrating the temperature, current and voltage sensors and carrying out the individual tests on each one of them, all three of them were then tested together.

4.5 The SoH Display Algorithm

When the key is moved to the ON position, the voltage, current and temperature of the battery are recorded. Since the battery temperature adjusts very slowly to changes in the environmental temperature, the internal heating of the battery can be ignored and so, the battery temperature taken to be that close to the battery (Thyagarajan *et al.*, 2014). Since the battery temperature affects the V_{oc} and performance of the battery, a temperature compensation algorithm was used to correct the V_{oc} and other voltage values before using them to compute the SoH.

A regression is a statistical modelling technique that fits a relationship describing joint variability between two or more variables which can thereafter be used for prediction purposes. The V and I values were designated as \mathbf{v} and \mathbf{c} for voltage and current respectively for use in the regression formulae, Equation 4.6 to Equation 4.15 (Ronald *et al.*, 2004):

$$\mathbf{v} = \mathbf{a} + \mathbf{bc} \quad (4.6)$$

where \mathbf{a} is the y-intercept and \mathbf{b} is the regression coefficient of \mathbf{v} on \mathbf{c} ;

$$S_{cc} = \sum c^2 - \frac{(\sum c)^2}{n} \quad (4.7)$$

$$S_{vv} = \sum v^2 - \frac{(\sum v)^2}{n} \quad (4.8)$$

$$S_{cv} = \sum cv - \frac{\sum c \sum v}{n} \quad (4.9)$$

$$\text{and } b = \frac{S_{cv}}{S_{cc}} \quad (4.10)$$

$$\text{y intercept } a = \bar{v} - b\bar{c} \quad (4.11)$$

the regression coefficient;

$$r = \frac{S_c}{\sqrt{S_{cc} S_{vv}}} \quad (4.12)$$

$$V = V_o + IR_{batt} \quad (4.13)$$

The V values obtained during engine cranking were plotted against the corresponding I values and a line of best, which is described by the Equation 4.6, plotted as illustrated in Figure 3.3. Equation 4.6 is a linear equation, like the Equation 4.13 where V_o is the y-intercept value like **a** and R_{batt} , the battery resistance, is like the regression coefficient **b**. Instead of plotting the V and I values obtained during engine cranking on a graph like the one shown in Figure 3.3 to get V_{loss} , those values were used in equations 4.6 to 4.13 to get the V_{loss} value which was eventually computed as;

$$V_{loss} = V_{oc} - V_o \quad (4.14)$$

The values of SoC and V_{loss} acquired during the engine cranking event were then compared with the voltage loss threshold (V_{lossth}) value and state of charge threshold (SoC_{th}) value stored in the memory of the Atmega 328 IC on the Arduino Uno R3 board. It is recommended that battery load testing be done when the battery's SoC is 75 % but the Spectro™ CA-12 battery load tester from Cadex Inc. uses a minimal charge of 60 % (Buchman, 2016).

To get the SoC_{th} , it was assumed that the BMS had an error margin of 3 % and another 1 % due to parasitic losses and so the SoC_{th} was taken to be 71 %. To get the V_{lossth} and voltage loss of a new battery ($V_{lossnew}$), a laboratory set-up as shown in Figure 4.12 was used to simulate the engine cranking event several times using a brand-new battery to get the average V_{loss} and $V_{lossnew}$ threshold. The tests on the LAB were conducted with the following measured parameters and assumed theoretical thresholds;

- i. $V_{lossnew} = 0.5 \text{ V}$
- ii. $SoC_{th} = 71 \%$
- iii. $V_{lossth} = 1.5 \text{ V}$
- iv. $SoH_{th} = 80 \%$

The SoH was used computed using the Equation 4.15 (Zhang, 2012);

$$\text{SoH} = \frac{V_{\text{loss}} - V_{\text{lossth}}}{V_{\text{lossnew}} - V_{\text{lossth}}} \times 100 \quad (4.15)$$

The index values of SoH that were less than zero were set at 0 % while those were greater than 1 were set at 100 % (Zhang, 2012). The SoH was displayed as a percentage in one of the 3 ways listed below with an indicative or instructive message to the motorist as;

85 % ≤ SoH ≤ 100 %: Good green LED turns on

80 % ≤ SoH ≤ 85 %: Fair and orange LED turns on

0 % ≤ SoH < 80 %: Replace battery and red LED turns on

The green, orange and red LEDs for indicating the SoH are different from the ones for power, reset and data-hold buttons on the user interface. The indicative LEDs can therefore be used by someone who doesn't know how to interpret the SoH displayed in percentage form.

4.5.1 Laboratory BMS Test

The laboratory setup for data collection comprised of the 500 A BLT model number 91129 from Chicago Electric^R Power Tools in the USA, five SLI batteries and the BMS. The BLT can be used on a 6 V or 12 V battery system and is capable of testing batteries that are rated in Ah as well as those rated in CCA. The laboratory set-up for simulating engine cranking using the 500 A battery BLT and the BMS was arranged as shown by the pictorial representation in Figure 4.12 showing the moll m3 plus k2 battery, the BMS encased in the white housing, the TFT display encased in the green housing and finally the blue BLT.

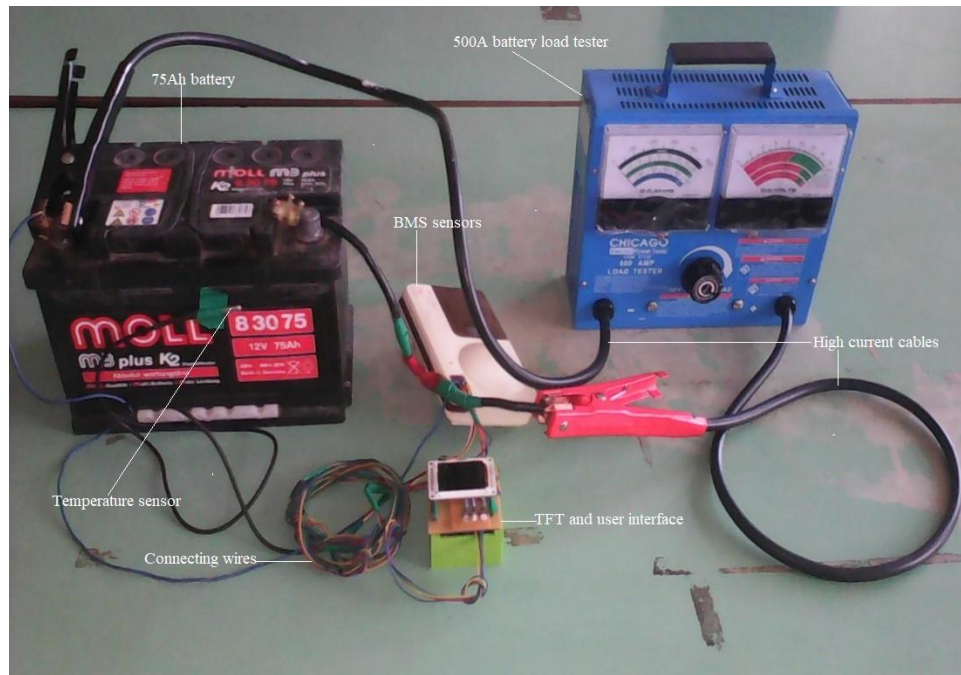


Figure 4.12: The pictorial setup of the 12 V SLI battery, the BMS and the 500 A BLT for simulating the car engine cranking event in the laboratory.

The BLT has two scales as shown in Figure 4.12 the first one being the I scale ranging from 0 A to 500 A while the second one is the V scale ranging from 0 V to 16 V. In the laboratory, the simulation of engine cranking event was accomplished by moving the I value on the first scale to a value between 120 A to 350 A using the black knob on the BLT and then turning on the BMS to start recording the V – I logs during the cranking period. The lower current limit was chosen to be 120 A because this was the least current drawn by the Isuzu truck, one of the five cars, during the actual engine cranking.

The acquired cranking data was saved in the SD card in the BMS in an excel sheet formatted with the listed 7 headings;

- i. column 1; the cranking event number
- ii. column 2; the open circuit voltage of the battery as measured by the BMS
- iii. column 3; the voltage loss associated with that specific cranking event
- iv. column 4; the state of charge of the battery for the specified cranking event
- v. column 5; the battery's temperature
- vi. column 6; the cranking duration in seconds

vii. column 8; the state of health of the battery

The 500 A BLT is designed to provide a fixed load, in this laboratory trial case a maximum of 230 A, to a 100 Ah Unistar battery. The BLT provides an indication of whether the battery could provide the preset current for a specified amount of time without failure. The BLT was cranked 18 times and the data saved in the data logger in the described excel format. From crank number (C#) 11, the acquired V values were then plotted against the corresponding I values and a line of best fit drawn to get the V_{loss} value. The V_{loss} for this cranking event was found by getting the difference between the measured V_{ocv} which was 12.55 V and the y-intercept voltage, V_o . The V – I values were then plotted on the same axis to show the behavior of the voltage and current during the engine cranking event.

The procedure of plotting the graph of a cranking event using the V – I logs was one way of getting the battery's V_{loss} , a method which if used for each cranking event undertaken in this research would have required 455 and 1256 graphs to be drawn for the laboratory and car-based results respectively. Instead of plotting the total of 1911 graphs, Equation 3.5 to Equation 3.14 in chapter 3 were used to compute the V_{loss} value which together with other parameters, was used compute the SoH of the battery. After successfully testing the BMS, it was used in the laboratory for collecting the data shown in section 5.3.

4.5.2 Field Setup of the Battery Monitoring System

The connection of the BMS in the car was done by disconnecting the cars' positive battery terminal and connecting the terminal to one end of the BMS' positive terminal and the other end of the BMS' positive terminal directly to the car battery. The negative terminal of the BMS, the blue wire in Figure 4.14, was connected to the negative terminal of the car battery. The temperature sensor, the black wire with a shiny silver end shown in Figure 4.13, was attached to the side of the car battery under test.



Figure 4.13: The battery monitoring system installed in the 250 Hp engine car



Figure 4.14: The battery monitoring system installed in the 115 Hp engine car

The user interactive interface and display unit of the BMS was secured onto an appropriate space next to the drivers' seat in the car under test as shown in the Figure 4.15 for the 250 Hp engine.



Figure 4.15: The battery monitoring system display, the green box, in the 250 Hp engine car

The BMS was installed in the 115 Hp engine and cranked 21 times and the data saved in the data logger in the excel format. It was from such tables bearing the cranking data for the five different batteries which were used in the five cars that the results shown in section 5.3 and 5.4 were drawn.

After successfully calibrating and testing the BMS in the 115 Hp engine, it was then used in all the cars for collecting the data presented in section 5.4. The battery under test was always fully charged before installing it alongside the BMS into the car. On the occasions in which the battery cranked the car's engine successfully and the car was driven, the cranking events were accomplished by stopping the car along the way turning off the engine and restarting it.

CHAPTER FIVE
RESULTS AND DISCUSSION

5.1 Laboratory Testing of the Sensors using the BLT, BMS and DMM

5.1.1 Voltage sensor test output

The voltage logs derived from the voltage sensor of the BMS as described in section 4.2.1 on page 34 alongside the same voltage logs as measured by the HT326 CAT IV Professional DMM are shown in Table 5.1.

Table 5.1: The calibration data for the voltage sensor obtained from the voltage sensor of the BMS and the DMM

BMS voltage reading (V) ± 0.47 V	DMM voltage reading (V) ± 0.35 V
12.52	12.65
12.41	12.51
12.38	12.49
12.29	12.41
12.27	12.39
12.21	12.31
12.17	12.27
12.16	12.26
12.12	12.21
12.11	12.18
12.05	12.12
11.93	12.01
11.10	11.09
10.99	11.01
9.99	9.92
9.78	9.69
9.54	9.41
9.49	9.34
9.34	9.22
9.25	9.11

The first column of Table 5.1 shows the measured voltage readings using the BMS while the second column shows the reference voltage measured by the DMM. The accuracy of the DMM was given as ± 0.35 V. The voltage measured using the BMS was plotted against the reference voltage as shown in Figure 5.1.

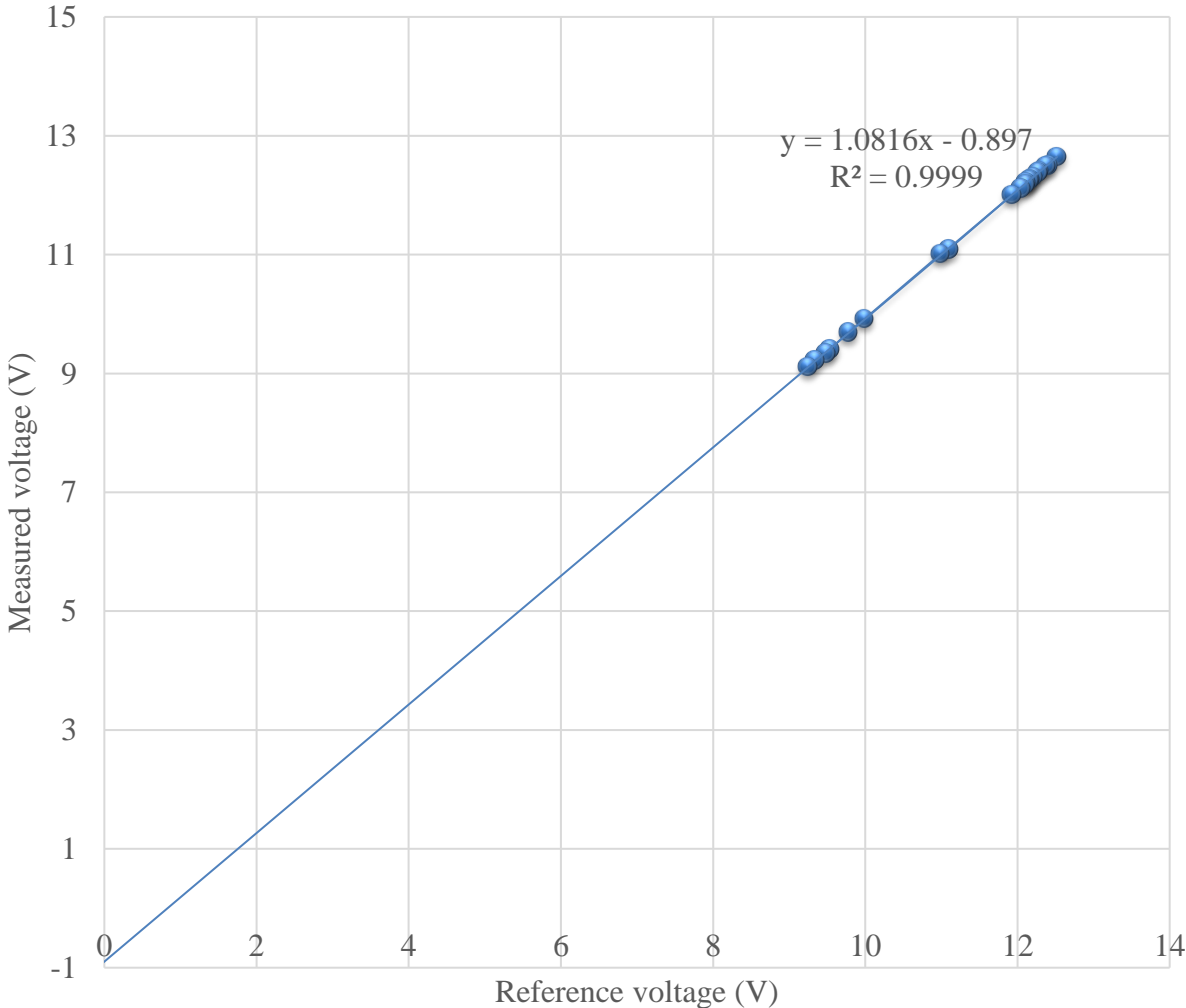


Figure 5.1: The calibration graph for the voltage sensor of the BMS

The linear equation derived from the graph of the measured voltage against the reference voltage was;

$$y = (1.0816x - 0.897) \tag{5.1}$$

To get the errors, standard deviations of the slope and of the y-intercept were computed using equations 4.3, 4.4 and 4.5 on pages 43 and 44.

The standard deviation based on the voltage calibration data;

in y-direction, S_{y_x} , was 0.22

of the slope, S_b , was 0.038

of the y-intercept, S_a , was 0.430.

The total error in the measured y-values, δy , was the sum of the error in the slope, δm , the error in the y-intercept, δc and the given ± 0.35 V error in the DMM as shown in Equation 5.2.

$$\begin{aligned}\delta y &= \delta m + \delta c + 0.35 \text{ V} \\ &= 0.430 + 0.038 + 0.35 \\ &= 0.818 \text{ V}\end{aligned}\tag{5.2}$$

The equation of calibration of the voltage sensor was therefore;

$$y_{BMSVcal} = (1.0816x - 0.897) \pm 0.818 \text{ V}\tag{5.3}$$

where $y_{BMSVcal}$ is the calibrated BMS voltage value.

5.1.2 Current sensor output

The current sensor output logs derived from the current sensor in the BMS as described in section 4.2.2 alongside their corresponding current logs using the Metrix MX 355 current clamp meter are shown in Table 5.2.

Table 5.2: The calibration data for the current sensor obtained using the BMS and the MX 355 clamp meter.

BMS current reading (A) ± 0.41 A	Metrix MX 355 current reading (A) ± 1.1 A
22.24	22.31
25.47	25.53
28.62	28.69
30.71	30.79
36.02	36.08
39.02	39.08
44.05	44.10
49.99	49.98
50.88	50.92
66.81	66.77
69.91	69.89
73.82	73.77
82.31	82.26
93.09	93.01
103.28	103.18
115.29	115.18
147.21	147.01
160.93	160.69
166.53	166.28
197.98	197.67
237.99	237.58
290.44	289.89

The first column of Table 5.2 shows the measured current readings using the BMS while the second column shows the reference current readings measured by the Metrix MX 355 current clamp meter. The accuracy of the Metrix MX 355 current clamp meter was given as ± 1.1 A. The measurements of current using the BMS were plotted against the reference current readings as shown in Figure 5.2.

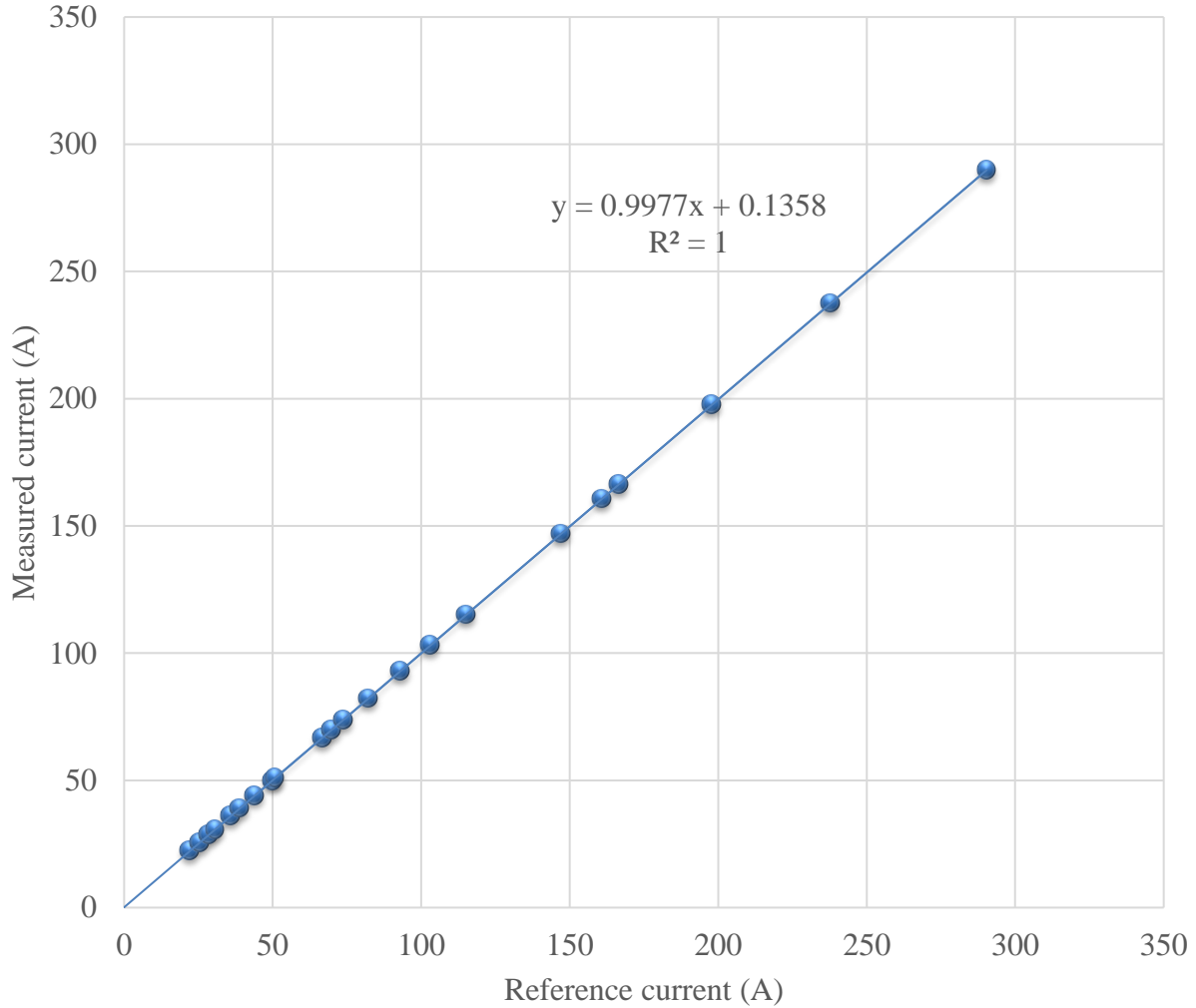


Figure 5.2: The calibration graph for the current sensor of the BMS

The linear equation derived from the graph of was;

$$y = (0.9977x + 0.1358) \quad (5.4)$$

To get the errors, standard deviations of the slope and that of the y-intercept were computed using equations 4.3, 4.4 and 4.5 on pages 43 and 44. The standard deviation based on the calibration data of the current sensor are shown below.

The standard deviation;

in y-direction, $S_{\frac{y}{x}}$, was 0.406

of the slope, S_b , was 0.148

and the y-intercept, S_a , was 0.001.

The total error in the measured y-values for current sensor was the sum of the error in the slope, the error in the y-intercept of the current calibration curve and the ± 1.1 A error in the clamp meter.

$$= 0.406 + 0.001 + 1.1 \text{ A}$$

$$= 1.507 \text{ A}$$

The calibrated BMS current value, $y_{BMS_{cal}}$, was;

$$y_{BMS_{cal}} = (0.9977x + 0.1358) \pm 1.51 \text{ A} \quad (5.5)$$

5.1.3 Temperature sensor output

The output logs derived from the temperature sensor of the BMS as described in section 4.2.3 alongside the corresponding temperature logs using the infra-red (IR) thermometer are shown in Table 5.3.

Table 5.3: The calibration data for the temperature sensor of the BMS and the IR thermometer

BMS temperature $\pm 0.643 \text{ }^\circ\text{C}$	IR laser thermometer $\pm 0.5 \text{ }^\circ\text{C}$
20.44	20.33
21.55	21.47
21.56	21.48
21.62	21.55
22.56	22.51
22.75	22.71
22.95	22.9
23.94	23.94
23.94	23.93
24.06	24.04
24.76	24.78
24.99	25.02
31.87	32.05
31.94	32.1
32.69	32.87
39.94	40.3
85.01	86.44
85.11	86.52
85.12	86.56
85.12	86.55
85.91	87.34

The first column of Table 5.3 shows the measured temperature readings using the BMS while the second column shows the reference temperature measured using the IR laser thermometer. The accuracy of the IR laser thermometer was given as $\pm 0.5\text{ }^{\circ}\text{C}$. The measured temperature readings from the BMS were plotted against the reference temperature as shown in Figure 5.3.

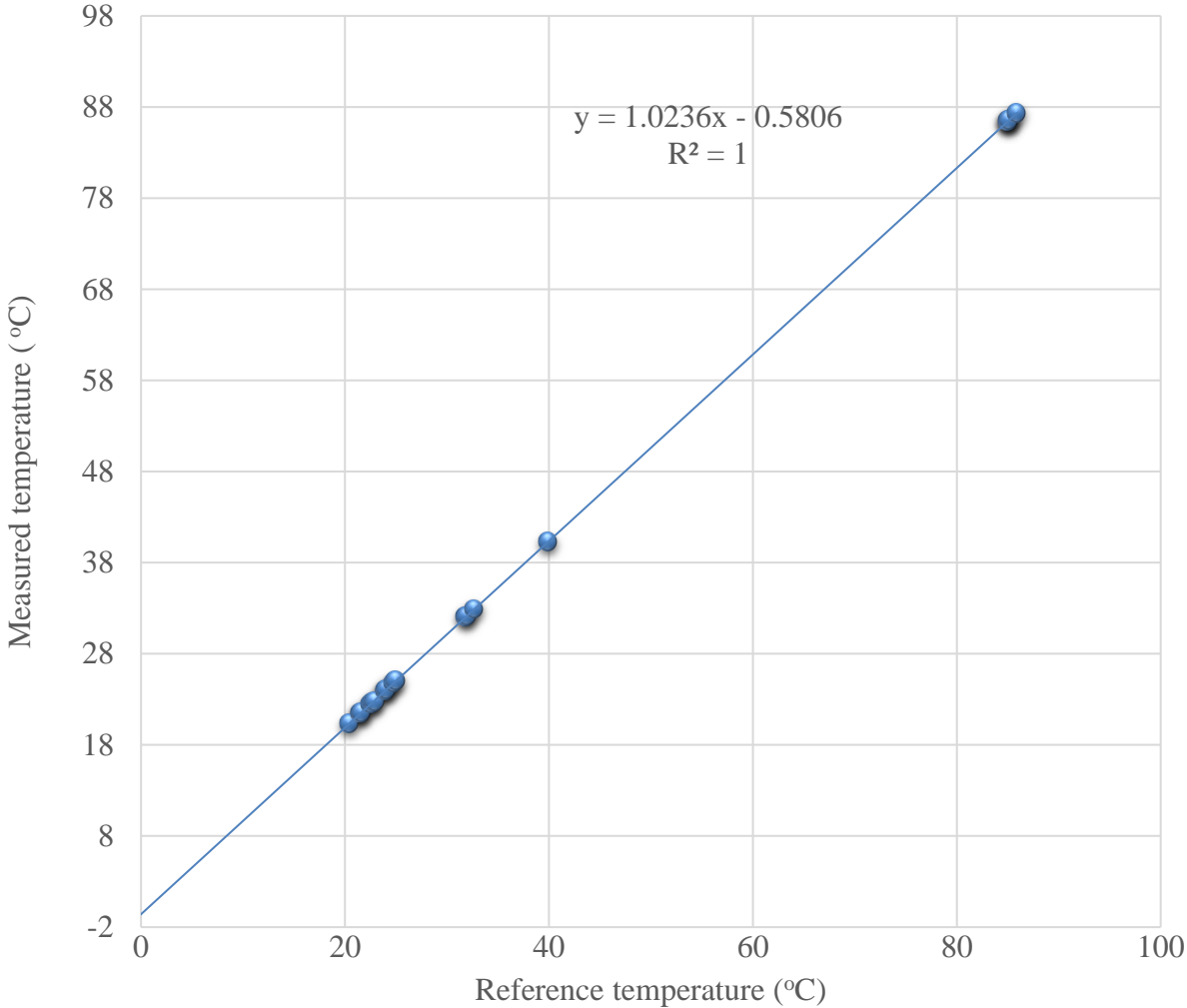


Figure 5.3: The calibration curve for the temperature sensor of the BMS

The linear equation derived from the graph of the measured temperature against the reference temperature was;

$$y = (1.0236x + 0.5806) \tag{5.7}$$

To get the errors, the standard deviations of the slope and that of the y-intercept for the temperature sensor were computed using equations 4.3, 4.4 and 4.5 on page 43 and 44

The standard deviation;

in y-direction, S_y , was 0.1.544

of the slope, S_b , was 0.013

and the y-intercept, S_a , was 0.630

The total error in the measured y-values of the temperature was the sum of the error in the slope, the error in the y-intercept of the temperature calibration graph and the stated ± 0.5 °C of the IR thermometer as shown below;

$$\begin{aligned} &= 0.630 + 0.013 + 0.5 \\ &= 1.143 \end{aligned}$$

The equation of calibration of the current sensor was therefore;

$$y_{BMS\text{cal}} = (1.0236x - 0.5806) \pm 1.14 \quad (5.8)$$

where $y_{BMS\text{cal}}$ is the calibrated BMS temperature value.

To get the calibration data of Tables 5.1, several sets of data were recorded and the calibration equation deduced for each set. The data collection was stopped when the gradient and the y-intercept values became nearly constant thus giving a more accurate approximation of the equation. The same procedure was used in the calibration data of the current and temperature sensors.

5.1.4 Combined V, I and T Analysis

The combined voltage, current and temperature logs from the sensors are shown in Table 5.4.

Table 5.4: The combined calibrated BMS voltage, current and temperature output readings

Current (A) ± 1.51 A	Voltage (V) ± 0.82 V	Temperature (°C) ± 1.14 °C
33.24	12.72	29.69
108.72	12.41	29.69
228.90	11.37	29.69
229.06	11.25	29.69
228.96	11.23	29.69
229.48	11.22	29.69
229.22	11.16	29.69
228.96	11.15	29.69
229.02	11.14	29.69
228.96	11.13	29.69
229.02	11.11	29.69
229.12	11.08	29.69
229.38	11.06	29.69
229.22	11.04	29.69
229.16	10.98	29.69
229.48	10.97	29.69
229.54	10.94	29.69
229.28	10.93	29.69

Table 5.4 shows the output from the three sensors when used concurrently to obtain the battery current, voltage and temperature logs during a single cranking event. The temperature of the battery remained constant during the cranking event but the voltage decreased as more current was drawn from the battery.

Table 5.5 on page 60 shows 18 cranking events carried out in the laboratory on the 100 Ah Unistar battery with the BLT preset to draw a current of 230 A during each cranking event.

Table 5.5: The computed data for 18 cranking events using the 100 Ah Unistar battery

Crank number (C#)	BMS V_{oc} (V) ± 0.82 V	Voltage loss (V) ± 0.01 V	SoC (%) $\pm 0.01\%$	Battery temperature ± 1.14 °C	Crank duration ± 0.01 s	SoH (%) ± 0.01
1	12.52	0.08	100	24.46	10.05	100
2	12.52	0.53	94.68	24.56	10.02	100
3	12.51	0.07	58.47	24.47	10.02	100
4	12.15	0.25	38.24	24.46	10.07	100
5	12.14	0.03	37.40	24.46	10.05	100
6	12.13	0.42	34.90	24.56	10.03	100
7	12.07	0.06	27.35	24.56	10.07	100
8	12.06	0.16	25.68	24.06	10.04	100
9	12.02	0.06	20.41	24.56	10.05	100
10	12.33	1.16	58.59	24.05	10.08	83.67
11	12.55	0.73	87.90	24.08	10.03	100
12	12.29	1.18	56.29	23.31	10.01	82.46
13	12.21	1.05	46.41	24.56	10.08	95.40
14	12.33	1.16	58.79	24.45	10.01	83.67
15	12.37	1.12	58.87	24.41	10.03	78.74
16	12.49	1.19	59.11	24.43	10.03	81.43
17	12.38	1.37	58.89	24.42	10.04	63.39
18	12.29	1.18	56.78	24.41	10.01	81.66

From Table 5.5, the V_{oc} decreased non-linearly following each cranking event. The temperature of the battery remained constant and its value was close to the ambient temperature which agrees with an observation made by Thyagarajan that the battery temperature can be taken to be the ambient temperature close to the battery under test (Thyagarajan *et al.*, 2014). When the cranking interval was 30 minutes as was the case between C# 10 and C# 11, the battery managed to recover some of the voltage and that was evidenced by the V_{oc} increasing from 12.33 V to 12.55 V corresponding to a SoC rise from 58.59 % to 87.00 %. Schoch *et al.* (2017), in their research on monitoring techniques for 12 V lead acid batteries in automobiles also observed this battery recovery phenomena of a battery in discharge state. The voltage and their corresponding current logs, 147 logs, for C# 11 in Table 5.5 are shown in Table 5.6.

Table 5.6: The V - I logs for the 100 Ah Unistar battery obtained for C# 11 using the BLT

V - I sample number	Current (A) ± 1.51 A	Voltage (V) ± 0.82 V	Time (seconds) ± 0.01 s
1	0.01	12.16	0.10
2	48.54	12.16	0.17
3	48.54	12.16	0.24
4	48.54	12.16	0.30
5	48.54	12.16	0.37
6	48.54	12.16	0.44
7	48.54	12.16	0.51
8	48.54	12.16	0.58
9	48.54	12.16	0.64
10	62.20	10.68	0.71
11	62.20	10.68	0.78
12	62.20	10.68	0.85
13	109.28	10.68	0.92
14	109.28	10.68	0.98
15	109.28	10.68	1.05
16	109.28	10.68	1.12
17	109.28	10.68	1.19
18	109.28	10.68	1.26
19	109.28	9.05	1.32
20	109.28	9.05	1.39
21	109.28	9.05	1.46
22	227.30	9.05	1.53
23	227.30	9.05	1.60
24	227.30	9.05	1.67
25	227.30	9.05	1.73
26	227.30	9.05	1.80
27	227.30	9.05	1.87
28	227.30	9.29	1.94
29	227.30	9.29	2.01
30	227.30	9.29	2.07
31	227.34	9.29	2.14
32	227.34	9.29	2.21
33	227.34	9.29	2.28
34	227.34	9.29	2.35
35	227.34	9.29	2.41
36	227.34	9.29	2.48
37	227.34	9.56	2.55
38	227.34	9.56	2.62

39	227.34	9.56	2.69
40	227.24	9.56	2.75
41	227.24	9.56	2.82
42	227.24	9.56	2.89
43	227.24	9.56	2.96
44	227.24	9.56	3.03
45	227.24	9.56	3.09
46	227.24	9.71	3.16
47	227.24	9.71	3.23
48	227.24	9.71	3.30
49	227.34	9.71	3.37
50	227.34	9.71	3.43
51	227.34	9.71	3.50
52	227.34	9.71	3.57
53	227.34	9.71	3.64
54	227.34	9.71	3.71
55	227.34	9.73	3.77
56	227.34	9.73	3.84
57	227.34	9.73	3.91
58	227.30	9.73	3.98
59	227.30	9.73	4.05
60	227.30	9.73	4.11
61	227.30	9.73	4.18
62	227.30	9.73	4.25
63	227.30	9.73	4.33
64	227.30	9.68	4.39
65	227.30	9.68	4.45
66	227.30	9.68	4.52
67	227.44	9.68	4.59
68	227.44	9.68	4.66
69	227.44	9.68	4.73
70	227.44	9.68	4.79
71	227.44	9.68	4.86
72	227.44	9.68	4.93
73	227.44	9.68	5.00
74	227.44	9.68	5.07
75	227.44	9.68	5.13
76	227.24	9.68	5.20
77	227.24	9.68	5.27
78	227.24	9.68	5.34
79	227.24	9.68	5.41
80	227.24	9.68	5.47

81	227.24	9.68	5.54
82	227.24	9.91	5.61
83	227.24	9.91	5.68
84	227.24	9.91	5.75
85	227.24	9.91	5.81
86	227.24	9.91	5.88
87	227.24	9.91	5.95
88	227.24	9.91	6.02
89	227.24	9.91	6.09
90	227.24	9.91	6.15
91	227.24	10.38	6.22
92	227.24	10.38	6.29
93	227.24	10.38	6.36
94	227.34	10.38	6.43
95	227.34	10.38	6.49
96	227.34	10.38	6.56
97	227.34	10.38	6.63
98	227.34	10.38	6.70
99	227.34	10.38	6.77
100	227.34	10.49	6.83
101	227.34	10.49	6.90
102	227.34	10.49	6.97
103	227.14	10.49	7.04
104	227.14	10.49	7.11
105	227.14	10.49	7.17
106	227.14	10.49	7.24
107	227.14	10.49	7.31
108	227.14	10.49	7.38
109	227.14	10.50	7.45
110	227.14	10.50	7.52
111	227.14	10.50	7.58
112	227.30	10.50	7.65
113	227.30	10.50	7.72
114	227.30	10.50	7.79
115	227.30	10.50	7.86
116	227.30	10.50	7.92
117	227.30	10.50	7.99
118	227.30	10.38	8.06
119	227.30	10.38	8.13
120	227.30	10.38	8.20
121	227.40	10.38	8.26
122	227.40	10.38	8.33

123	227.40	10.38	8.40
124	227.40	10.38	8.47
125	227.40	10.38	8.54
126	227.40	10.38	8.60
127	227.40	10.20	8.67
128	227.40	10.20	8.74
129	227.40	10.20	8.81
130	227.34	10.20	8.88
131	227.34	10.20	8.94
132	227.34	10.20	9.01
133	227.34	10.20	9.08
134	227.34	10.20	9.15
135	227.34	10.20	9.22
136	227.34	10.27	9.28
137	227.34	10.27	9.35
138	227.34	10.27	9.42
139	227.40	10.27	9.49
140	227.40	10.27	9.56
141	227.40	10.27	9.62
142	227.40	10.27	9.69
143	227.40	10.27	9.76
144	227.40	10.27	9.83
145	227.40	10.60	9.90
146	227.40	10.60	9.96
147	227.40	10.60	10.03

From Table 5.6, it can be observed that the current drawn from the battery rose from 0.01 A to 48.54 A then to 62.20 A and finally to 109.28 A in the first 1.29 seconds. Within this time, the voltage dropped from 12.16 V to 9.05 V with the initial V_{oc} for this crank was being 12.55 V as shown in Table 5.5. The voltage then fluctuated between 9.05 V and 9.91 V for 4.83 seconds and then fluctuated between 10.20 V and 10.60 V within the last 3.67 seconds of cranking. The current drawn thereafter increased from 109.28 A to values between 222.14 A and 227.44 A in the remaining 8.5 seconds. The value of 109.28 A was recorded 9 times in 0.54 seconds. Similarly, the values 48.54 A, 62.2 A, 227.14 A, 227.24 A, 227.30 A, 227.34 A, 227.40 A and 227.44 A were each recorded more than 7 times. This V- I trend is load specific i.e this BLT models the demand whose trend follows that pattern. This is like the uniqueness of the current drawn by different car

ignition starter motors. The plot of the voltage values against current for C# 11 are shown in Figure 5.4.

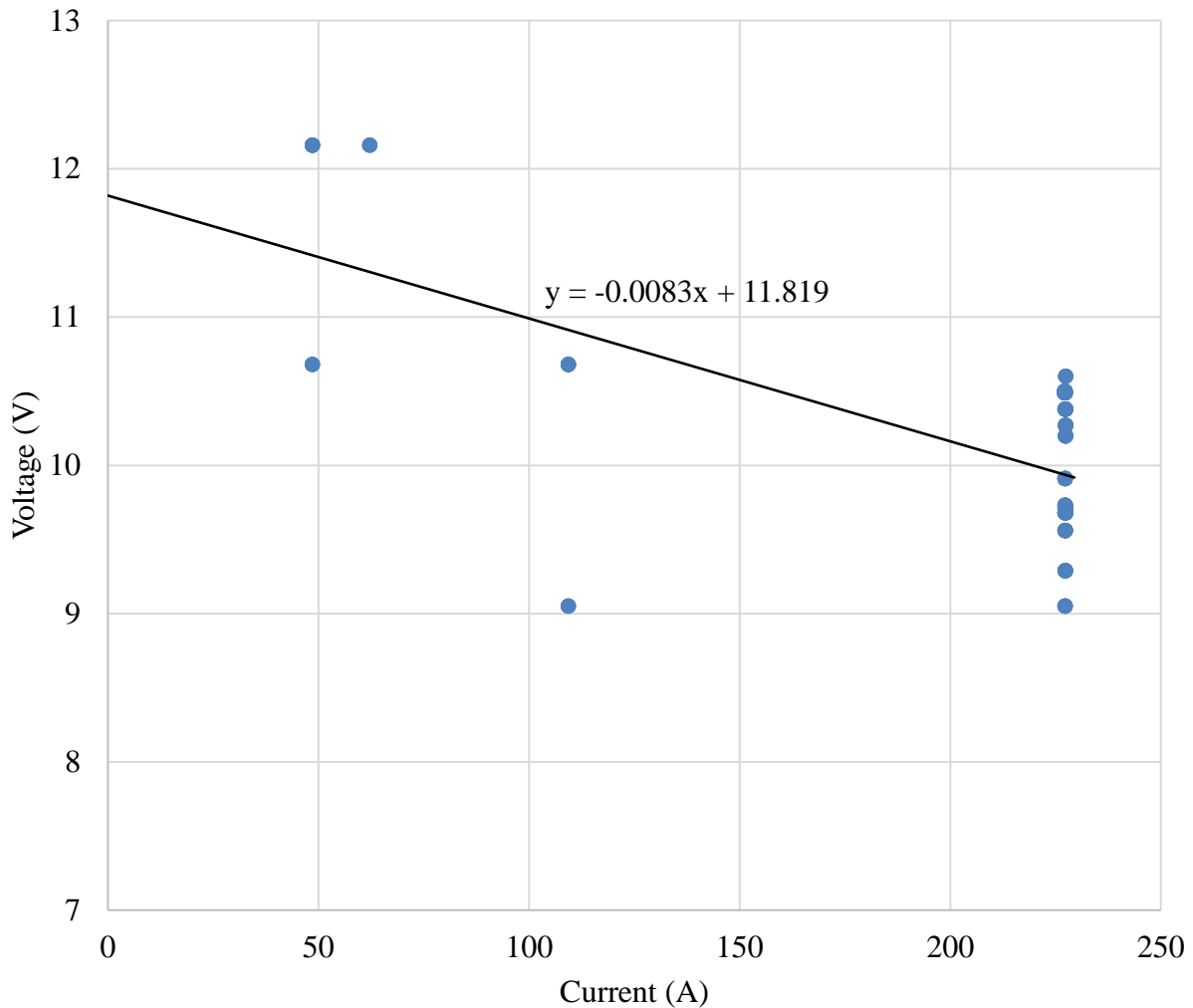


Figure 5.4: The battery current-voltage characteristics for C# 11 for the 100 Ah Unistar battery

Based on Figure 5.1, most of the V- I logs were constant and so they appear to be clustered between 222.14 A – 227.44 A as shown in the figure. This is so because unlike the actual car engine, the BLT used for cranking presents a fixed load to the battery and that is why the current stayed almost constant at 227.14 A and 227.44 A and the voltage at 10.5 V during the cranking period. The V_{loss} for C# 11 was 0.731 V and it's TFT display appeared as shown in Figure 5.5.

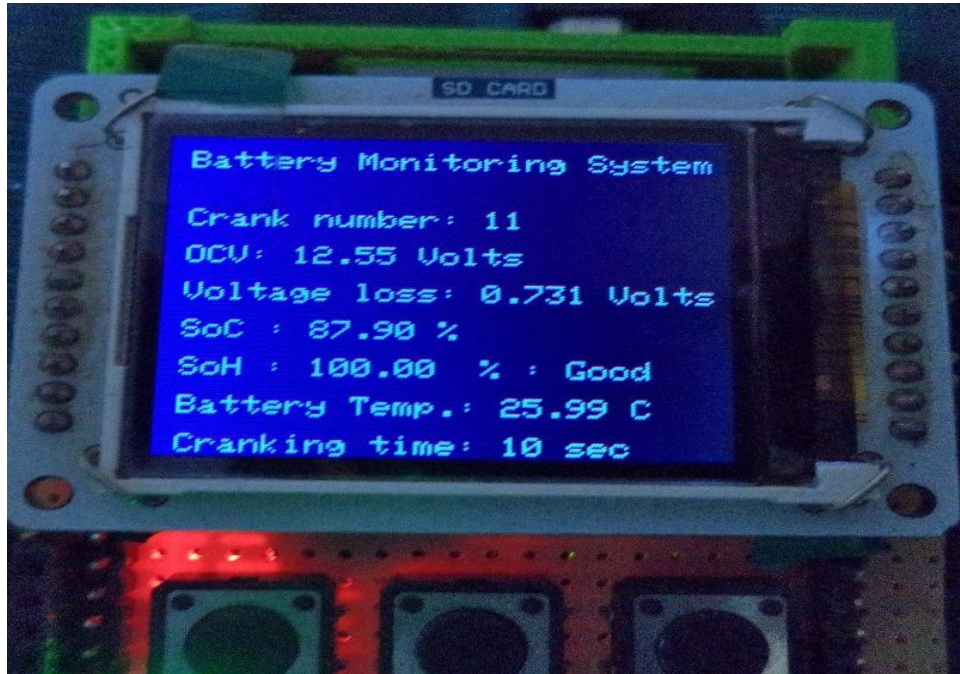


Figure 5.5: The TFT display for the C# 11 for the 100 Ah Unistar battery

The variation of voltage and current signals during this cranking event, C#11, is shown in Figure 5.6.

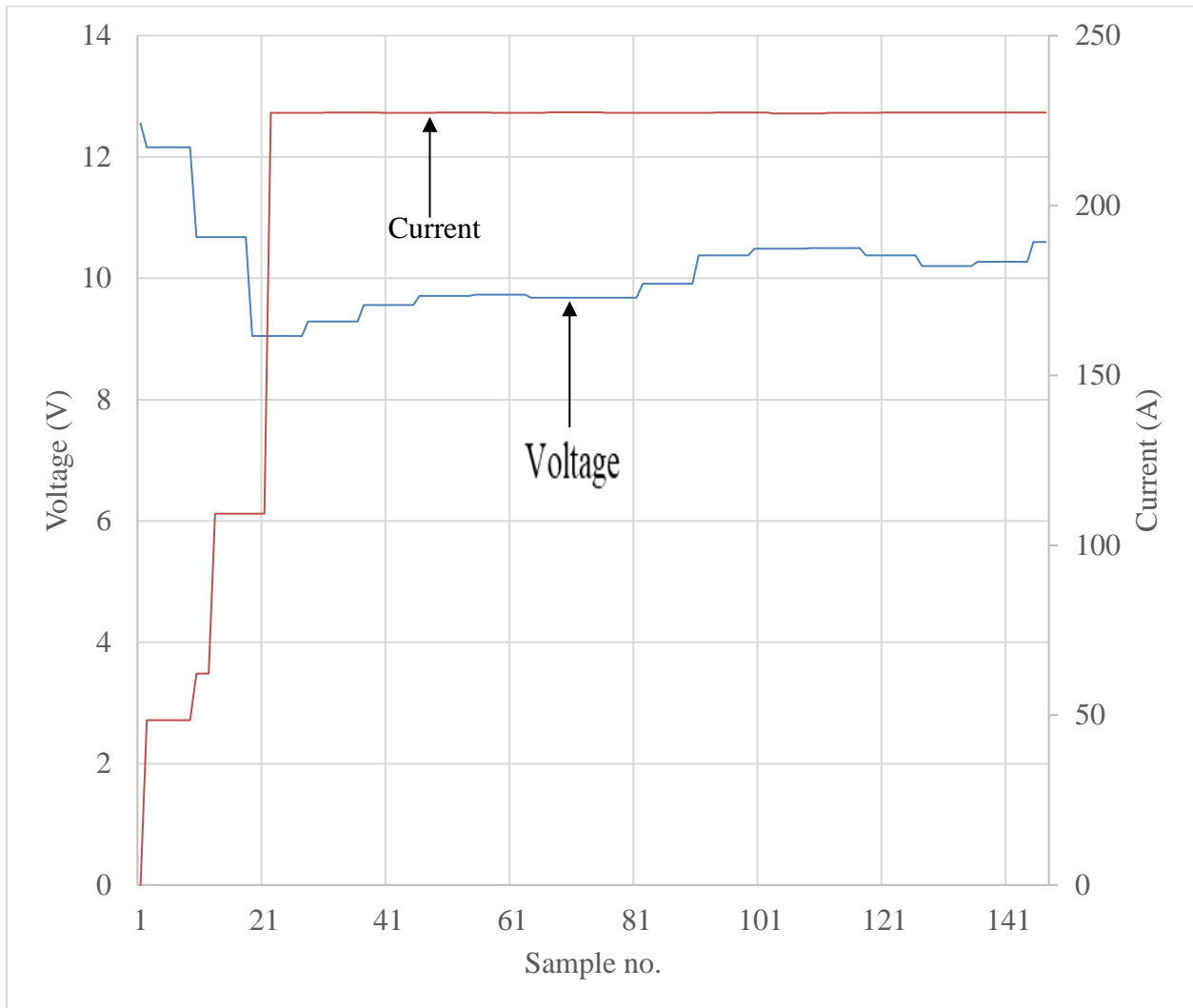


Figure 5.6: The current - voltage characteristics of the 100 Ah Unistar battery for C# 11

Based on Figure 5.6, the voltage dropped from a V_{oc} of 12.55 V to 12.16 V then to the lowest value of 9.05 V at which point the current increased sharply from 109.28 A to 227.30 A. The current was initially at 0.01 A just before the cranking request was made. This observation based on the first 21 samples of V – I logs represents the point at which enough current for cranking was drawn by the load and so from this point onwards, the voltage begins rising from the lowest value of 9.05 V to 10.68 V. After the first 21 samples of V – I, the current stays almost constant between 227.14 A and 227.44 A as is shown by the nearly straight line representing the current. This trend of the

battery voltage dropping to a low value when a load is applied to it and then eventually increasing after delivering enough current to crank the load was also observed by Larry Juang (Juang, 2010).

5.2 Field Test using the BMS and the car

5.2.1 Voltage, current and temperature display

The voltage, current and temperature sensor output logs of the BMS when installed in the car were derived using Equation 5.3, Equation 5.5 and Equation 5.8 respectively.

5.2.2 Combined V, I and T Analysis

The combined voltage, current and temperature logs from the current, voltage and temperature sensors are shown in Table 5.7 on page 69.

Table 5.7: The combined V, I and T logs for a single cranking event in the 125 Hp engine

Current (A) ± 1.15 A	Voltage (V) ± 0.82 V	Temperature (°C) ± 1.14 °C
41.55	12.62	34.55
135.90	12.41	34.55
286.13	11.37	34.55
286.33	11.25	34.55
286.20	11.23	34.55
286.20	11.21	34.55
286.85	11.20	34.55
286.20	11.20	34.55
286.13	11.17	34.55
286.40	11.16	34.55
286.53	11.16	34.55
286.20	11.15	34.55
286.33	11.13	34.55
286.20	11.11	34.55
286.28	11.10	34.55
286.20	11.09	34.55
286.20	11.09	34.55
286.28	11.09	34.55
286.20	11.08	34.55
286.20	11.07	34.55
286.40	11.07	34.55
286.20	11.07	34.55
286.40	11.06	34.55
286.20	11.06	34.55
286.20	11.04	34.55
286.40	10.99	34.55
286.20	10.99	34.55
286.45	10.98	34.55
286.73	10.98	34.55
286.53	10.97	34.55
286.40	10.94	34.55
286.28	10.93	34.55
286.45	10.91	34.55

Table 5.7 shows the logs from the current, voltage and temperature sensors of the BMS which was installed in the car with a 125 Hp engine. The logs were taken during one cranking event that lasted

for 0.5 ± 0.01 seconds. The temperature of the battery was constant within the cranking period whereas the voltage dropped from 12.62 V to 10.91 V when the load, the car starter, was engaged. The voltage drop was caused by the large current of 286.55 A being drawn by the starter for cranking the car. The fully computed data for 21 cranking events in the 125 Hp engine using the 100 Ah Unistar battery are shown in Table 5.8.

Table 5.8: A sample of the data for 21 cranking events in the 125 Hp engine

Crank number	BMS V_{oc} (V) ± 1.51 V	Voltage loss (V) ± 0.01 V	SoC (%) ± 0.01 %	Battery temperature ($^{\circ}$ C) ± 1.15 $^{\circ}$ C	Cranking duration ± 0.01 s	SoH (%) ± 0.01 %
1	12.51	0.07	83.27	23.31	0.65	100
2	12.31	0.03	58.47	23.31	0.66	100
3	12.31	0.33	58.47	23.31	0.67	100
4	12.25	0.04	52.11	23.31	0.74	100
5	12.26	0.77	52.72	23.31	0.75	100
6	12.23	0.00	49.82	23.31	0.59	100
7	12.25	0.12	51.99	23.31	0.73	100
8	12.25	0.09	51.99	23.31	0.65	100
9	12.25	0.73	51.99	23.31	0.67	100
10	12.21	0.95	44.77	25.37	0.85	100
11	12.21	1.05	46.45	23.37	0.77	95.40
12	12.29	1.18	56.29	23.31	0.79	82.46
13	12.36	7.44	64.91	23.31	0.98	0
14	12.20	5.65	44.78	23.31	0.87	0
15	12.15	2.74	38.07	23.37	0.90	0
16	12.14	11.3	37.23	23.37	1.03	0
17	12.52	3.41	84.75	23.37	1.09	0
18	12.36	5.56	64.91	23.37	0.84	0
19	12.23	3.83	49.82	23.37	0.80	0
20	12.26	7.13	52.71	23.37	0.89	0
21	12.26	6.92	52.71	23.37	2.56	0

From Table 5.8, the initial V_{oc} was 12.51 V with a SoC of 83.27 % and following each cranking event there was an associated V_{loss} . As the V_{loss} increased, it took a longer time to crank the engine as can be seen from the cranking duration logs. The SoH was 100 % on the first 10 cranks in which the battery cranked the engine successfully as well as on C# 11 and C# 12. From C# 13 to C# 21, the battery failed to crank the engine because the V_{loss} was between 2.74 V and 11.30 V which was

much higher than $V_{\text{loss th}}$ of 1.5V. The battery was also not charging fully since the cranking events were carried out while the car was in a stationary position. The car used was drawing a current of 280 A on each cranking event and this also led to the battery failing to crank. TFT screen display for C# 10 appeared as shown in Figure 5.7.

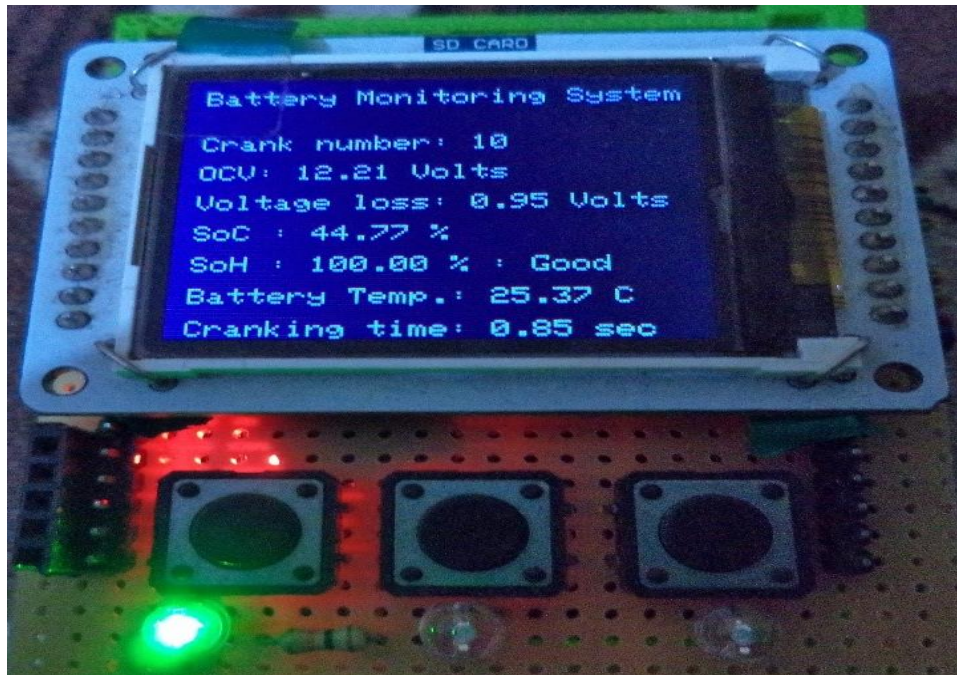


Figure 5.7: TFT display of C# 10 for the 125 Hp engine car using the 100 Ah Unistar battery

The variation of the V and I values during the cranking event are shown in Figure 5.8 on page 72.

Figure 5.8 represents 495 V - I logs based on C# 10, of Table 5.5, for the 100 Ah Unistar battery installed in the car with the 125 Hp engine.

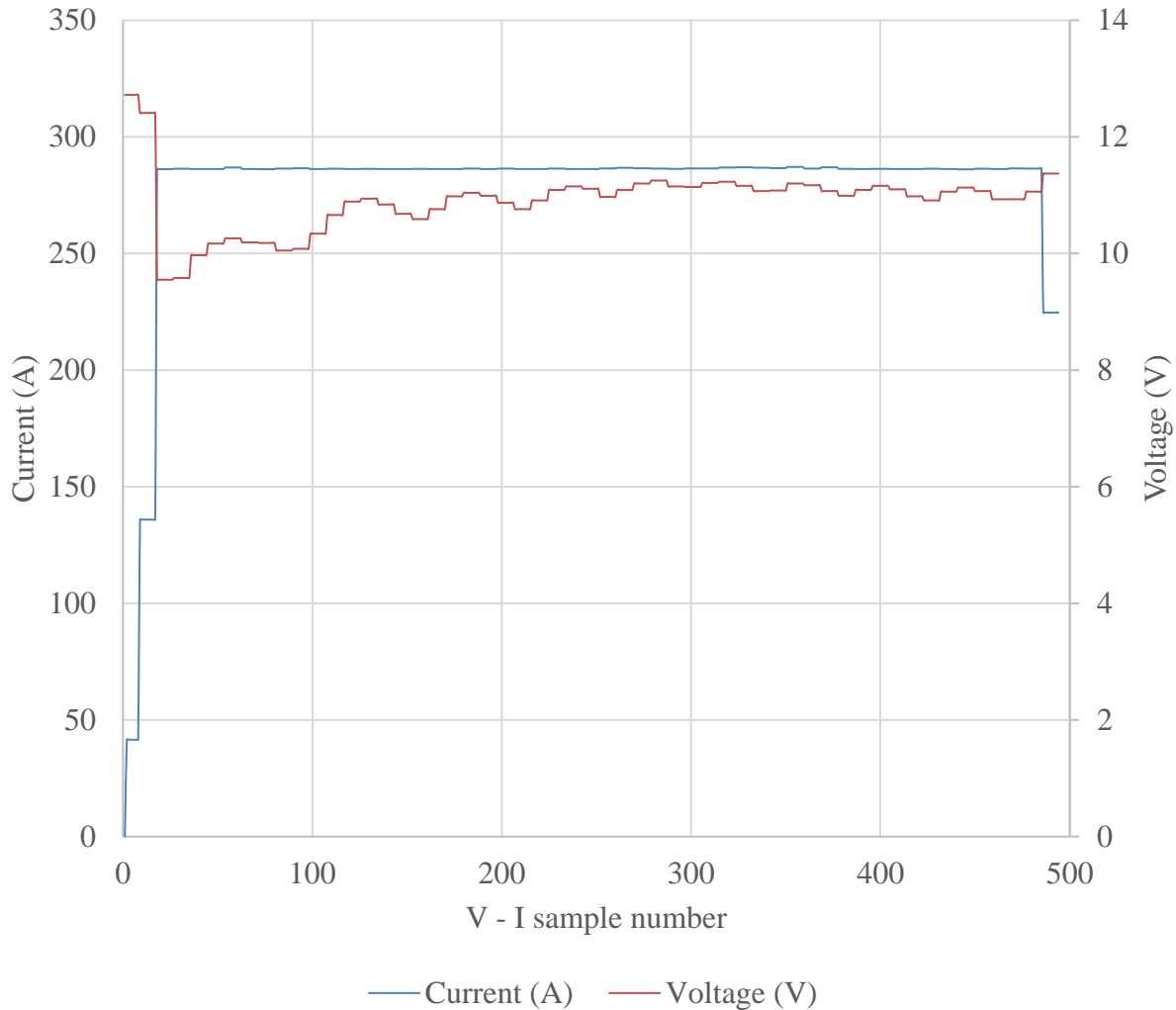


Figure 5.8: The current - voltage characteristics of the 100Ah Unistar battery in the 125 Hp engine for C# 10

From Figure 5.8, the voltage of the battery just before cranking was 12.62 V while the current was zero. When a cranking event was initiated, the voltage dropped to a low of 9.55 V and a current drawn increased within a very short time from 0 - 286.2 A on the 18 sample of V - I. At this point, of 9.55 V and 286.2 A, the greatest torque was produced by the starter motor sufficient for successful cranking of the 125 Hp engine. Thereafter, the voltage began increasing while the current fluctuated between 286.08 A and 287.10 A then dropped to 224.88 A as the cranking event came to an end. The fluctuations in current are caused by the dynamics of fuel injection and

combustion in the engine cylinders. The V- I trend during engine cranking are consistent with those of Moseley *et al.*, (2017) in their work on lead acid batteries for future automobiles.

5.3 Laboratory V, I and T Test Analysis for the BMS

5.3.1 The 110 Ah Land Rover Varta battery

Figure 5.9 shows the cranking data for the brand-new 110 Ah Land Rover Varta battery.

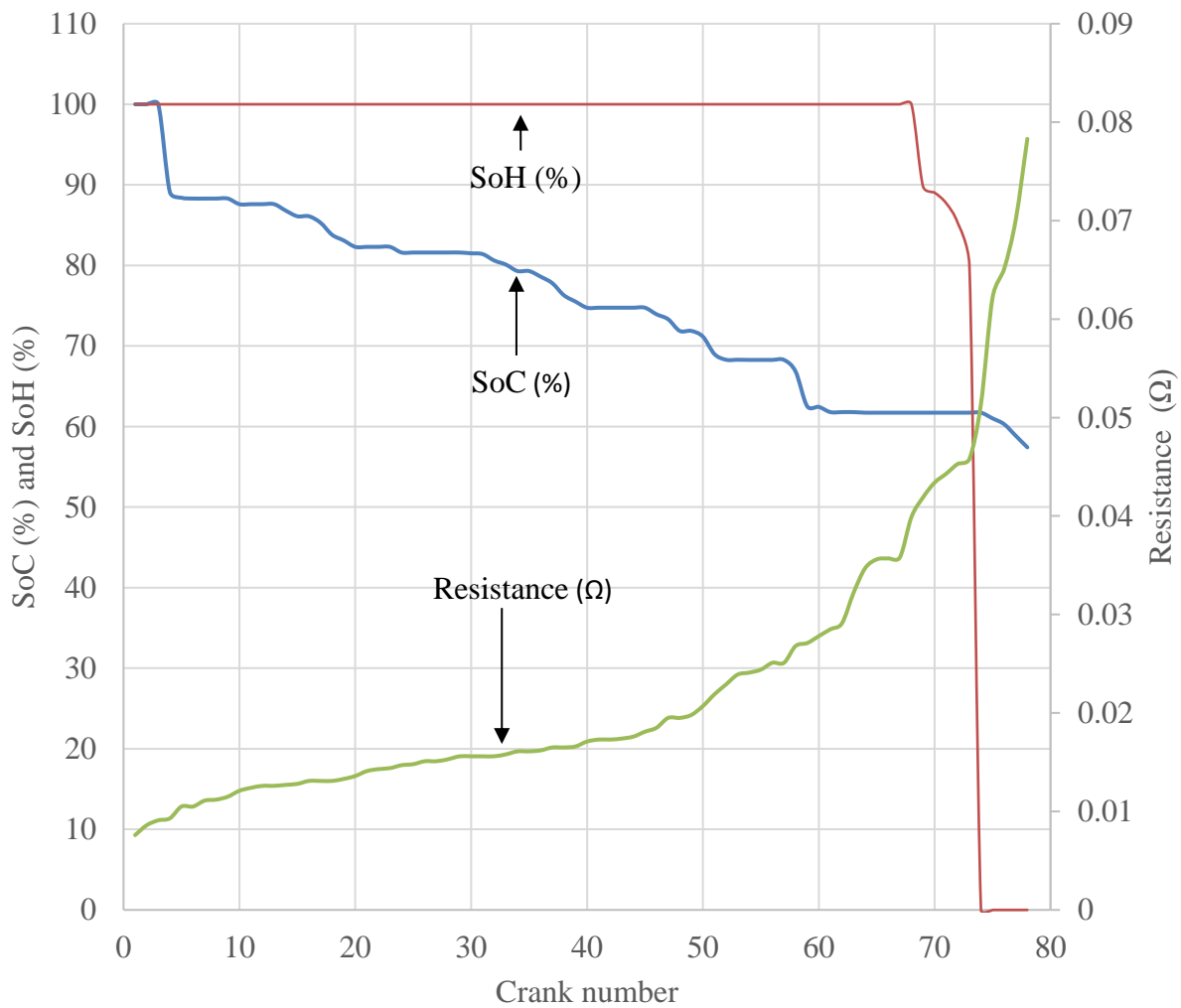


Figure 5.9: The 78 cranking events at sequential intervals of 10 cranks in 40 minutes for the brand new 110 Ah Land Rover Varta battery in the laboratory

Figure 5.9 shows 78 cranks with each crank taking an average cranking time of 10 seconds. The SoH was 100 % for the first 68 cranks but thereafter, it began reducing and finally dropped to zero on C# 74 to C# 78. The SoH was sustained at 100 % regardless of the subsequent reduction in SoC because this battery was brand new and so the cumulative effects of resistance and other forms of battery deterioration had not begun. On C# 70, the SoH began reducing non-linearly with the reducing SoC. The SoC between C# 69 and C# 73 were constant at 61.72 %, but the SoH was reducing because at this point, the V_{loss} values were increasing and consequently lowering the SoH.

The range of resistance for the whole cranking period was between 0.0076 Ω - 0.0783 Ω . At the point where the SoH began reducing, the resistance was 0.0514 Ω while the SoC was 61.72 %. The time interval between the cranks was between 5 -10 minutes to allow the BLT to cool down since its temperature kept rising with each crank. Besides the increase in V_{loss} , the resistance was also increasing with the number of cranks. As more current was being drawn, the movement of electrons in the battery causes an increase in temperature and consequently the resistance. High resistance causes the battery to heat up and the voltage to drop under load.

This trend of reduction in SoC and SoH of the battery whenever a battery is discharging was also deduced by Rezvanizani and other researchers, (Rezvanizani *et al.*, 2014), who were doing a similar research on advances in SLI battery health monitoring and prognostics for vehicles safety and mobility. The TFT display for C# 9 and C# 73 are shown in Figures 5.10 and Figure 5.11 respectively.

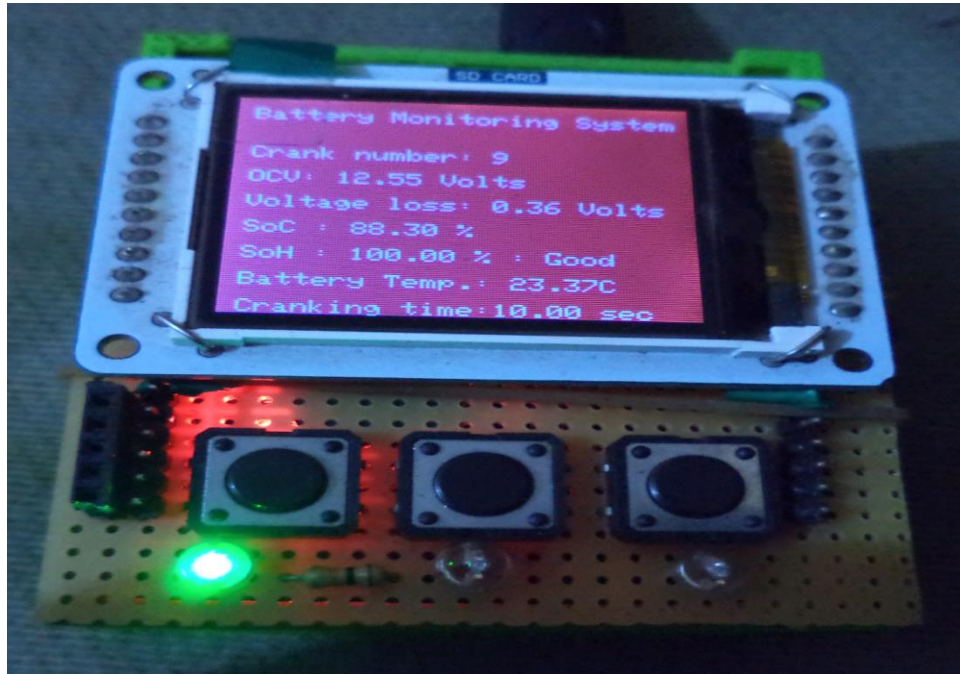


Figure 5.10: The TFT display for C# 9 for the brand new 110 Ah Land Rover Varta battery

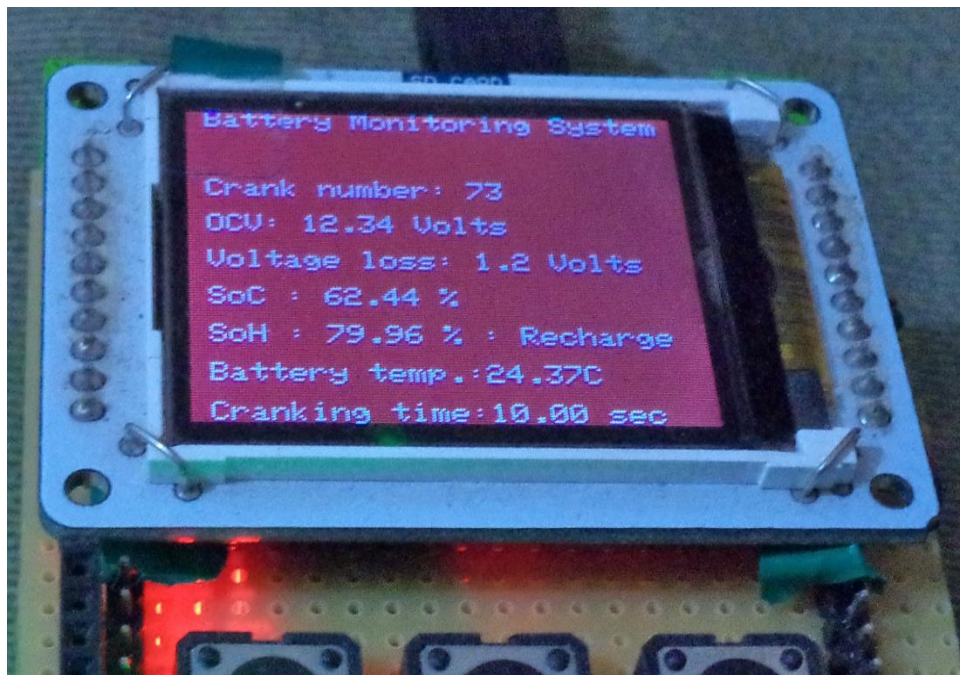


Figure 5.11: The TFT display for C# 73 for the brand new 110 Ah Land Rover Varta battery

The summarized SoH indication for the Land Rover Varta battery in the laboratory is shown in Table 5.9;

Table 5.9: The summary of the SoH and SoC of the 110 Ah Land Rover Varta battery

C#	1 - 68	69	70	71	72	73	74 - 78
SoH (%)	100	89.79	89.03	87.71	85.24	79.96	0
SoC (%)	100 – 61.72	61.72	61.72	61.72	61.72	61.72	61.72

From Table 5.9, the new battery sustained a SoH of 100 % for many cranks, 68 in this case, each lasting 10s in which a current of 300 A was drawn from the battery. This implies that the V_{loss} associated with a new battery is small and so it can deliver the electrical power for a longer period before deterioration sets in. From C# 69 to C# 73, a brand-new battery having a low SoC can have a SoH that is above threshold if the V_{loss} associated with cranking is below threshold. The V_{loss} increased C# 70 leading to the SoH dropping to 0 %, thus the battery could not deliver enough power for cranking from this point onwards.

5.3.2 The 75 Ah Chloride Exide Battery

Figure 5.12 shows the cranking data for the brand-new 75 Ah Chloride Exide battery.

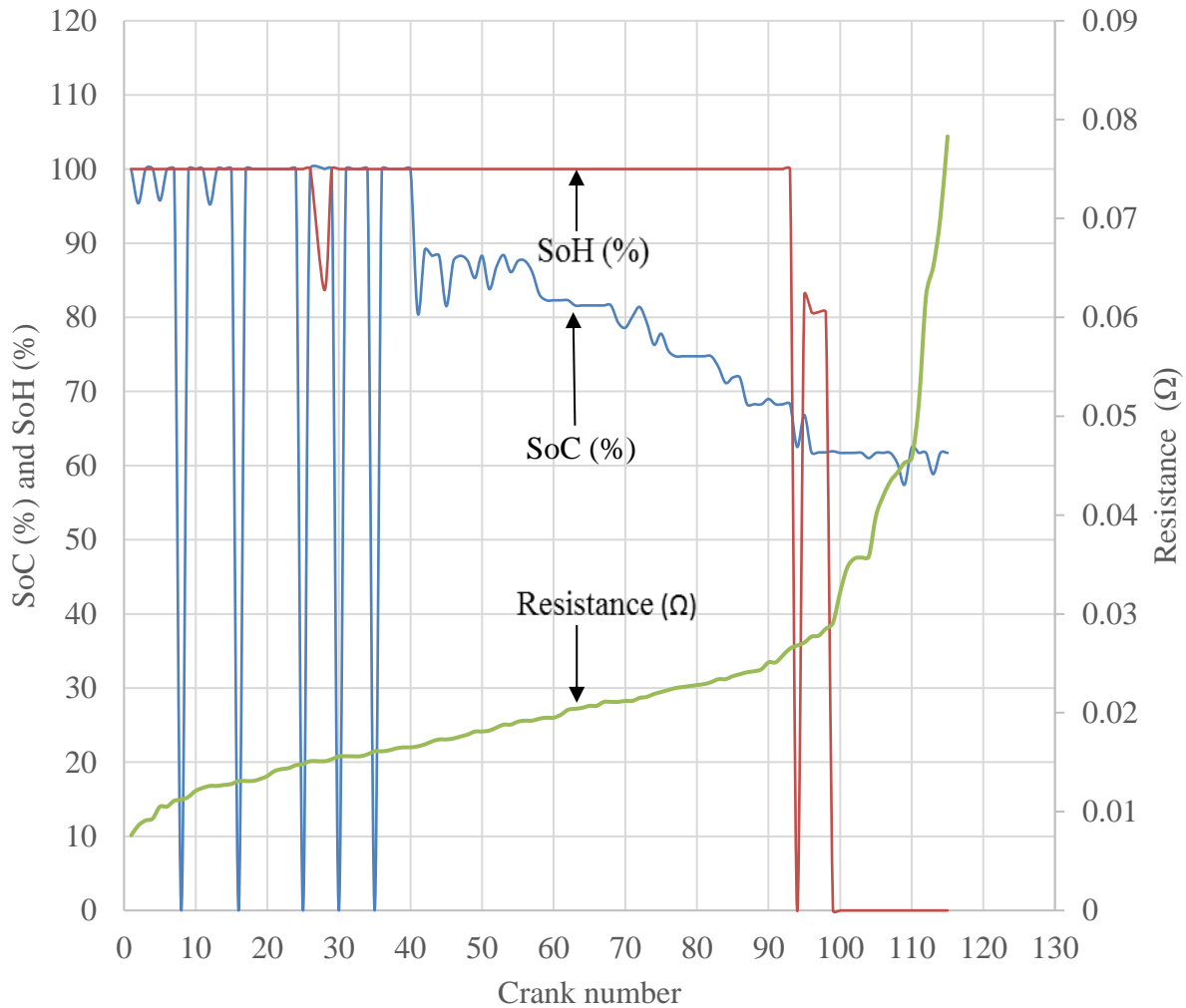


Figure 5.12: The SoC and SoH for the brand-new Chloride Exide battery in the laboratory

From Figure 5.12, the SoH of the Chloride Exide battery was 100 % from the C# 1 up to C# 93, apart from the C# 28 which was 83.67 %. On C# 94, the SoH dropped to zero due to a higher V_{loss} , however the next four cranks reached the SoH threshold of 80 % and thereafter, the SoH dropped to 0 % for the next 17 cranks. The battery was not charging and once the stored energy was used up the SoC decreased.

The SoC was between 95 % to 100 % for the first 40 cranks apart from the C# 8, C# 16, C# 25, C# 30 and C# 35 in which it fell to 0%. For these cranks, the temperature sensor erroneously read the temperature as -127 °C and from it's manufacturer, this error occurs when the power supply to the sensor is interrupted by transient voltage. This value can therefore be ignored using the program code or by resetting the BMS using the reset button. The resistance of the battery for C# 8, C# 16, C# 25, C# 30 and C# 35 were 0.0112 Ω , 0.0131 Ω , 0.0148 Ω , 0.0156 Ω and 0.0161 Ω respectively. The SoC reading of 0 % did not hinder successful cranking during these cranks and the preceding cranks as can be seen in Figure 5.12. The values of the preceding resistance are low as compared to other values of resistance, e.g 0.0291 Ω on C# 99 at which cranking failure occurred. This implies that high resistance diminishes cranking ability. The SoC between C# 41 and C# 59 decreased and then increased severally because the time interval between the cranks was 15 minutes and so the battery was able to recover part of its lost voltage. This battery recovered again on C# 72, C# 75 and C# 94, however the SoC kept reducing with each crank and eventually failed to crank when it reached 61.93 % at C# 99. The resistance of the battery was between 0.0076 Ω and 0.0783 Ω corresponding to 100 % and 0% SoH respectively.

The TFT display for C# 48 and C# 114 are shown in Figures 5.13 and Figure 5.14 respectively.

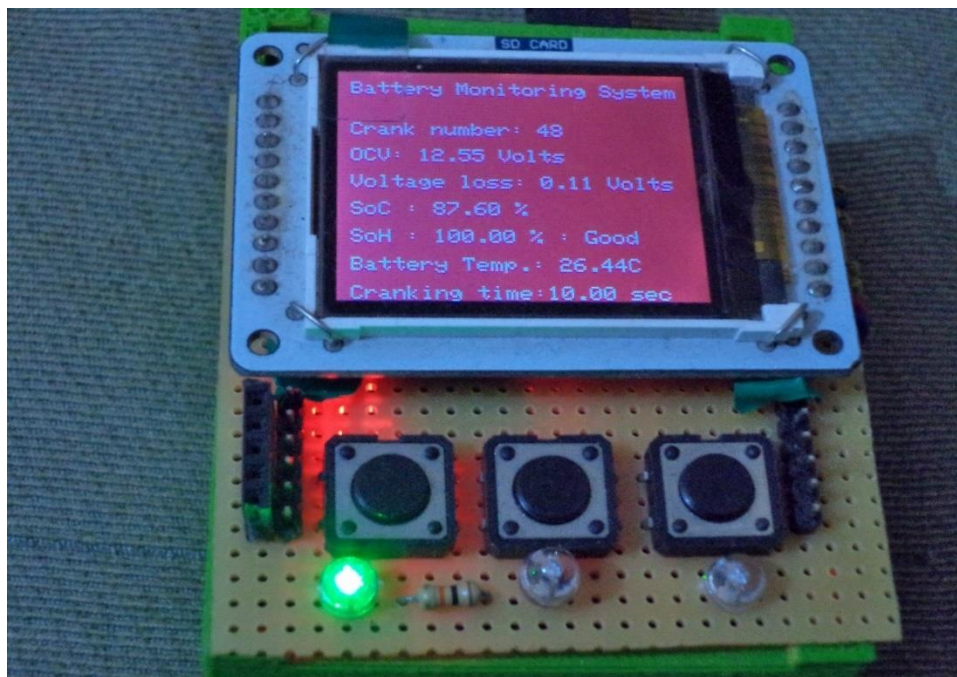


Figure 5.13: The TFT display for C# 48 for the brand new 75 Ah Chloride Exide battery

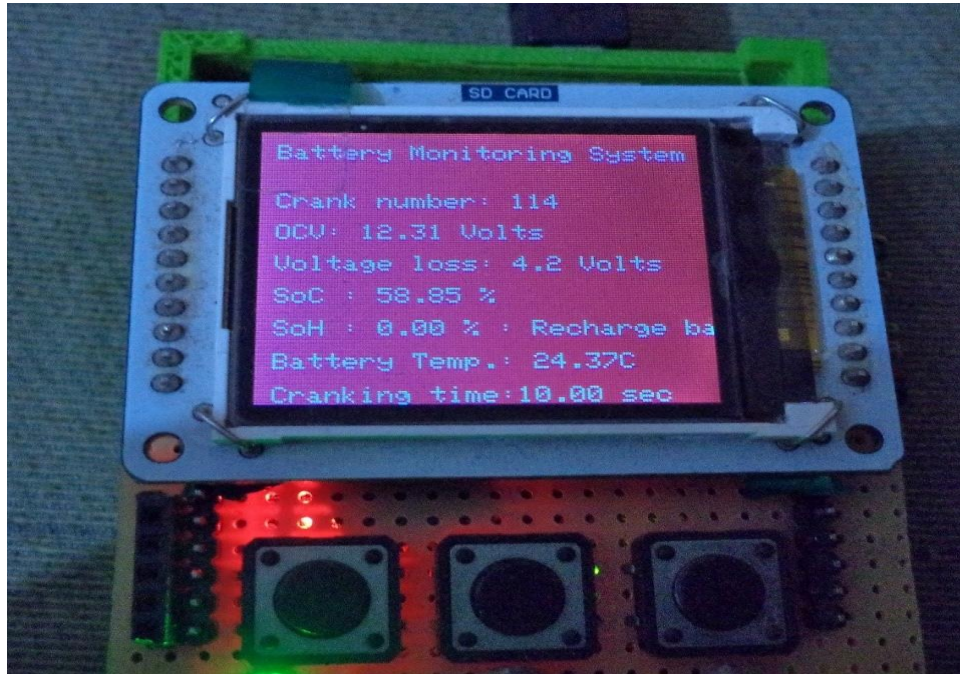


Figure 5.14: The TFT display for C# 114 for the brand new 75 Ah Chloride Exide battery

The summarized SoH and SoC indication for the Chloride Exide battery is shown in Table 5.10.

Table 5.10: The summary of the SoH and SoC of the 75 Ah Chloride Exide battery

C#	1 - 93	94	95 – 98	99 – 115
SoH (%)	100	0	80.70 – 83.02	0
SoC (%)	100 – 68.27	62.52	66.83 – 61.79	61.93 – 61.72

From Table 5.10, the battery cranked successful on the first 93 cranks since the battery was new. The V_{loss} was more than $V_{loss_{th}}$ on C# 94 thereby causing the SoH to be 0%. This battery was not being charged and so the voltage kept on reducing with each crank. Between C# 94 and C# 95, the battery was left to rest for a while during which time its chemical activities slowed down leading to recovery of SoC from 62.52 % to 66.83 %. During C# 99 to C#115, the SoC had reduced and so V_{loss} during cranking increased causing the SoH to be 0%. The SoC was 0 % on C# 8, C# 16, C#2 5, C# 30 and C# 35 as well.

5.3.3 The 110 Ah Yuasa battery

Figure 5.15 shows the cranking data for the 110 Ah Yuasa battery in the laboratory.

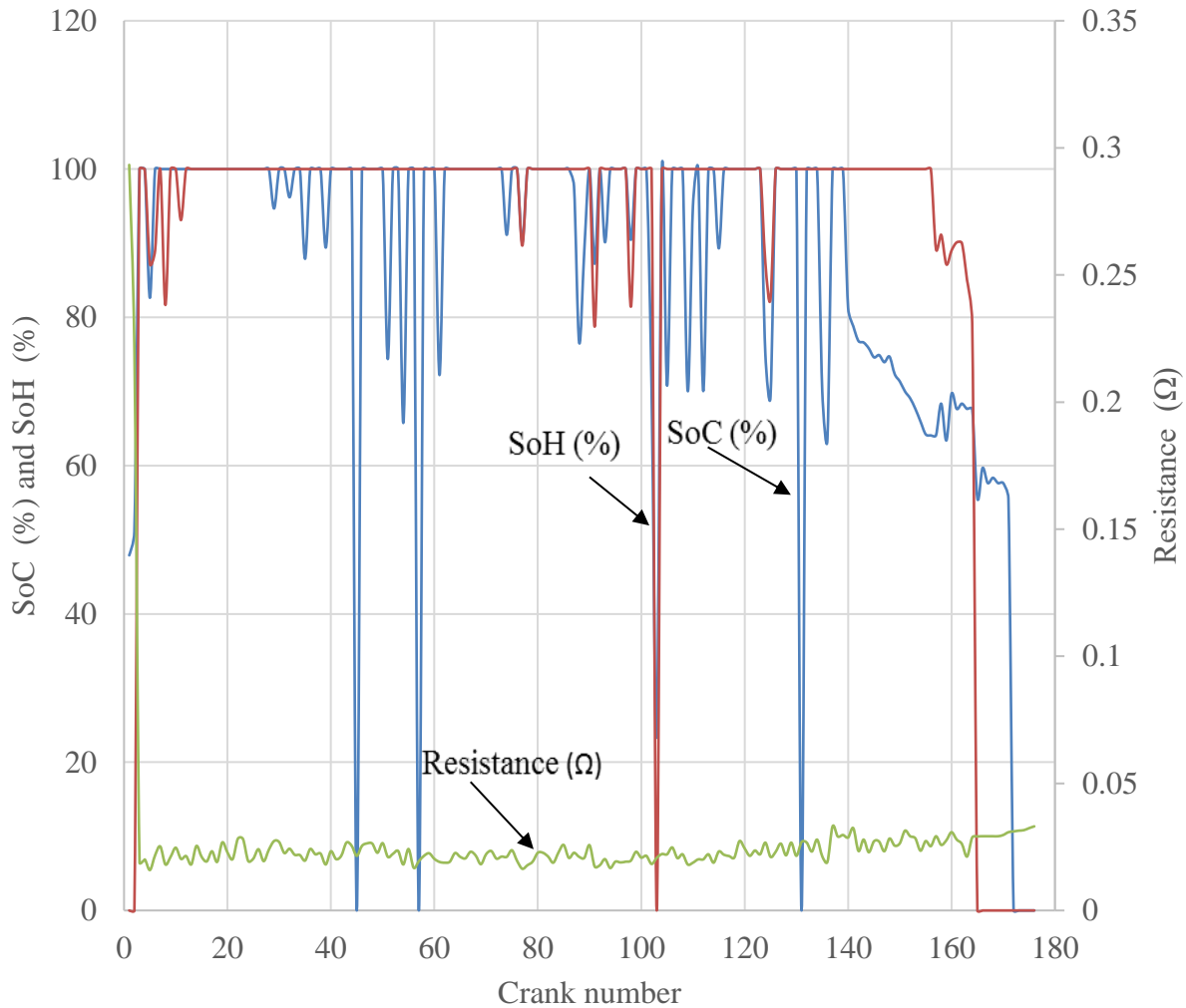


Figure 5.15: The SoH and SoC against crank number for the 110 Ah Yuasa battery in the laboratory

The resistance of the Yuasa battery for the first two cranks was 0.2933Ω and 0.2211Ω while the SoH was 0 % in both cases as shown in Figure 5.12. This was caused by a loose connection of the battery clips to the battery terminals but once tightened, the SoC and SoH readings rose to 100 % on C# 3. The overall resistance of the battery increased by a factor of 4.0×10^{-5} which was deduced from the trendline of the resistance. From the C# 3 to C# 102, the SoC and SoH were above their threshold values of 71 % and 80 % respectively. On the C# 45, C# 57 and C# 131, the SoC was 0

% whereas the SoH was 100 % due to the temperature sensor reading -127 °C. From C# 140, the SoC began reducing until it finally got to 0 % on C# 172 and remained so until C# 176. The SoH began reducing from C# 157 where the resistance was 0.0279 Ω and on reaching C# 165 where the resistance was 0.0291 Ω, it dropped to 0 % and remained so until C# 176. TFT display for C# 54 is shown in Figure 5.16.

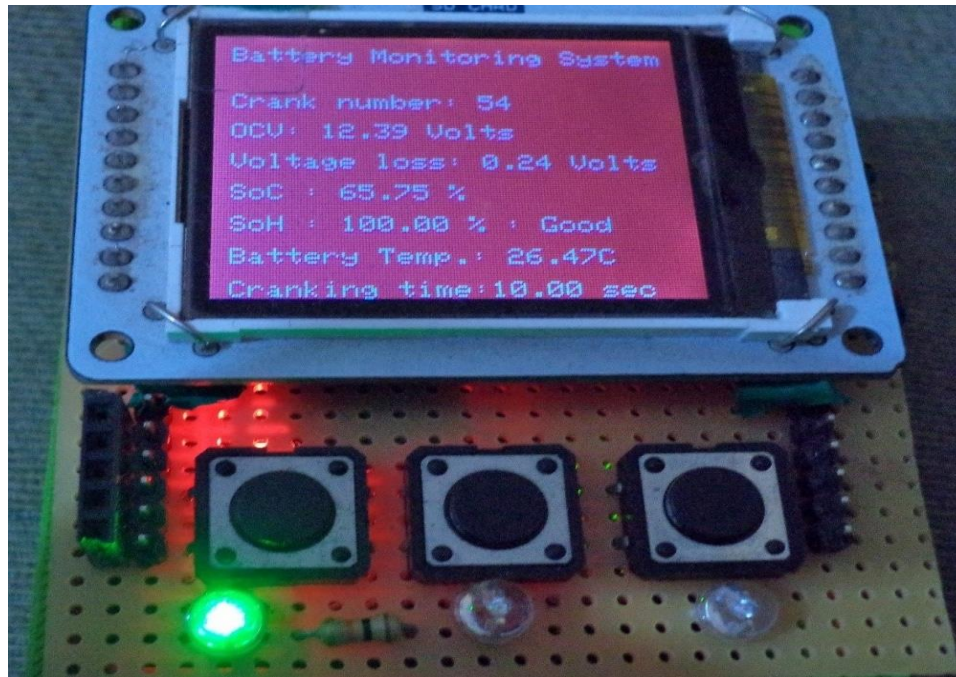


Figure 5.16: The TFT display for C# 54 for the 110 Ah Yuasa battery

The summarized SoH and SoC indication for the Yuasa battery is shown in Table 5.11.

Table 5.11: The summary of the SoH and SoC of the 110 Ah Yuasa battery

C#	1 - 2	3 - 102	103	104 - 156	157 - 164	165 - 176
SoH (%)	0	78.74 - 100	0	82.50 - 100	79.21 - 91.14	0
SoC (%)	47.90 - 51.10	65.75 - 100	23.67	63.59 - 100	64.09 - 67.64	0 - 59.68

From Table 5.11, the SoH was 0 % on the first two cranks because of a loose battery terminal and so cranking was unsuccessful. The SoC for C# 45, C# 57 and C# 131 were 0 % because the temperature sensor read -127 °C due to a voltage spike in the car's electrical system. The other cranks between C# 3 and C# 156 successful cranking was realized. From C# 157, the chemical energy in the battery reduced non-linearly until it got to 0 %.

5.3.4 The 100 Ah Unistar Battery

Figure 5.17 shows the cranking data for the 110 Ah Unistar battery in the laboratory.

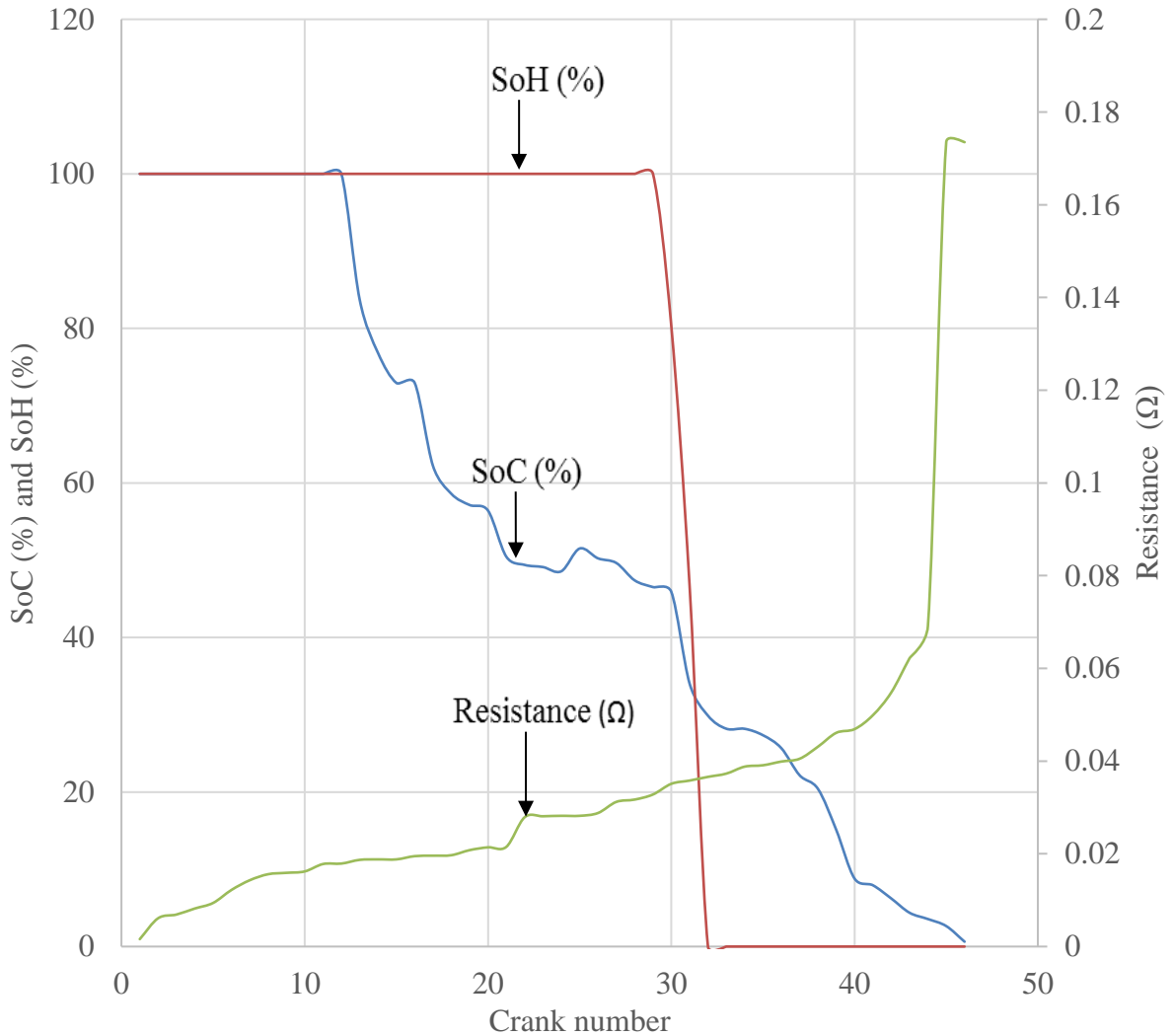


Figure 5.17: The cranking data for the 110 Ah Unistar battery in the laboratory

The SoC and SoH for the Unistar battery were both 100 % up until C# 12 and thereafter, the SoC started reducing. The SoH remained at 100 % until C# 29 and on C# 30, it dropped to 80.33 %. At the cranking failure point, that is C# 31, the SoC was 34.02 %, SoH was 46.62 °C and the resistance 0.0358 Ω. The range of resistance for the 47 cranking events was between 0.0016 Ω and 0.1735 Ω. The SoC_{th} , 71 %, was reached at C# 16 and so the battery should have been charged at this point before proceeding with more cranking events but since the current being drawn from this battery

was between 100 A and 120 A, the SoH was above threshold. There were 15 more successful cranks after the SoC_{th} value had been reached as can be seen from the corresponding SoH values reading 100 %.

The TFT display for C# 2, C# 31 and C# 45 are shown in Figure 5.18, Figure 5.19 and Figure 5.20 respectively.

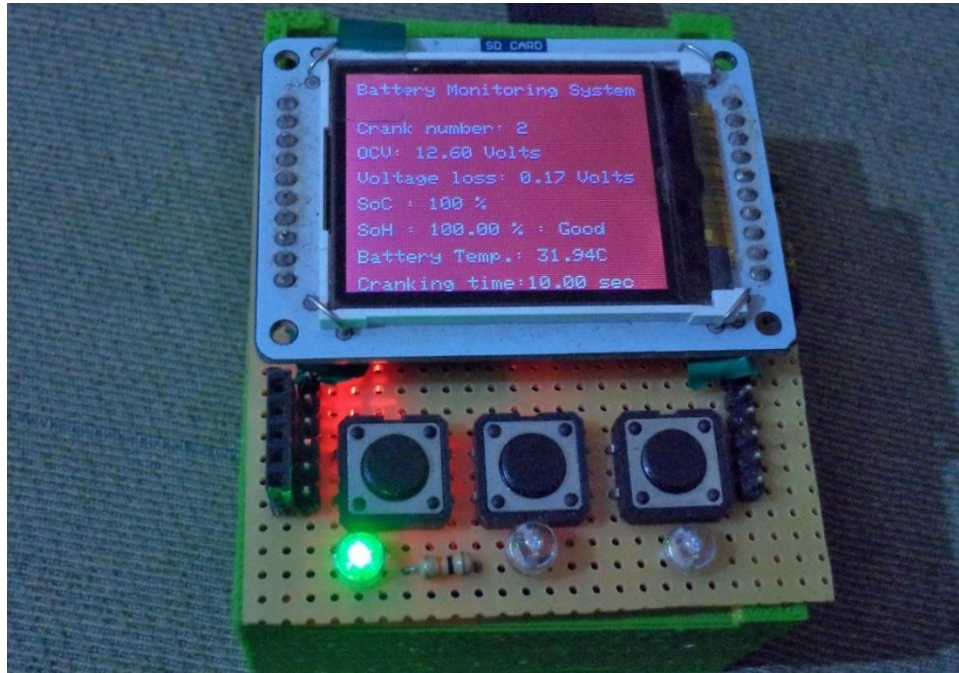


Figure 5.18: The TFT display for C# 2 for the 100 Ah Unistar battery

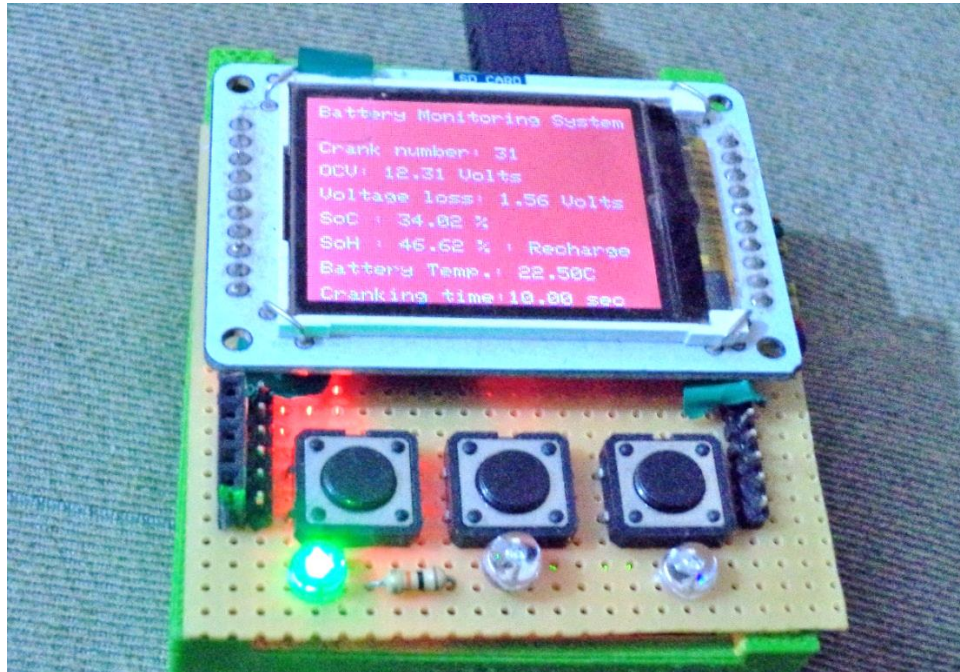


Figure 5.19: The TFT display for C# 31 for the 100 Ah Unistar battery

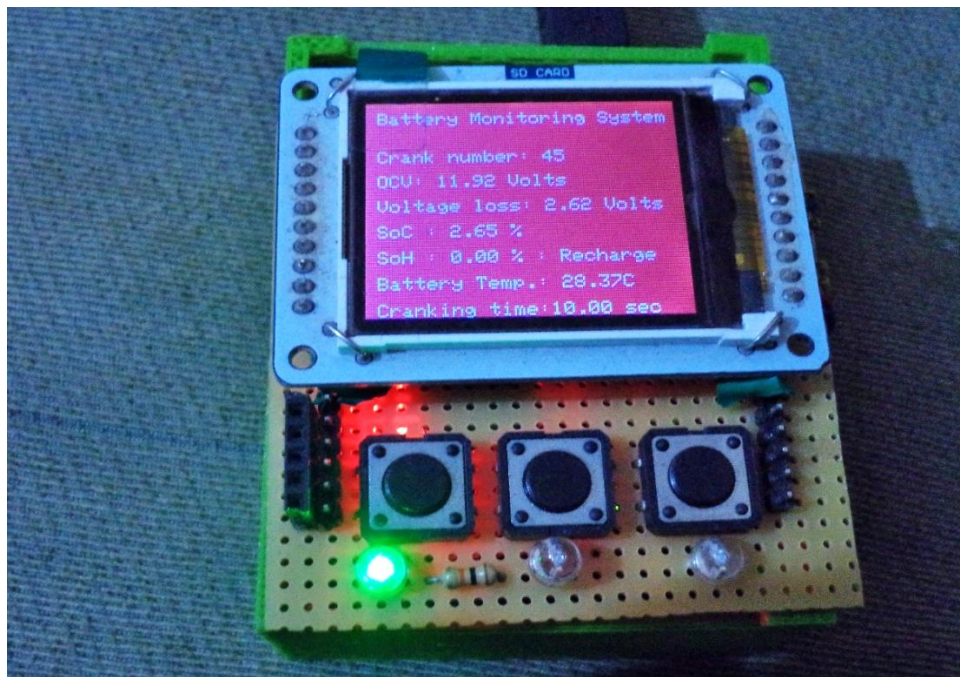


Figure 5.20: The TFT display for C# 45 for the 100 Ah Unistar battery

The summarized SoH and SoC indication for the Unistar battery is shown in Table 5.12.

Table 5.12: The summary of the SoH and SoC of the 100 Ah Unistar battery

C#	1-12	13 - 29	30	35-46	32 - 46
SoH (%)	100	100	80.33	46.62	0
SoC (%)	100	36.52 - 83.69	35.91	34.02	0.63 – 29.88

From Table 5.12, the battery cranked successfully on the first 30 cranks after which it failed. The battery was 2 years old and so its health had deteriorated such that it failed after 30 cranking events otherwise the SoC should have stayed above threshold for more than the recorded 16 cranks before decreasing. The battery cranked successfully with the SoC being below the SoC threshold of 71% which implies that the threshold value can be lower than the recommended 75 %. This finding was also proved to be true by Cadex Inc. (Buchman, 2016) who use the SoC_{th} of 60 % in their Spectro™ CA-12 battery load tester battery equipment.

5.3.5 The 75 Ah moll m3 plus K2 battery

Figure 5.21 shows the cranking data for the moll m3 plus K2 battery.

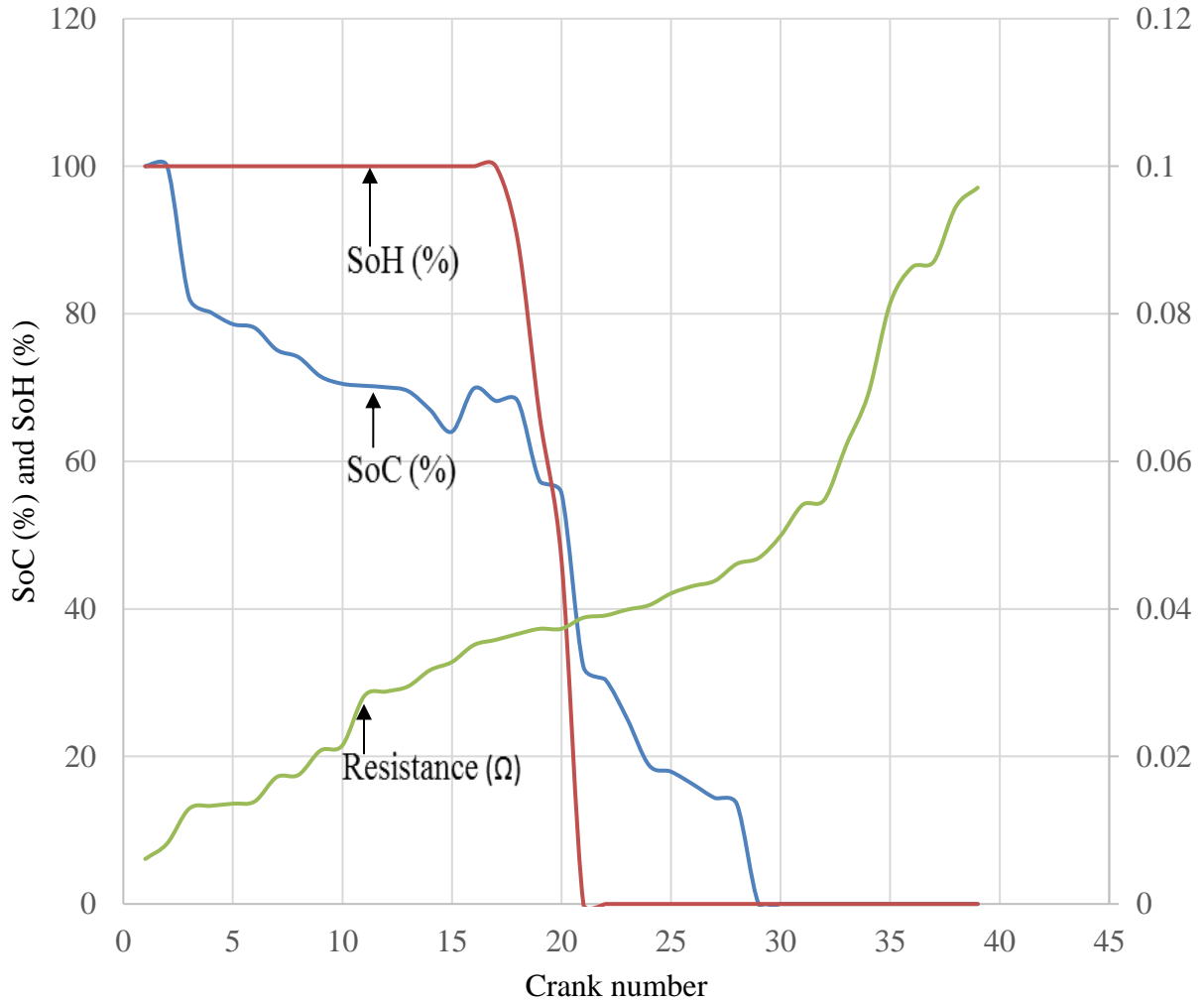


Figure 5.21: The cranking data for the 75 Ah moll m3 plus k2 battery in the laboratory

The SoH of the moll m3 plus k2 battery was 100 % for the first 17 cranks and thereafter it fell to 90.01 %, 66.16 %, 46.42 % and then to 0 % on C# 21 to C# 39. The SoC was 100 % for the first two cranks then it fell below the SoC_{th} and kept reducing till it got to 0 % at C# 29 and the next 10 cranks as well. With the SoC below the 71 % threshold, the SoH was above the 80 % threshold for 15 more cranks thus affirming that the SoC_{th} can be lower than the standard 75 % and successful cranking still be realised. The resistance was between 0.0061 Ω and 0.0971 Ω for all the 39

cranking events. At the point where the SoH fell below threshold, the resistance was 0.0372Ω while the SoC was 55.68 %. The SoH dropped from 90.01 % on C# 18 to 60 % on C# 19 then 46.62 % on C# 21 and thereafter to 0 % for the next 19 cranks.

The summarized SoH and SoC indication for the moll m3 plus K2 plus battery in the laboratory is shown in Table 5.13.

Table 5.13: Summary of the SoH and SoC of the 75 Ah moll m3 plus K2 plus battery

C#	1 – 2	3 – 17	18 – 20	21 - 28	29
SoH (%)	100	100	90.01 – 46.62	13.17 – 32.17	0
SoC (%)	100	62.02 – 82.18	55.68 – 68.18	0	0

From Table 5.13, the battery cranked successfully on the first 17 cranks with the lowest SoC being 62.02 %. This battery had been in use for 2 years and so most of the active material had deteriorated. The charge retention capacity had reduced considerably and so, that it failed after only 20 cranks and its behavior became unpredictable thereafter.

5.4 Field results from the BMS in the car

5.4.1 The 80 Hp engine

The cranking data for the moll m3 plus k2 battery installed in the 80 Hp engine is shown in Figure 5.22. The current drawn during cranking as measured by the 400 A metrix MX 355 clamp meter was 120 A. The average values of the battery temperature, the V - I logs and the cranking duration were 24.81 °C, 1769 and 0.95 seconds respectively.

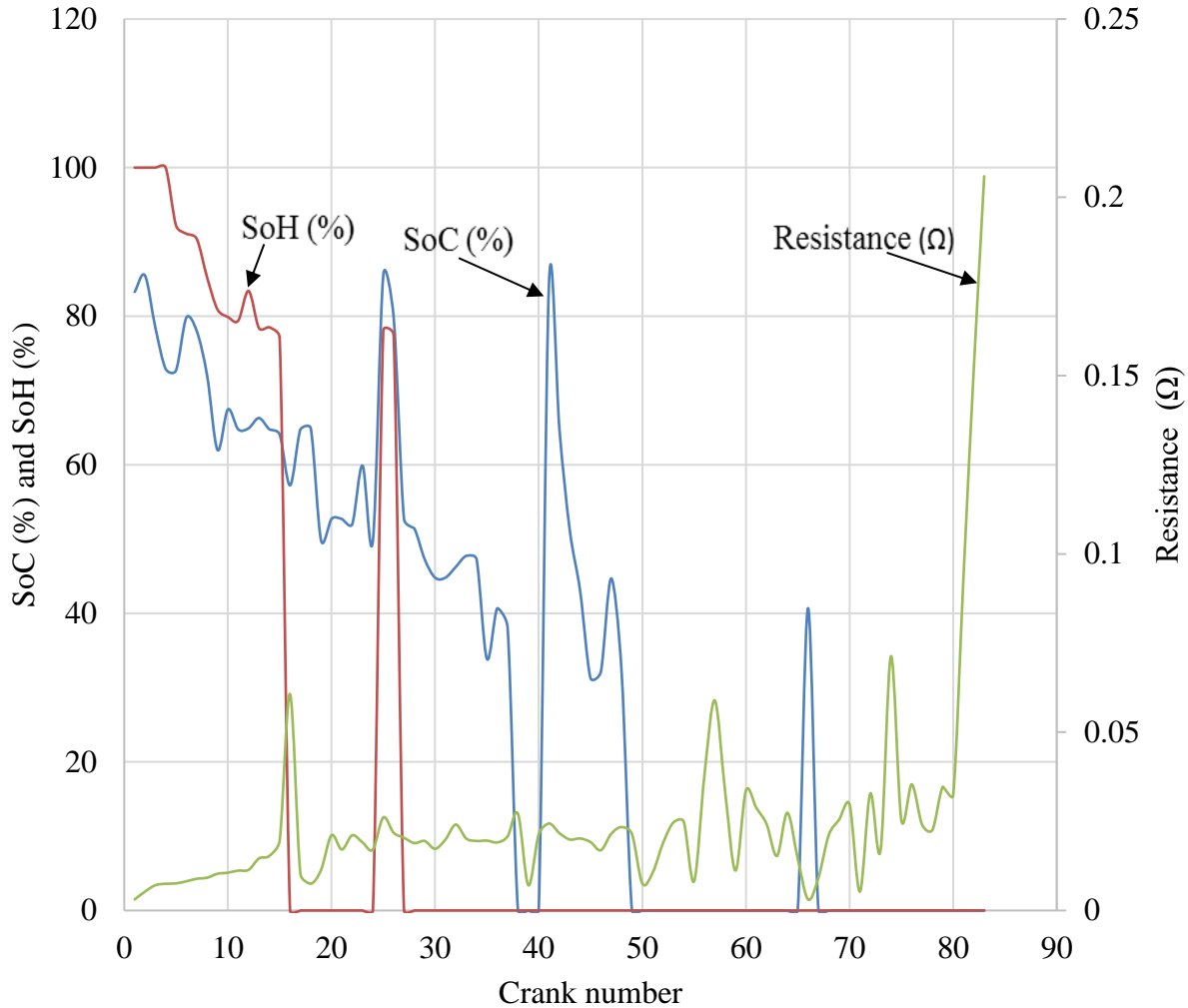


Figure 5.22: The SoC and SoH against crank number for the 75 Ah moll m3 plus K2 plus battery

From Figure 5.22, the 80 Hp engine was cranked 16 times on the first day on which it was driven for 5 km around Eastlands area in Nairobi. The battery’s SoC was between 64 % and 85 %, regardless of it being charged by the alternator implying that the ability of the battery to store charge had deteriorated. The battery was able to crank the engine on 15 occasions out of the 16 cranks with the SoH being between 77.10 % – 91.10 %. The resistance of the battery for the 15 cranks was between 0.0031 Ω – 0.0196 Ω while the temperature of the battery was 27 °C.

On the second day, the battery had a SoC of 57.23 % but was unable to crank the 80 Hp engine since its SoH was 0 %. This means that the battery had some charge but the ability to deliver this charge to the crank the engine was below threshold and so cranking was unsuccessful. A battery

can therefore be fully charged but have a SoH of 0 %, implying that the ability to deliver the required amount of charge to run a load is not sufficient. Eight more cranking attempts also failed since the SoH was 0 %. The failure to crank was due to the SoC being below threshold such that the voltage loss exceeded the voltage loss threshold of 1.5V leading to the low SoH. After C# 25, the battery was given a rest period an hour within which the SoC increased to 85.51 % on C# 26 and 79.87 % on C# 27. This behavior of the battery also confirms the findings of Prengaman, (2017), that the behavior of a failing battery becomes unpredictable when its SoH falls below 80 %. The engine cranked successfully on C# 26 and C# 27 with the corresponding resistance being 0.0261 Ω and 0.0218 Ω while the SoH was 78.10 % and 77.50 %. On C# 28, the SoC fell to 52.71 % and then kept reducing all through to C# 37 before falling to 0% on C# 38, C# 39 and C# 40. The SoH was 0 % from C# 27 to C# 40 and the battery's resistance was between 0.0204 Ω – 0.0213 Ω . Regardless of the battery being charged by the alternator, it's SoC was quite low and the SoH was 0 %. This can be attributed to a reduction in the active materials of the battery which are directly proportional to the battery's deliverable capacity as discussed by (Maria *et al.*, 2011) in section 1.1.

On the third day, the SoC had risen to 84.66 % on C# 41 but thereafter it reduced to 32.14 %, dropped to 0 %, rose to 50.75 % and after 4 more cranks, it dropped to 0 % for the last 16 cranks with the highest resistance recorded being 0.2059 Ω . This 75 Ah moll m3 plus K2 plus battery had been used for 2 years in a car and so its health had reduced considerably. When a battery starts failing, its behavior becomes unpredictable and so the voltage rise on the third day was a confirmation of this observation.

The display on the TFT screen for C# 35 representing the failed cranks appeared as shown in Figure 5.23 implying that the battery needed to be replaced since the SoH had fallen below the 80% threshold.

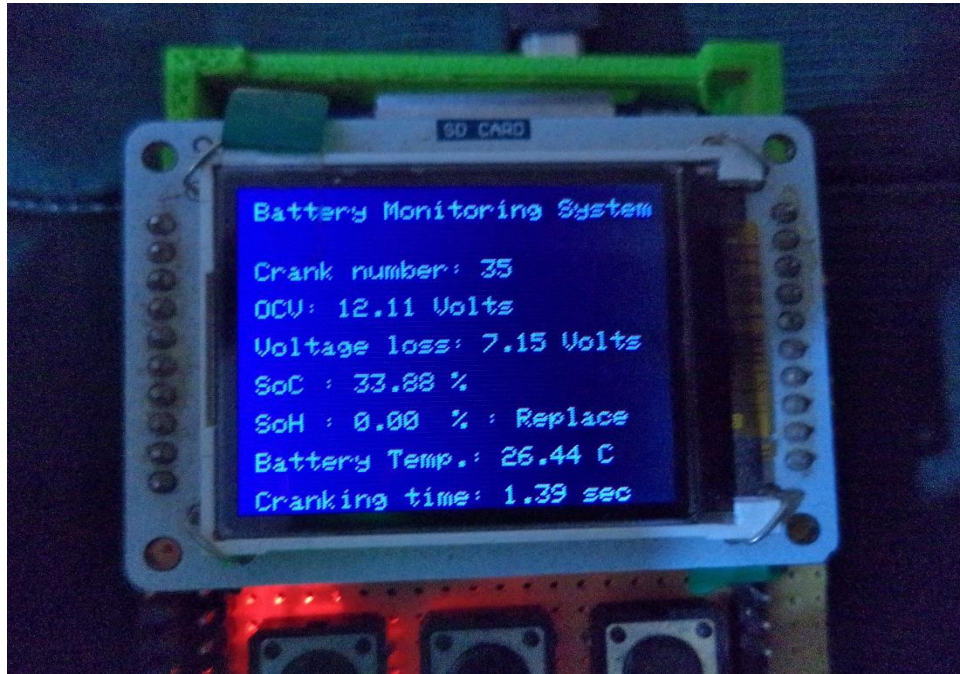


Figure 5.23: The TFT display for C# 35 for the 75 Ah moll m3 plus k2 battery in the 80 Hp engine

The summarized SoH indication for the 75 Ah moll m3 plus K2 plus battery in the 80 Hp engine is shown in Table 5.14.

Table 5.14: The summary of the SoH and SoC for the 75 Ah moll m3 plus K2 plus battery

C#	SoH (%)	SoC (%)
1 - 4	100	72.90 – 85.47
5 - 15	77.10 – 92.20	61.99 – 79.82
16 - 24	0	49.81 – 57.23
25	78.10	85.51
26	77.50	79.87
27 - 37	0	38.08 – 51.42
38 - 40	0	0
41 - 48	0	31.28 - 84.66
49 - 83	0	0

From Table 5.14, the battery was able to crank the engine on 18 cranks out of 83. The engine cranked successfully even with the SoH being below the SoC_{th} value of 80 % otherwise the battery could have been prematurely replaced. Manufactures of German luxury cars found out that

batteries returned from every 400 such cars for repairs, half of them were in good working condition (Lonnie *et al.*,2013).

The cranking data for the Yuasa battery when installed in the 80 Hp engine is displayed in Figure 5.24. The car was driven for 5 km in Nairobi within which 49 cranks were taken. The average number of V - I logs for each cranking event was 287.

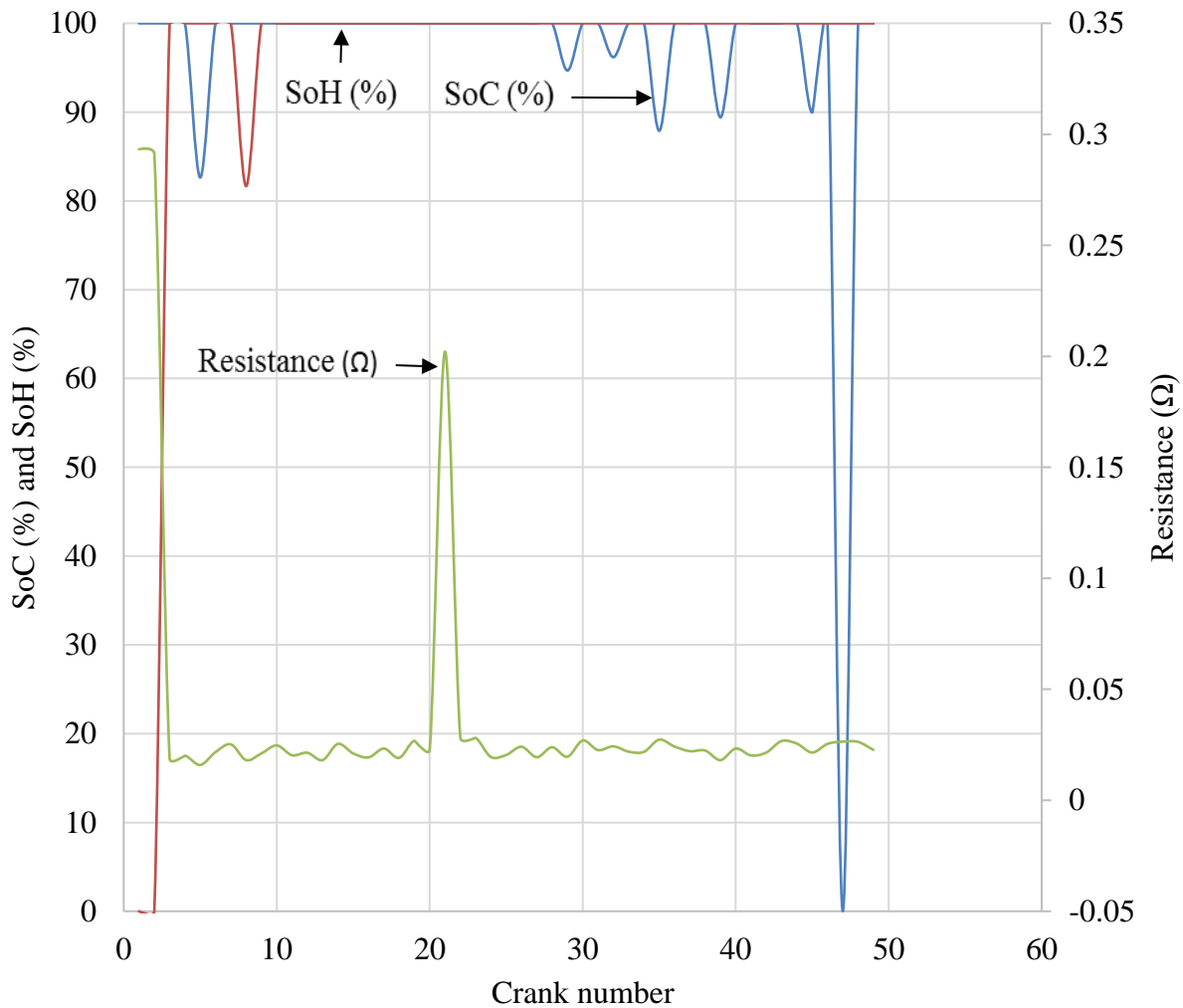


Figure 5.24: The SoC and SoH against crank number for the 110 Ah Yuasa battery in the 80 Hp car

From Figure 5.24, the SoH for C# 1 and C# 2 was 0 % with the corresponding resistance being 0.2933 Ω and 0.2911 Ω for the C# 1 and C# 2 respectively. The battery cranked the 80 Hp engine successfully on C# 3 after which the engine was revved for some time before take-off. From C# 3

to C# 49, the SoH was 100 % except for C# 8 which was 81.66 %. The SoC was 100 % from the C# 3 to C# 26 and thereafter alternated between 87.89 % and 100 %. On C# 47, the SoH was 100 % while the SoC was 0 % and the resistance was 0.0264 Ω but the battery successfully cranked the engine. The range of resistance for the 49 cranks was 0.0159 Ω - 0.2933 Ω with the highest resistance being on the C# 1 and C# 2. The cranking time for the C# 1 and C# 2 was 2 seconds for each while the average cranking time for the remaining cranks was 0.56 seconds and the battery temperature 35 °C.

The display on the TFT screen for C# 1 and C# 47 appeared as shown in Figure 5.25 and Figure 5.26 respectively.

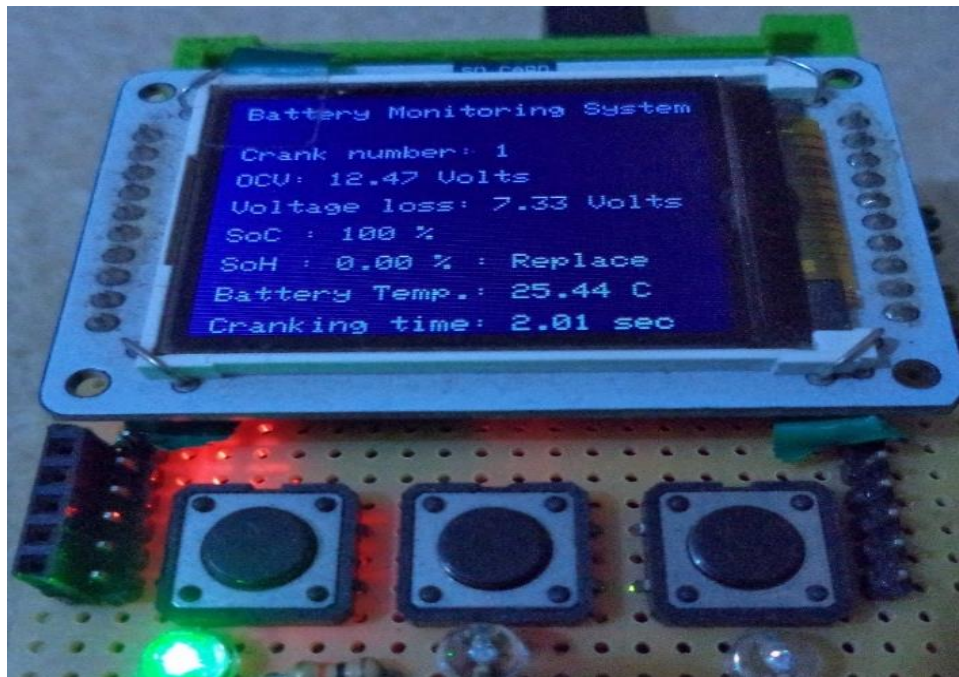


Figure 5.25: The TFT display for C# 1 for the 110 Ah Yuasa battery

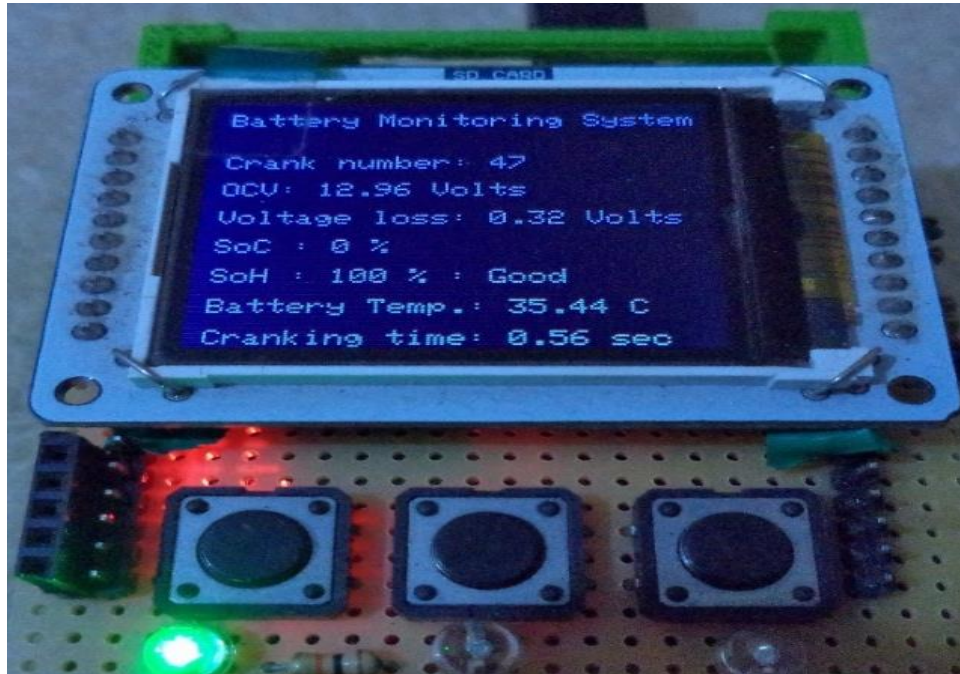


Figure 5.26: The TFT display for C# 47 for the 110 Ah Yuasa battery

The summarized SoH indication for the 110Ah Yuasa battery in the 80 Hp engine is shown in Table 5.15.

Table 5.15: The summary of the SoH and SoC for the 110 Ah Yuasa battery in the 80 Hp engine

C#	1 – 2	3 – 7	8	9 – 49
SoH (%)	0	100	81.66	100
SoC (%)	100	82.63 - 100	100	82.63 - 100

The low SoC on C# 1 and C# 2 was due to the high resistance experienced during the first 2 cranks and on C# 21 which had a resistance of 0.2021 Ω , which were quite high and outliers when compared to the rest of the resistance values. The battery was however able to crank the engine 47 times thereafter from C# 3 to C# 47.

The cranking data for the Unistar battery when installed in the 80 Hp engine is shown in Figure 5:27. The temperature of the battery was 49.45 $^{\circ}\text{C}$ on average for the two days in which it was used in the 80 Hp engine. The average V - I logs for each crank was 211.

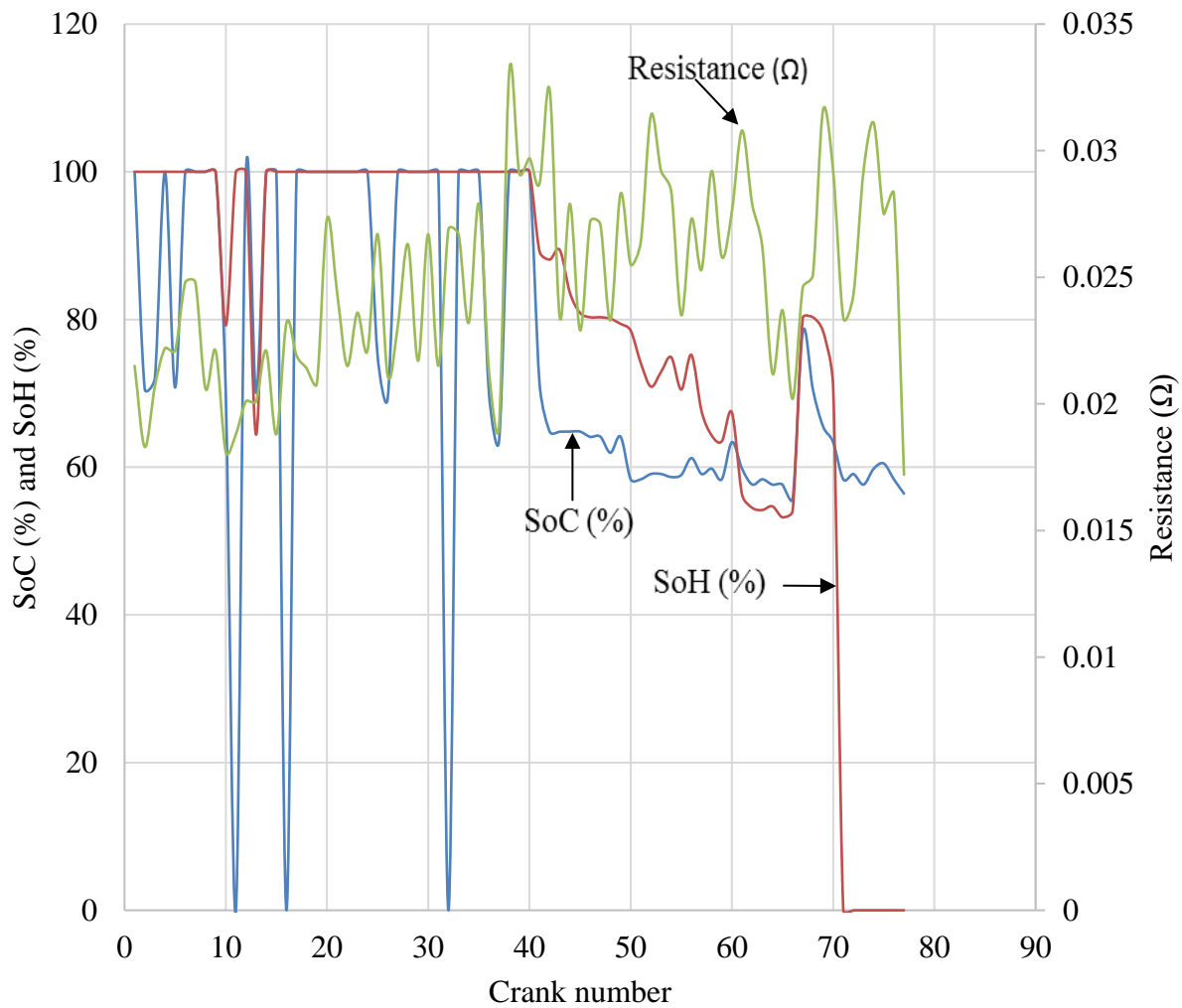


Figure 5.27: The SoC and SoH against crank number for the 100 Ah Unistar battery in the 80 Hp car

Based on Figure 5.27, there were 40 cranks on the first day in which the SoH was 100 % for all the cranks except C# 10 and C# 13 which were 79.2 % and 64.4 % respectively. The SoC was 0 % on C# 11, C# 16 and C# 32 but their SoH was 100 % and so the engine cranked successfully. The resistance for the 40 cranks ranged between 0.0181 Ω and 0.0331 Ω . The lowest SoH that was able to crank the 80 Hp engine was 64.3 % while the average cranking time was 0.59 seconds. The SoH of 64.3 % is lower than the SoH_{th} of 80 % and so according to the SoH algorithm discussed in section 3.5, this battery was supposed to be replaced.

There were 37 cranks on the second day with the SoC ranging between 50 % and 70 % while the SoH was between 53.2 % and 89.2 %. The lowest SoH that cranked the engine successfully was 64.3 % and the resistance for the 37 cranks was between 0.0172 Ω – 0.0331 Ω . The SoC fell below the SoC_{th} of 71 % on several cranks but the battery cranked the car engine successfully because of the low current draw of 120 A by the 80 Hp engine during cranking. Regardless of the charging, the SoC kept reducing while the resistance kept increasing and eventually affecting the SoH of the battery. The TFT display for C# 26 and C# 32 are shown in Figure 5.28 and Figure 5.31 respectively.

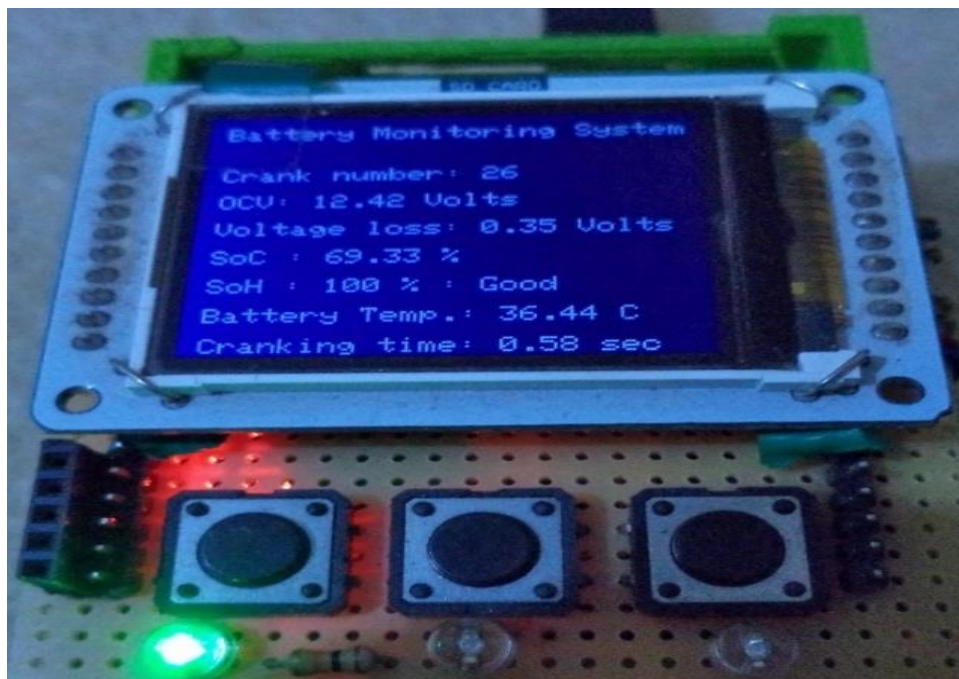


Figure 5.28: The TFT display for C# 26 for the 100 Ah Unistar battery

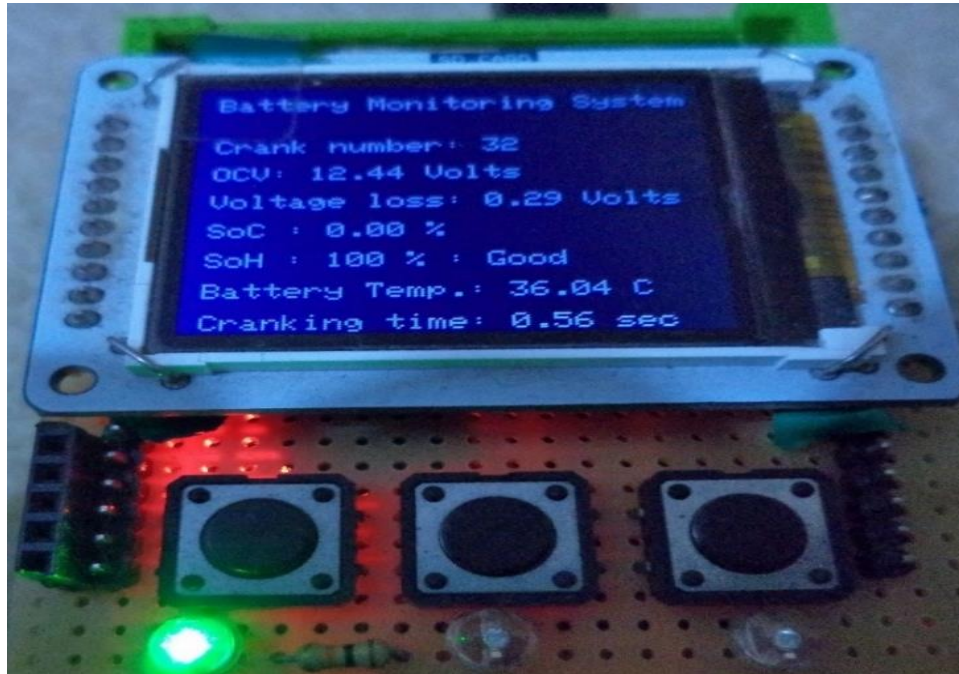


Figure 5.29: The TFT display for C# 32 for the 100 Ah Unistar battery

The summarized SoH and SoC indication for the 100 Ah Unistar battery in the 80 Hp engine is shown in Table 5.16.

Table 5.16: The summary of the SoH and SoC for the 100 Ah Unistar battery in the 80 Hp engine

C#	SoH (%)	SoC (%)
1 - 9	100	70.57 - 100
10	79.20	70.06
11 - 12	100	0 and 100
13	64.40	70.05
14 - 40	100	63.59 - 100
41 - 48	89.20 – 80.10	61.95 – 71.28
49 - 56	79.40 – 75.20	64.13 – 58.67
57 - 66	54.10 – 67.60	55.70 – 63.39
67 - 70	70.90 – 80.30	63.38 – 78.30
71 - 77	0	56.42 – 60.50

From Table 5.16, there was a total of 77 cranks using the 80 Hp engine. A loose cable connection caused the SoC to read 0 % on 3 occasions. The battery’s ability to crank the engine with a SoH of 64.3 %, C# 13, which is below the recommended 80 %, agrees with the findings of Chen and

other researchers that showed that a battery's threshold values and ultimate performance depends upon the type and specifications of application to which it is put (Chen *et al.*, 2012). From C# 71 to C# 77, the battery's ability to accept and retain the charge had gone down.

5.4.2 The 115 Hp engine

The moll m3 plus k2 battery's cranking data from the 115 Hp is shown in Figure 5.30.

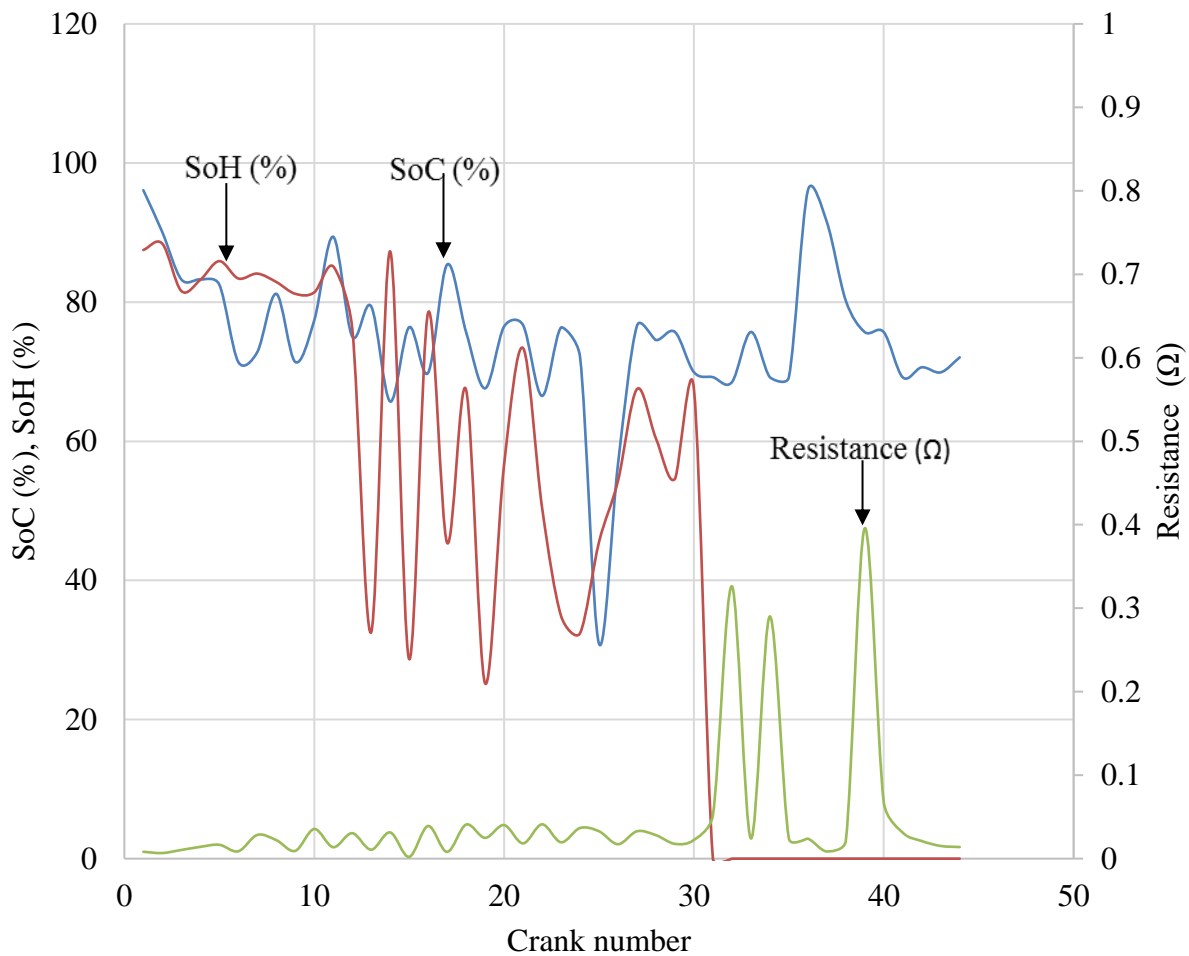


Figure 5.30: SoC and SoH against crank number for the 75 Ah moll m3 plus k2 battery in the 115 Hp car

Based on Figure 5.30, the first 10 cranks were taken over 5 km covered by the car. The battery resistance for the first 10 cranks was between 0.0082 Ω and 0.0355 Ω and on all these occasions, the engine cranked successfully. The average cranking time for each crank was 0.96 seconds which

was slightly higher compared to the average cranking time of a brand-new battery of 0.49 seconds. From C# 10 to C# 30, the battery cranked on 9 occasions and failed on 11. The average V - I logs taken was 1286 for each crank while the temperature of the battery was 26.25 °C. The lowest recorded value of SoH at which cranking was successful was 67.4 % which agrees with the findings of Chen *et al.*, (2012) that showed that a battery's performance depends on the type and specifications of the application to which it is put. The TFT display for C# 11 is shown in Figure 5.31.

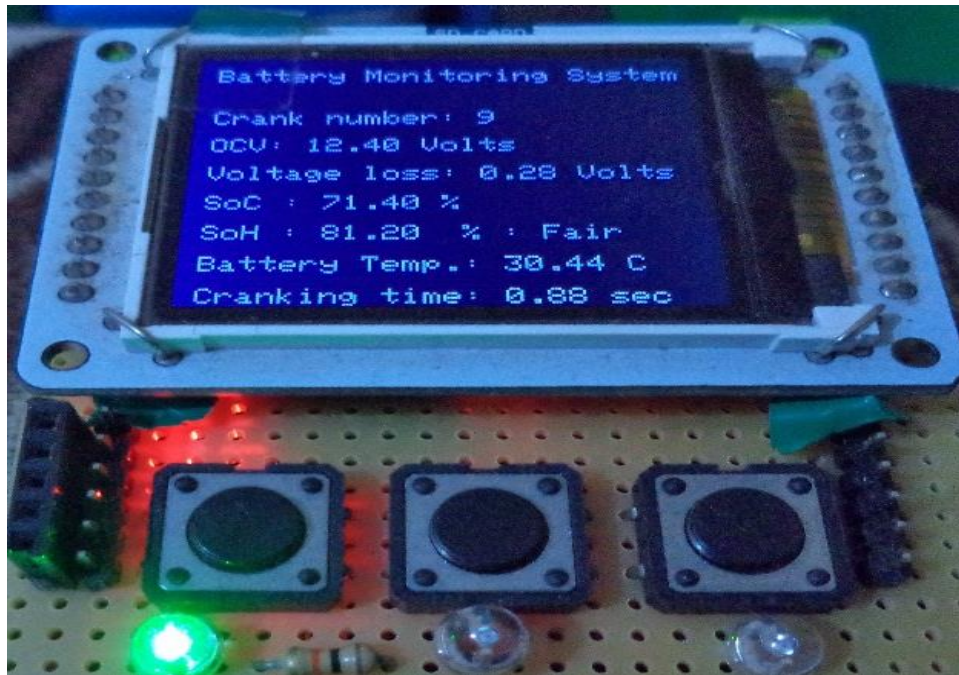


Figure 5.31: The TFT display for C# 9 for the 75 Ah moll m3 plus k2 battery in the 115 Hp engine

The summarized SoH indication for the 75 Ah moll m3 plus k2 battery in the 115 Hp engine is shown in Table 5.17.

Table 5.17: The summary of the SoH and SoC indication for the 75 Ah moll m3 plus k2 battery in the 115 Hp car

C#	1 – 10	11 – 16	17 – 30	31 – 49
SoH (%)	87.50 – 81.40	85.14 – 78.50	67.50 – 45.40	0
SoC (%)	71.40 – 96.09	65.71 – 89.40	30.90 – 85.40	68.49 – 91.52

From Table 5.17, the battery cranked the engine on the first 10 cranks. In the next 30 cranks, cranking was successful on 9 occasion with the SoC ranging between 67.40 % and 85.14 %. Since the SoC of 67.40 % was the lowest value on which cranking was possible, it implies that the SoH threshold depends on the application to which the battery is put. With the SoC being between 28.68 % and 56.60 % cranking was unsuccessful. C# 31 to C# 49 had a high SoC values but the SoH was 0 % and so cranking failed on all of them. The highest SoC among the last 18 cranks was 91.52 % but the SoH was 0 % implying that the voltage loss associated with this cranking event was higher than the V_{lossth} of 1.5 V. Whenever the V_{loss} exceeded V_{lossth} the SoH was 0 % and cranking was not successful.

The cranking data for the Unistar battery when installed in the 115 Hp is shown in Figure 5.32.

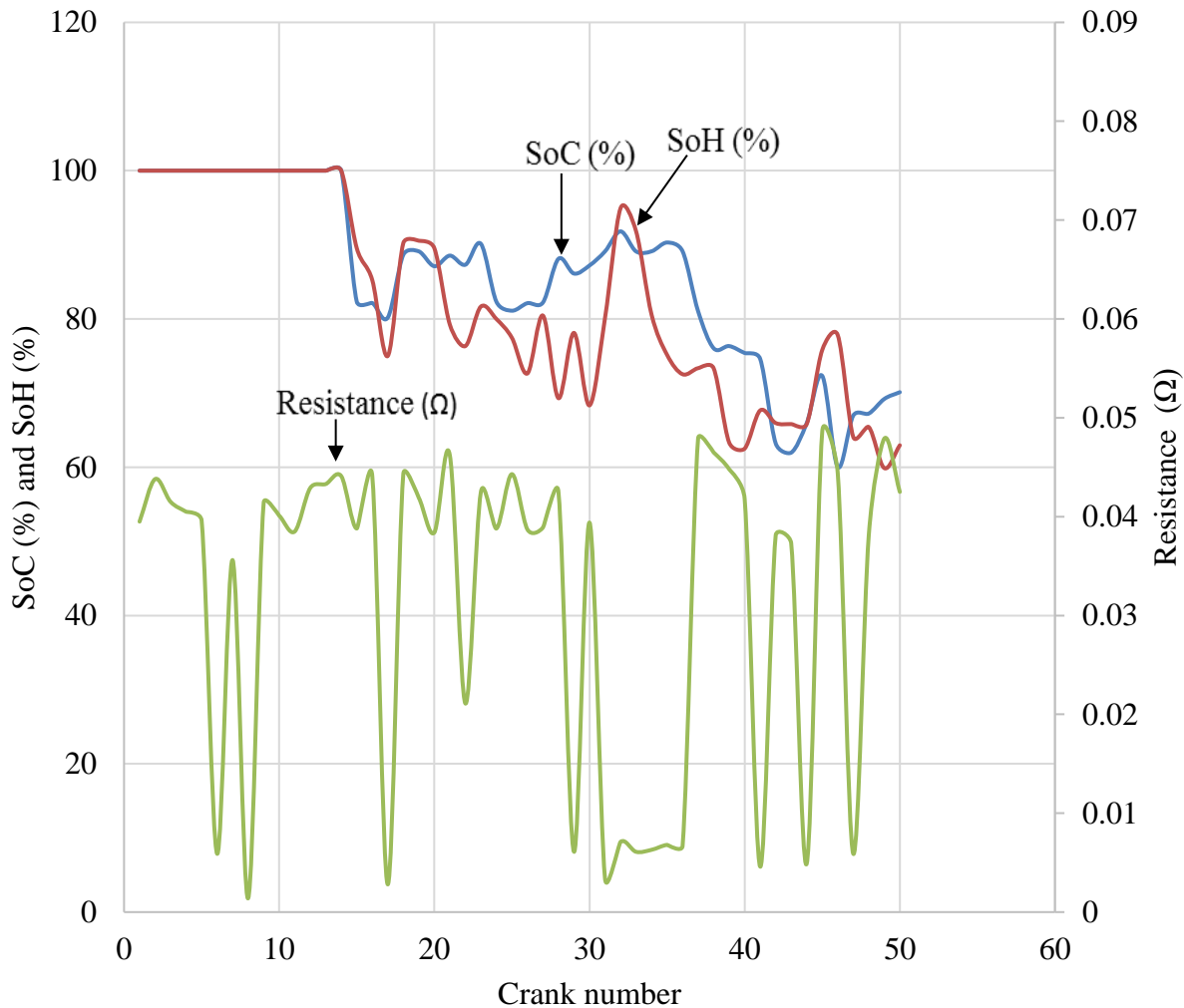


Figure 5.32: The SoC and SoH against Crank number for the 100 Ah Unistar battery in the 115 Hp car

Figure 5.32 shows the 50 cranking events using the Unistar battery installed in the 115 Hp engine. The first 25 cranks were recorded over 5 km covered by the car within Nairobi. The rest of the cranks were taken with the car in a stationary position. In the first 14 cranks, both the SoH and SoC were 100 % and the car cranked in 0.56 seconds. From C# 15 to C# 50, the cranking time increased to an average of 0.72 seconds due to reduction of the SoC and an increase in battery resistance and consequently a reduction in the SoH. The increase in battery resistance and consequent reduction in the SoC of the battery can also be used as an indicator of the SoH of the battery as this agrees with the findings of Thyagarajan *et al.*, (2014) that any battery parameter that

changes with its usage can be used to indicate its SoH. The engine cranked successfully up to the point where the SoH was 74.62 %, below which there was no cranking. The range of resistance for this battery when used in the 115 Hp engine was 0.0014 Ω – 0.0486 Ω while the temperature was 33.31 °C. The average number of V - I logs for each cranking event was 1199. The summarized SoH indication for the 100 Ah Unistar battery in the 115 Hp engine is shown in Table 5.18.

Table 5.18: The summary of the SoH and SoC indication for the 100 Ah Unistar battery in the 115 Hp engine

C#	1 – 14	15 - 37	38 - 50
SoH (%)	100	81.04 – 90.81	60.02 – 76.05
SoC (%)	100	68.34 – 94.93	59.88 – 77.82

From Table 5.18, the Unistar battery had a SoC and SoH of 100 % on C# 1 to C# 14 and was able to crank the engine. Both the SoH and SoC reduced in the next 22 cranks regardless of the battery being charged by the alternator meaning that the charge retention capacity of the battery had reduced. In the last 12 cranks, the SoC and SoH reduced further due to low charge retention capacity and short charging time since the car was stationary. The active materials of a battery usually store the charge of the battery and so when they are depleted, this ability will be lowered, an observation that was also made by (Prengaman ,2017) in their work on current collectors and active materials for the lead acid battery.

The cranking data for the Yuasa battery when installed in the 115 Hp engine is shown in Figure 5.33.

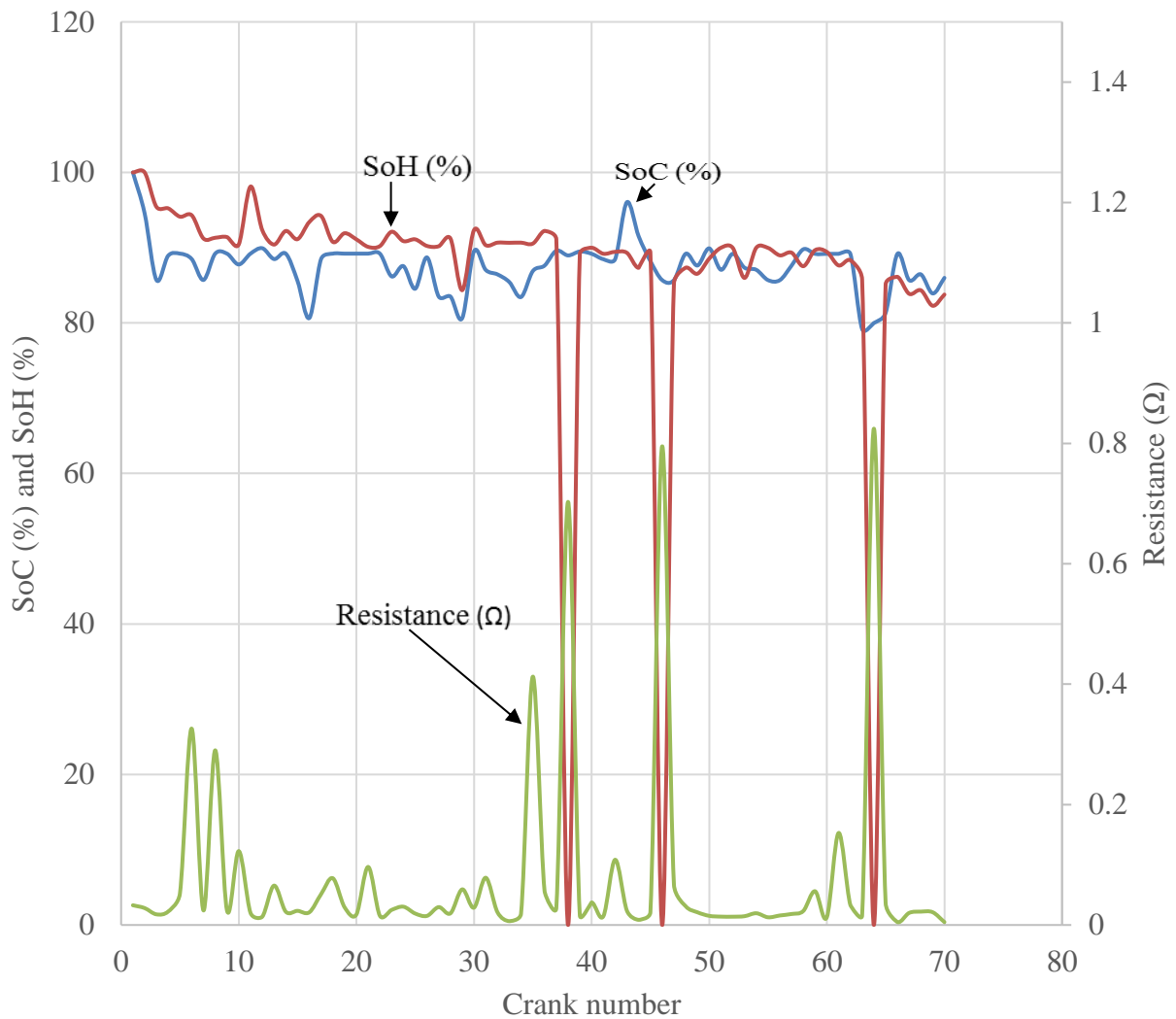


Figure 5.33: The SoC and SoH against crank number for the 110 Ah Yuasa battery in the 115 Hp engine

A total of 70 cranks was performed on the Yuasa battery in the 115 Hp engine for a period of two days. The temperature of the battery was 27.9 °C on the first day and 29.3 °C on the second day. The current drawn during engine cranking was between 180 A and 200 A.

On the first day, a total of 40 cranks were recorded over a distance on 5 km. The battery was able to crank the engine on all the cranks apart from C# 38 which also corresponded with the highest resistance recorded on the first day. When the battery exhibits a high resistance, its SoC and SoH reduces thereby lowering its ability to crank the engine. The range of resistance on the first day

was between $0.0064 \Omega - 0.7028 \Omega$. The SoC of the battery was between 80 % - 90 % regardless of being charged by the cars' generator implying that the active materials had deteriorated and so could not accept charge efficiently. Whenever the resistance of the battery was high, cranking was unsuccessful and the cranking time also increased. During charging and discharging, chemical reactions in the battery have associated losses in the active mass involved in the reaction. Part of the energy is lost through sound and heat with part of it being lost as vapor leading to a reduction in the active materials of the battery. These losses cause a reduction in the battery's charging efficiency, which is the ratio of available energy from a fully discharged battery to the amount of energy needed to completely charge the battery. Coulombic efficiency or charge acceptance is therefore reduced by the losses occurring during the charging and discharging process. In general, the coulombic efficiency for a new battery is usually high however and it reduces as the battery ages.

On the second day, a total of 30 cranks were recorded over 5 km with the battery resistance ranging between $0.0048 \Omega - 0.8244 \Omega$. The SoH was 0% for C# 46 where the resistance was 0.7951Ω and the SoC of 85.69 %. The SoH was also 0 % on the C# 64 with SoC of 79.99 % and a resistance of 0.8244Ω . The average cranking time was 0.47 seconds while the number of V - I logs taken for every crank was 962. The TFT display for C# 64 is shown in Figure 5.34.

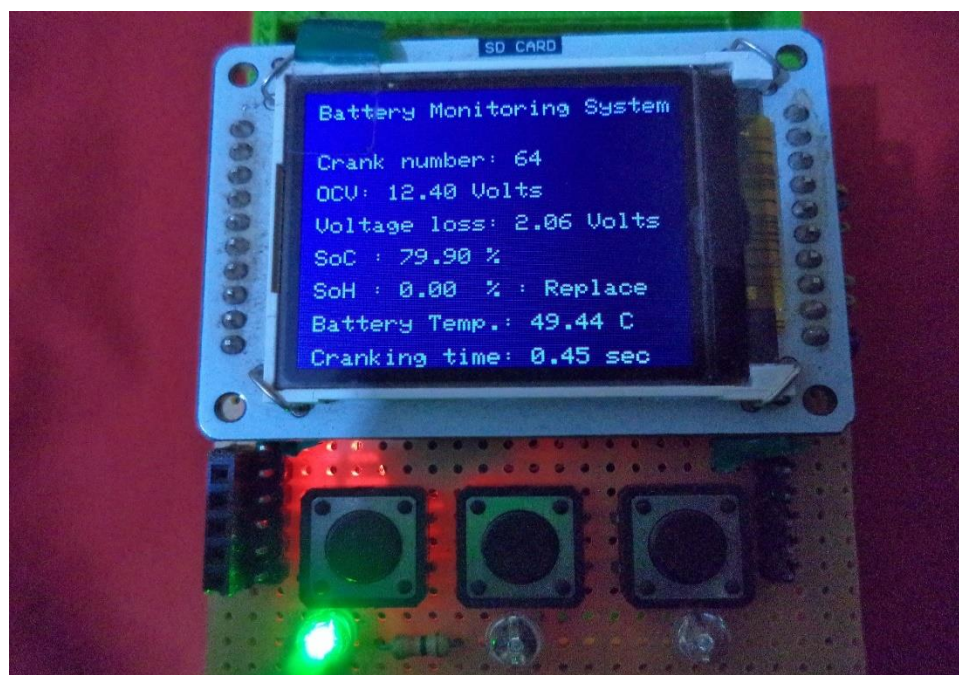


Figure 5.34: The TFT display for C# 64 for the 110 Ah Yuasa battery in the 115 Hp engine

The summarized SoH and SoC indication for the Yuasa battery in the 115 Hp engine is shown in Table 5.19.

Table 5.19: The summary of the SoH and SoC indication for the 110 Ah Yuasa battery in the 115 Hp engine

C#	SoH (%)	SoC (%)
1 - 2	100	94.45 – 100
3 - 37	83.45 -98.12	80.63 – 89.93
38	0	88.97
41 - 45	88.21 – 96.04	87.32 – 89.45
46	0	85.69
47 - 63	85.23 -89.99	79.89 – 89.91
64	0	79.99
65 - 70	82.28 – 86.13	81.33 – 89.18

Based on Table 5.19, the SoH for the Yuasa battery was between 82.28 % and 100 % for the two days it was used. Since the SoH was high, the cranking time was 0.47 s which was quite low as compared to other values. The SoC was between 79.18 % and 100 % which implied that the battery was charging but not getting full due to the short charging time.

5.4.3 The 100 Hp engine

The Yuasa battery's data when used in the 110 Hp engine is shown in Figure 5.35 on page 105.

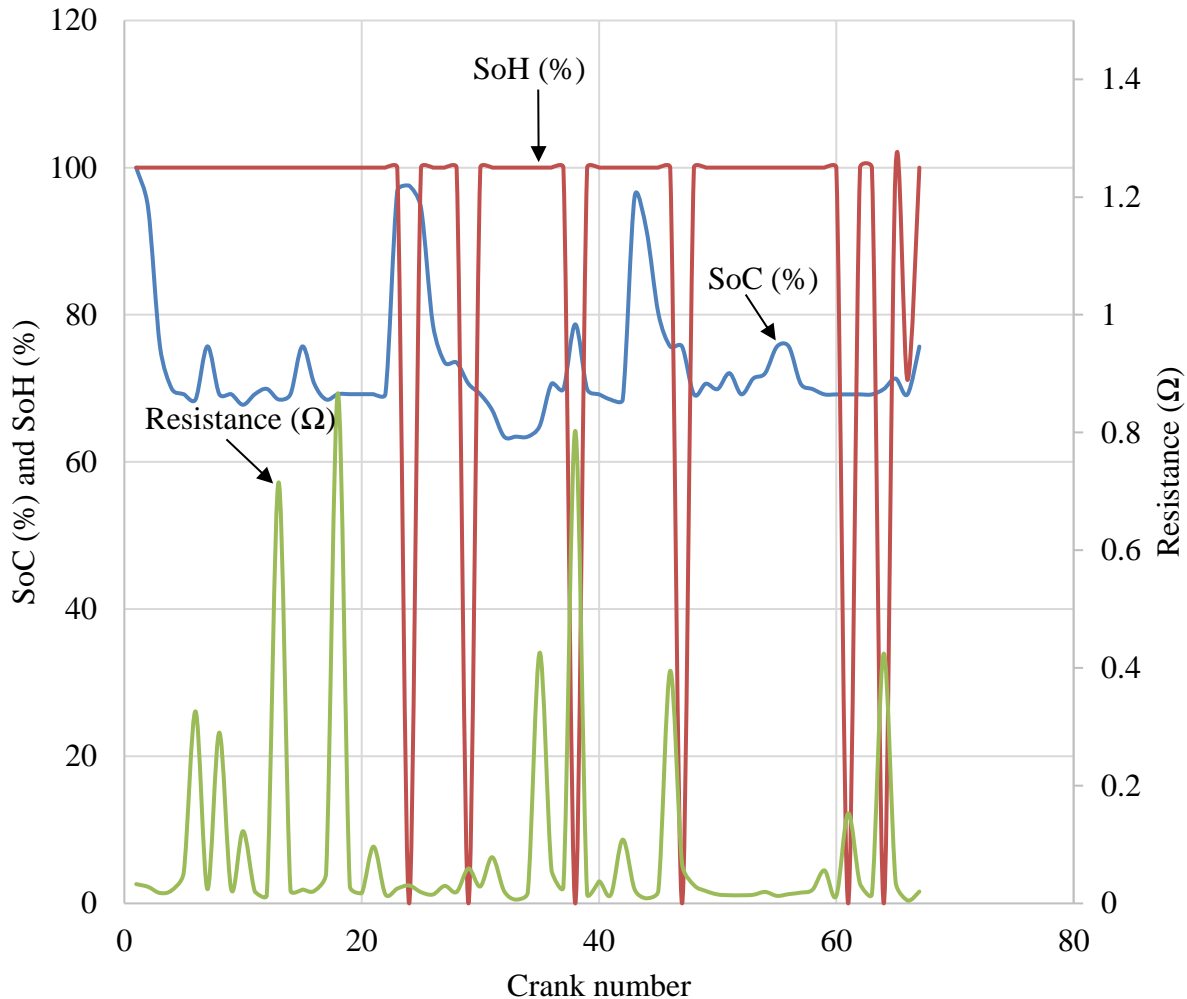


Figure 5.35: The SoH and SoC against crank number for the 110 Ah Yuasa battery in 100 Hp car

Based on Figure 5.35, there were 67 cranking events recorded for the Yuasa battery in the 100 Hp engine. Cranking was successful on 61 out of the 67 cranking events and the average cranking time was 0.48 second. The SoH was 0 % on crank C# 25, C# 28, C# 38, C# 47, C# 60 and C# 63 in which cranking was not successful. This SoH was 0 % because of a faulty wiring of the BMS in the engine. The average V - I logs taken was 676 for each crank while the temperature of the battery was 27.25 °C. The lowest recorded value of SoH at which cranking was successful was 71.13 % while the SoC was between 67.77 % and 100 %. The battery was able to charge on a few occasions like C# 7, C# 15, C# 43 and C# 56 which show a noticeable increase in SoC as can be seen in Figure 5.32. Since the charging wasn't long enough, the SoC kept decreasing thereafter.

The summarized SoH and SoC indication for the Yuasa battery in the 100 Hp engine is shown in Table 5.20.

Table 5.20: The summary of the SoH and SoC indication for the 110 Ah Yuasa battery in the 100 Hp engine

C#	SoH (%)	SoC (%)
1 - 23	100	67.77 – 100
24	0	97.55
25 - 28	100	73.51 - 94.54
29	0	70.63
30 - 37	100	63.44 – 70.62
38	0	78.71
39 - 46	100	68.47 – 96.04
47	0	75.69
48 - 59	100	69.19 – 75.69
60	0	69.18
61	100	69.18
62 - 63	100	69.18
64	0	69.90
65	100	71.12
66	71.13	69.18
67	100	75.68

From Table 5.20, the Yuasa battery was used for cranking the engine 67 times. On C# 24, the SoC was nearly 100 % but the engine could not be crank because the V_{loss} associated with this crank was very high. The SoH was 0 % on C# 24 implying that the battery was unable to deliver the correct amount of power to crank the engine. The same phenomenon was repeated on C# 29, C# 38, C# 47 and C# 56.

5.4.4 The 125 Hp engine

The cranking data for the brand-new Chloride Exide battery when installed in the 125 Hp engine that draws between 250 A – 280 A during cranking is shown in Figure 5.36 on page 107. The car was driven from Nairobi to Oloitoktok and back in two days there by covering 500 km and recording 249 engine cranking events.

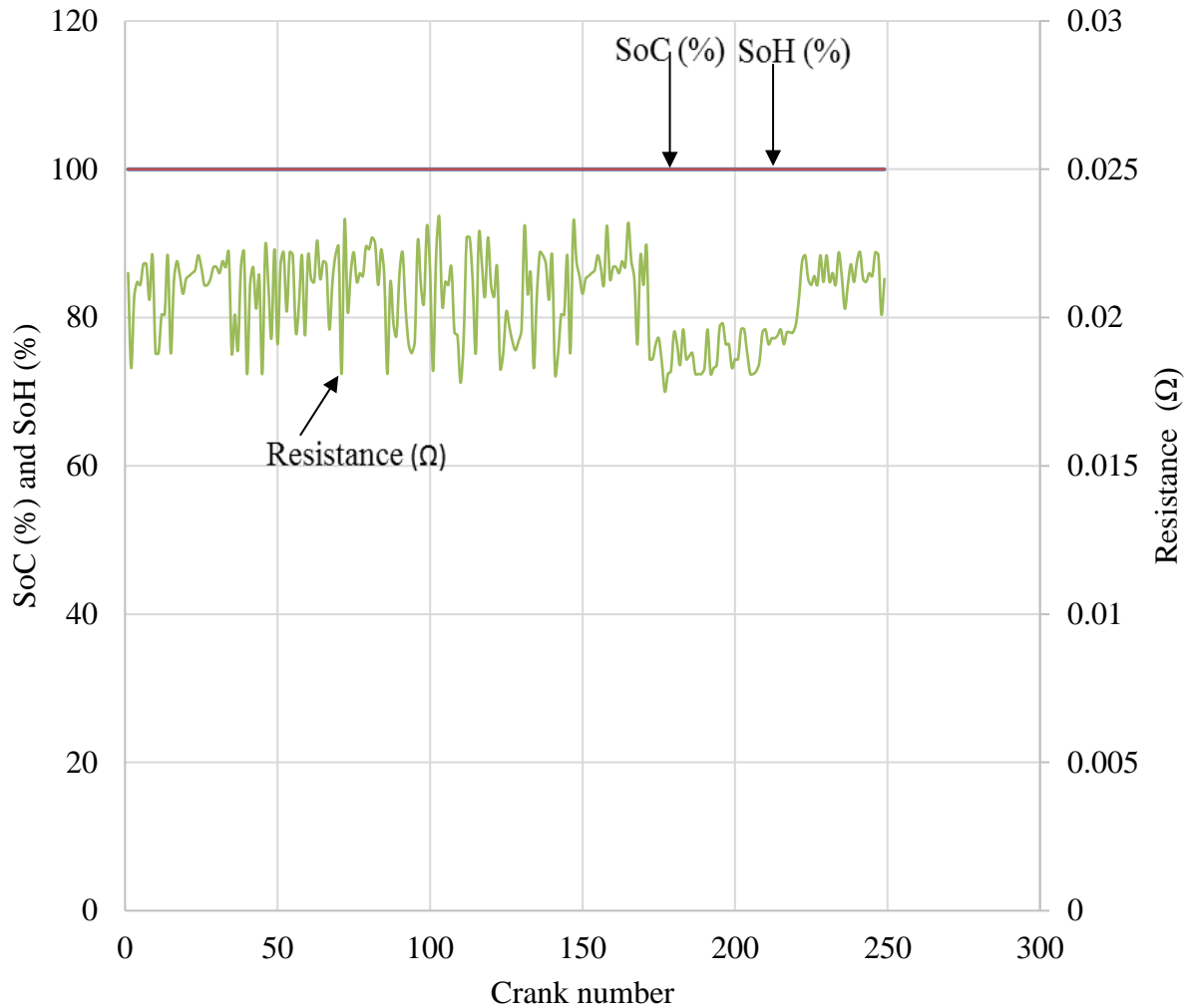


Figure 5.36: The SoH and SoC against crank number for the brand new 75 Ah Chloride Exide battery in the 125 Hp car

The Chloride Exide battery was brand new and so both the SoH and SoC were 100 % throughout the two-day period and that is why the blue color for indicating the SoC merged with the red one that indicates the SoH of the battery. The resistance of the battery was between 0.0076 Ω – 0.0783 Ω and the cranks were taken on both days. The car was driven from Nairobi for 3 hours consecutively to Oloitoktok and likewise on return to Nairobi on the following day and so the battery's temperature was 84.47 °C. A brand-new battery in good health has high cranking power and low resistance and so it delivers its energy efficiently for cranking.

5.4.5 The 250 Hp engine

The cranking data for the Unistar battery installed in the 250 Hp engine is shown in Figure 5.37.

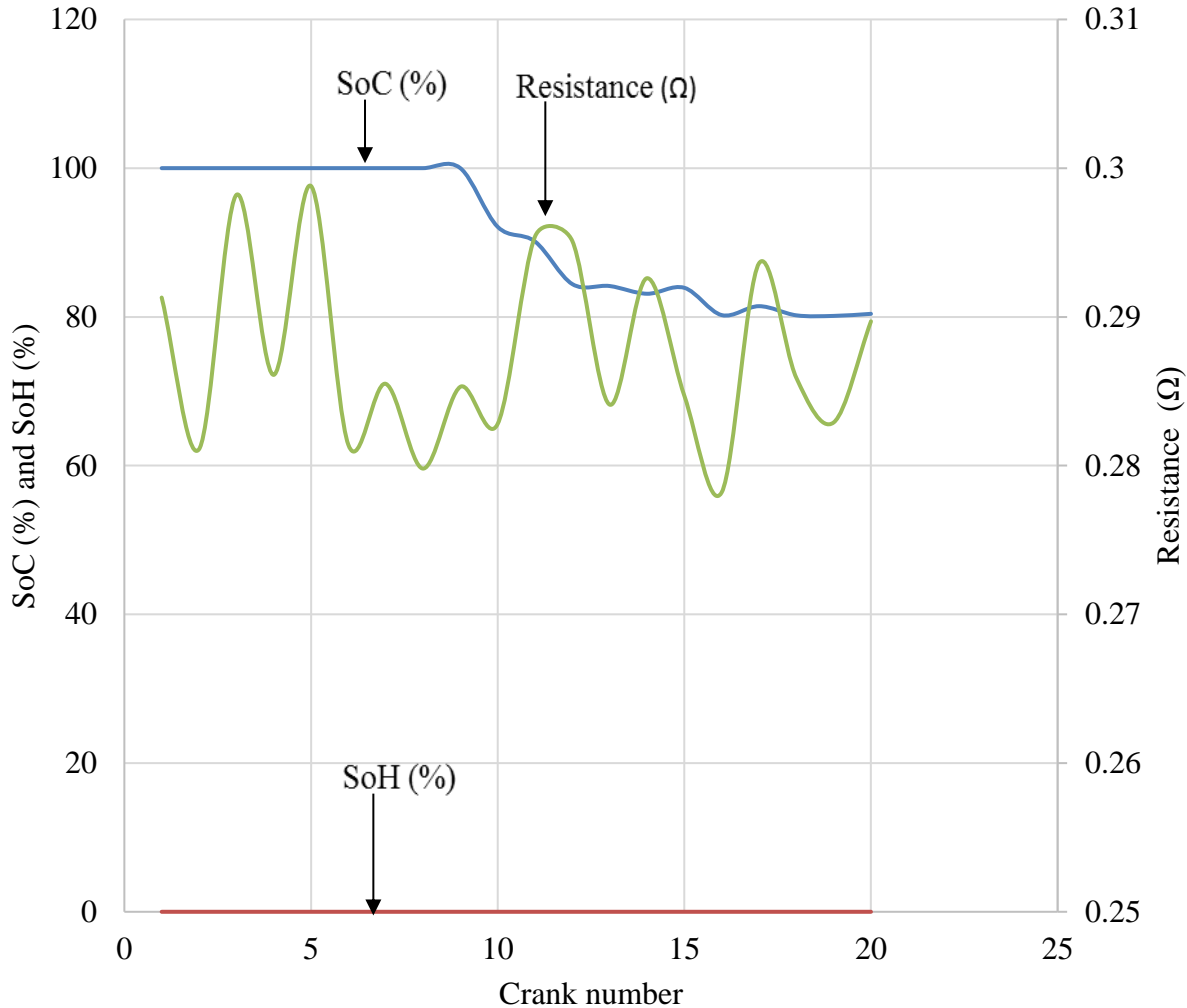


Figure 5.37: The SoH and SoC against crank number for the 100 Ah Unistar battery in the 250 Hp engine

From Figure 5.37, the SoC was 100 % on the first nine cranks and thereafter it began to reduce. Regardless of the SoC being 100 %, the battery failed to crank the 250 Hp engine on all the 20 cranks since it's SoH was 0%. The resistance of the battery was between 0.2782 Ω – 0.2988 Ω. An increase in battery resistance and decrease in the SoH leads to an increase of cranking time. the temperature of the battery was 24.25 °C while the number of V - I logs for each cranking event was 200. The average time taken for each crank was 2 seconds which was high as compared to the lowest cranking time of 0.47 seconds on other occasions.

The Unistar battery cranked the 80 Hp engine having a starter that draws a current of 120 A during cranking but failed in the to crank the 250 Hp engine that had a starter that draws 300 A during cranking. The power requirements from a battery are and SoH threshold are dictated by the application to which the battery is applied. This result agrees with the discussion by Sayed *et al.*, (2014) that there is no fixed definition for SoH thereby leaving scholars and manufacturers to calibrate their own SoH thresholds based on customized applications. The engine capacity and starter motor types have been identified as factors that influence cranking by Karden (2017) in the book on development trends for future automobile and their demand on the battery. The summarized SoH and SoC indication for the 100 Ah Unistar battery in the 250 Hp engine are shown in Table 5.21.

Table 5.21: The summary of the SoH and SoC indication for the 100 Ah Unistar battery in the 250 Hp engine

C#	1 – 9	10 – 20
SoH (%)	0	0
SoC (%)	100	80.13 – 92.11

From Table 5.21, the Unistar battery was unable to crank the 250 Hp engine since its status had deteriorated so much. A battery can work very well with one application but fail when used on a different one that has higher power requirements. The 250 Hp engine draws a higher current during cranking than the other cars and so its power requirements were much higher than those of the rest of the cars. Therefore, higher engine capacity and type of starter motor influence the power demands of the vehicle during engine cranking.

The cranking data for the Yuasa battery installed in the 250 Hp engine is shown in Figure 5.38.

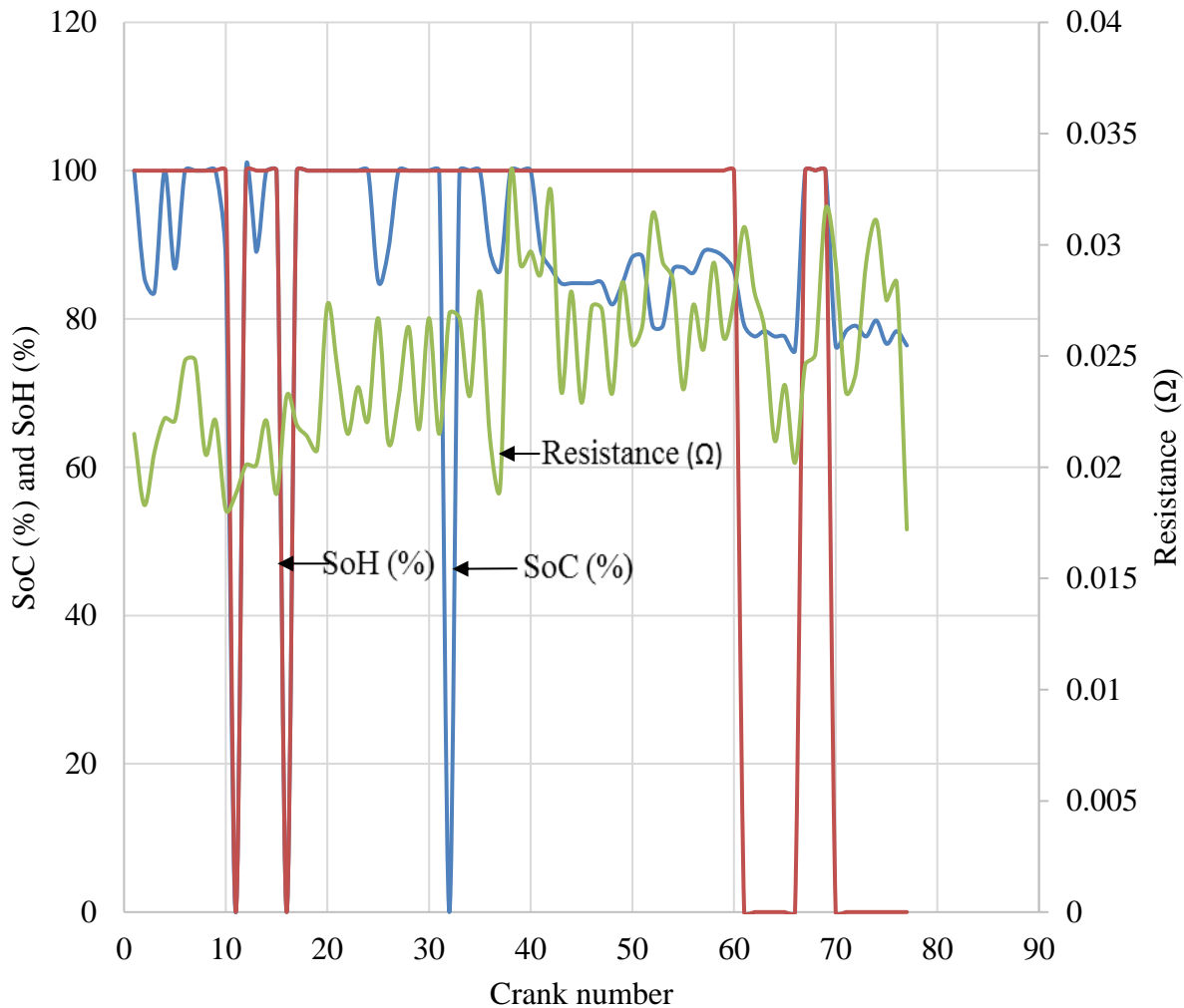


Figure 5.38: The SoH and SoC against crank number for the 110 Ah Yuasa battery in the 250 Hp engine

The first 40 cranks shown in Figure 5.38 were taken on the first day of using the Yuasa battery in the 250 Hp engine. The range of the resistance was $0.0172 \Omega - 0.0248 \Omega$ on the first day and $0.0248 \Omega - 0.0331 \Omega$ on the second day in which 37 cranks were taken. The car covered 5 km on the first day but on the second, the cranks were taken while the car was in a stationary position. The battery temperature was $29.75 \text{ }^\circ\text{C}$ on the first day when the cranks were taken and $26.41 \text{ }^\circ\text{C}$ on the second day. For the first 40 cranks, the SoH was 100 % except on C# 11, C# 16 and C# 32 where it was 0 %. The SoC reduced gradually from 89.28 % on C# 41 to 76.42 % on C# 77 while the SoH was 100 % for C# 41 to C# 60 except C# 67, C# 68 and C# 69. The temperature of the

battery on the second day was 26.41 °C. The TFT display for C# 32 and C# 61 is shown in Figure 5.39 and Figure 5.40 respectively.

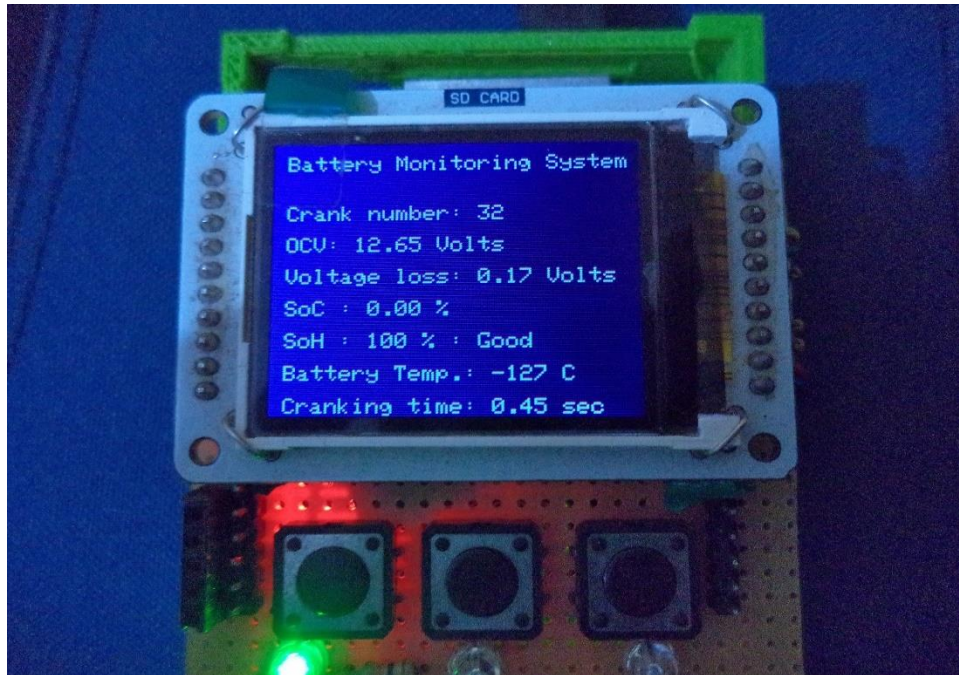


Figure 5.39: The TFT display of C# 32 of the 110 Ah Yuasa battery in the 250 Hp engine

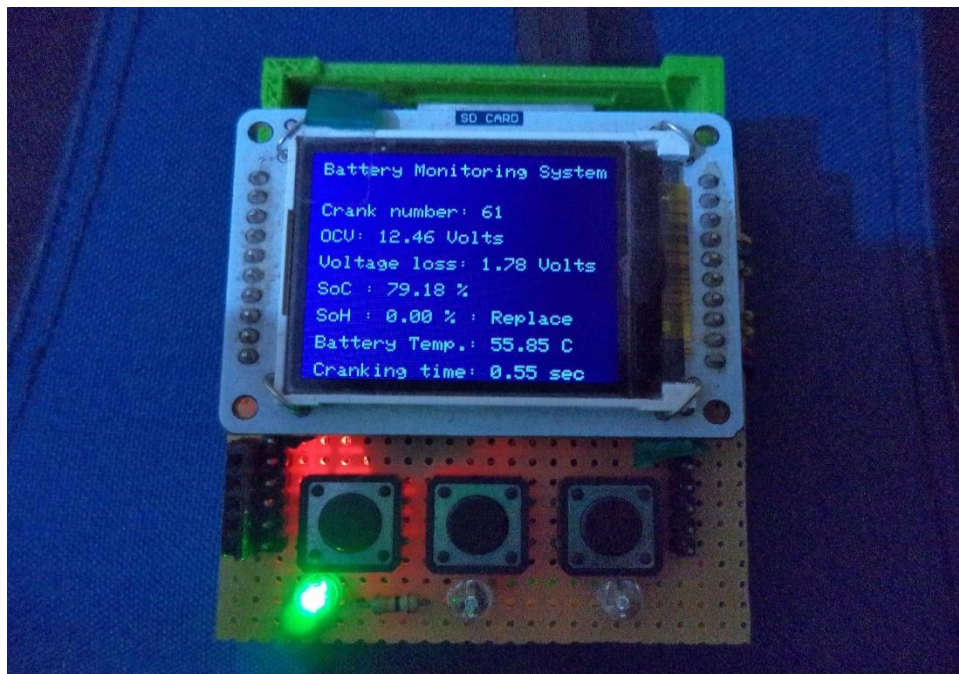


Figure 5.40: The TFT display of C# 61 of the 110 Ah Yuasa battery in the 250 Hp engine

The summarized SoH and SoC indication for the 110 Ah Yuasa battery in the 250 Hp engine is shown in Table 5.22.

Table 5.22: The summary of the SoH and SoC indication for 110 Ah Yuasa battery

C#	SoH (%)	SoC (%)
1 - 10	100	83.67 - 100
11	0	0
12 - 15	100	89.05 - 100
16	0	0
17 - 24	100	100
25 - 31	100	85.08 – 100
32	100	0
33 - 60	100	79.08 – 100
61 - 66	0	75.79 – 79.18
67 - 69	100	100
70 - 77	0	76.38 – 79.78

From Table 5.22, the Yuasa battery successfully cranked the engine on the first 10 cranks since the SoH was above threshold. On C# 11 and C# 16, both SoC and SoH was 0 % because of the battery terminals were loosely connected. On C# 32, the temperature sensor erroneously read -127 °C which caused the SoC to read 0 % and the SoH to be 100 % and so cranking was still successful. This sensor error is accounted for in the manufacturers data sheet and so the BMS needs to be reset using the reset button. For the C# 61 to C# 66 and C# 70 to C# 77, the SoH was 0 % was above 75.79 % in both cases but due to high voltage loss during cranking, the battery was unable to crank the engine. Cranking was successful on all the other cranking events.

The cranking data for the 110 Ah Land Rover Varta battery in the 250 Hp engine is shown in Figure 5.41. The 250 Hp engine car was driven from Nairobi to Mwea Irrigation Scheme and back covering 220 km every day for 5 consecutive days.

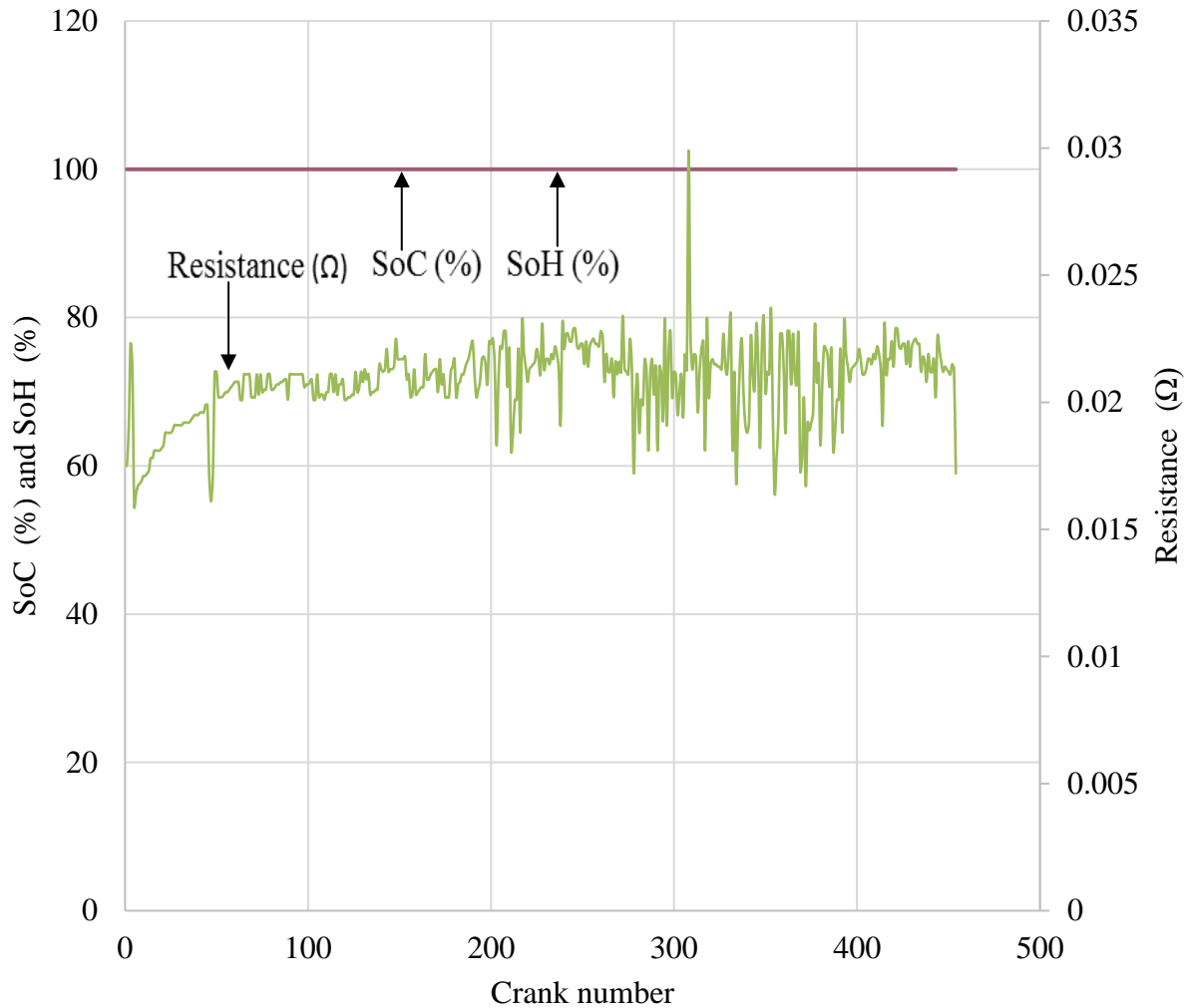


Figure 5.41: The SoH and SoC against crank number for the 110 Ah Land Rover Varta battery in the 250 Hp engine

The SoC and SoH of the battery was 100 % for all the five days since the battery was brand new. The average cranking time for all the cranks was 0.49 seconds. The temperature of the battery was 23.7 °C for the first crank in the morning just before departure and it gradually increased to 85 °C and remained high throughout the rest of the journey. The resistance was between 0.0159 Ω – 0.0237 Ω apart from crank number 308 where it shot up to 0.0299 Ω.

The cranking data for the moll m3 plus k2 battery in the 250 Hp engine is shown in Figure 5.42.

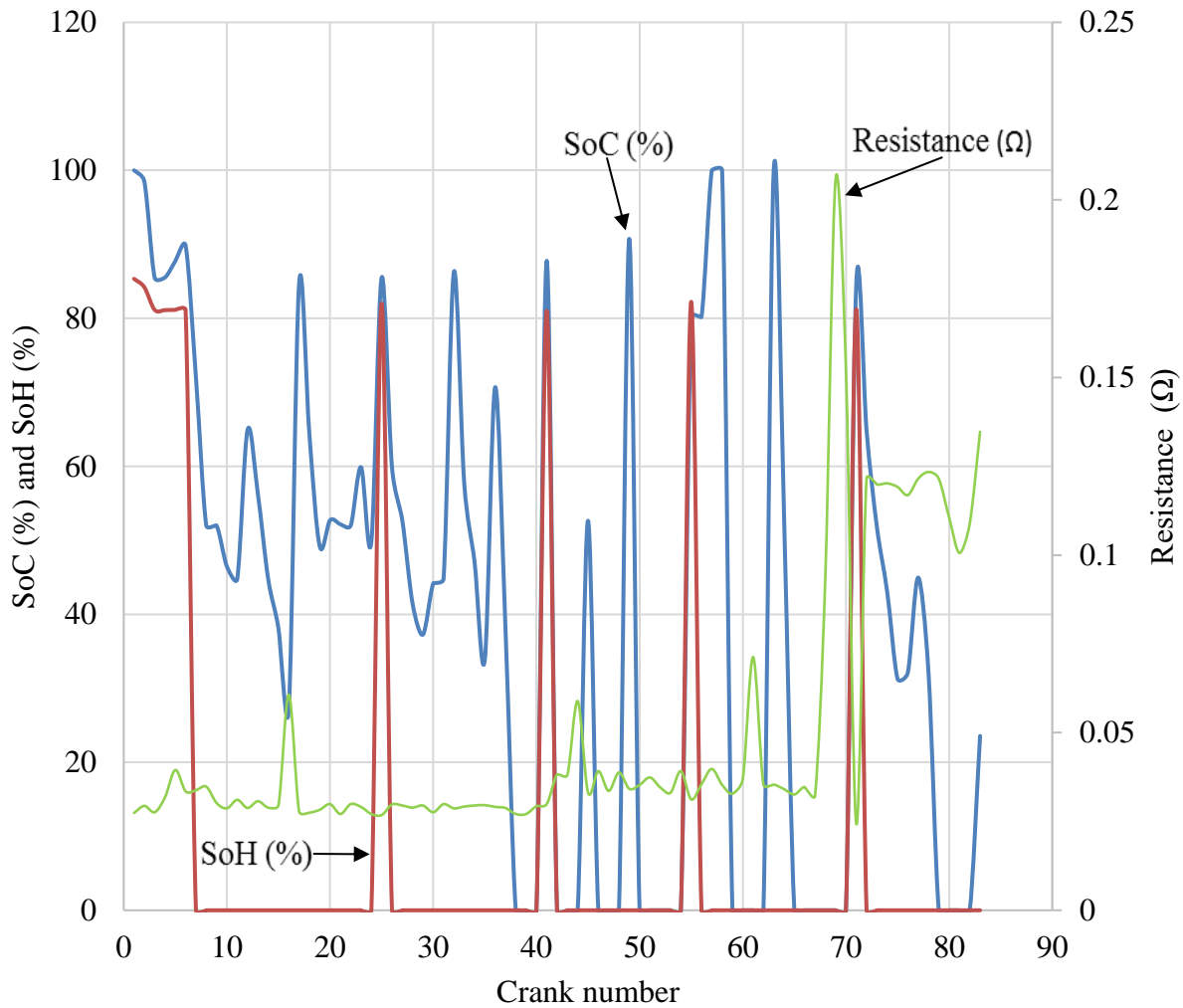


Figure 5.42: SoH and SoC against crank number for the 75 Ah moll m3 plus k2 battery in the 250 Hp engine

Based on Figure 5.42, the battery cranked the engine successfully on the first 6 cranks while the car was stationary. On the second crank, the SoC began reducing which was quite soon implying that the ability of the battery to retain charge had reduced. The battery was able to crank the engine on C# 25, C# 41, C# 55 and C# 71 on which the SoC had risen above the threshold value of 71 % and a corresponding reduced resistance compared with the rest of the resistance values in this series. The range of resistance for the 83 cranks was 0.0244 Ω – 0.2059 Ω with the resistance increasing in the second half of the cranking events. The temperature of the battery was 23.56 °C

while the V-I samples was 1500 for each crank and the cranking time was 0.89 seconds. The TFT display for C# 38 and C# 58 are shown in Figure 5.43 and Figure 5.44 respectively.

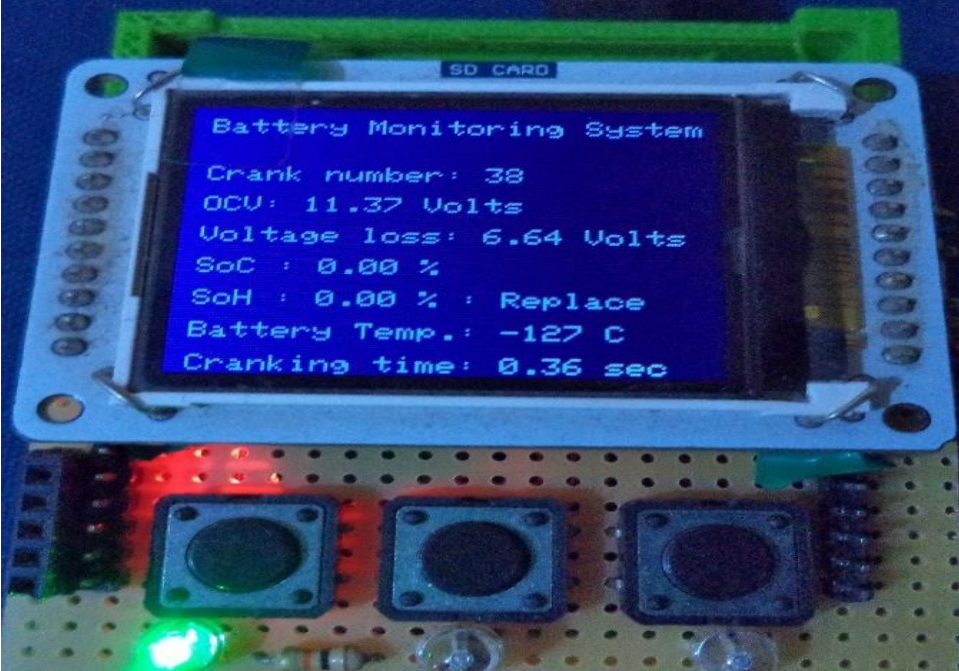


Figure 5.43: The TFT display for C# 38 for the 75 Ah moll m3 plus k2 battery in the 250 Hp engine

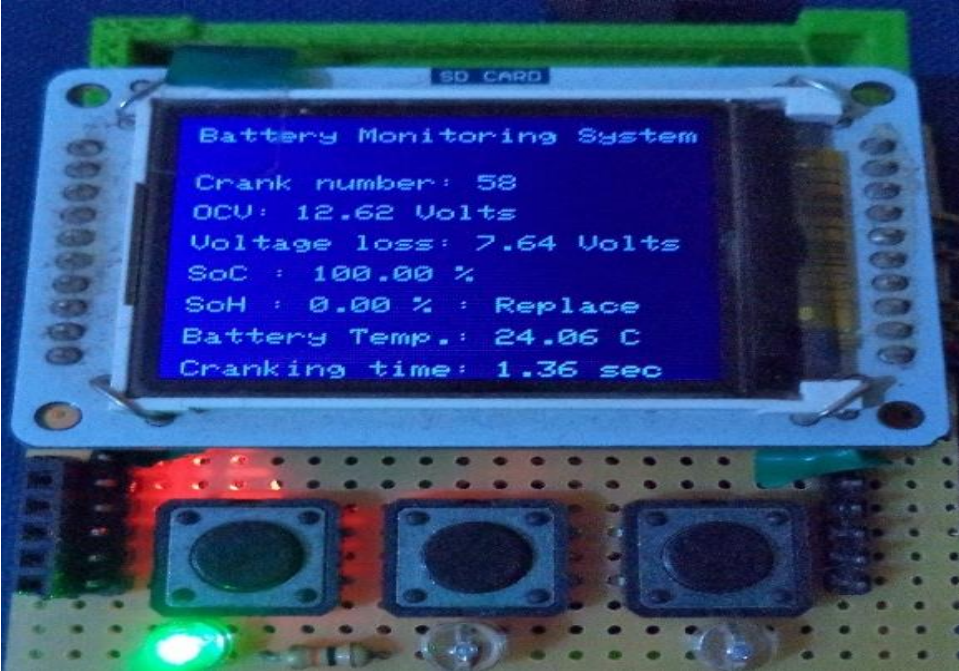


Figure 5.44: The TFT display for C# 58 for the 75 Ah moll m3 plus k2 battery in the 250 Hp engine

The summarized SoH and SoC indication for the 75 Ah moll m3 plus k2 battery in the 250 Hp engine is shown in Table 5.23.

Table 5.23: The summary of the SoH and SoC indication for the 75 Ah moll m3 plus k2

C#	SoH (%)	SoC (%)
1 - 6	81.09 - 85.34	85.47 - 100
7 - 24	0	27.23 - 84.75
25	82	85.51
26 - 37	0	33.88 - 86.26
38 - 40	0	0
41	80.99	87.77
42 - 44	0	0
45	0	52.64
46 - 48	0	0
49	0	90.75
50 - 54	0	0
55	82.23	80.22
56 - 58	0	80.18 - 100
59 - 62	0	0
63	0	100
64	0	53.31
65 - 70	0	0
71	81.23	84.66
72 - 78	0	31.28 - 84.66
79 - 82	0	0
83	0	23.56

From Table 5.23, the battery managed to crank on C# 1 to C# 6, C# 25, C# 41, C# 55 and C# 71 because the SoH was above threshold. Regardless of charging, the SoC and SoH was 0 % on C# 40 to C# 42, C# 46 to C# 48 and C# 50 to C# 54 because this battery had been in use for 2 years and its active materials had been depleted. Cranking was not successful on the remaining cranks since the V_{loss} was above threshold.

5.5 Performance of the batteries in the field

The Land Rover battery had a SoH of 100 % for the first 68 cranks carried out in the laboratory before failing at the C# 74. This battery was brand new and so it performed very well. The range of resistance for the whole cranking period was between 0.0076 Ω - 0.0783 Ω . When used in the

250 Hp car, the SoC and SoH was 100 % throughout the period it was used with an average cranking time of 0.49 s. In the car, the resistance was between 0.0159 Ω and 0.0237 Ω which was higher than the one in the laboratory because of additional electronic components in the car.

In the laboratory, the SoH of the Chloride Exide battery was 100 % for 93 cranks and thereafter dropped to 0 %. The resistance of the battery was between 0.0076 Ω and 0.0783 Ω corresponding to 100 % and 0% SoH respectively. In the 125 Hp engine, the Chloride Exide battery's SoH and SoC were 100 % throughout the two-day period.

The Yuasa battery when installed in the 80 Hp engine had a resistance between 0.0159 Ω and 0.2933 Ω while the average cranking time was 0.56 s. In the 115 Hp engine, the battery was able to crank the engine except where the resistance was high. The range of resistance was between 0.0064 Ω and 0.7028 Ω and the average cranking time was 0.47 s. In the 250 Hp engine, the resistance was between 0.0172 Ω and 0.0331 Ω . The average cranking time in the 100 Hp engine was 0.48 s.

The SoC and SoH for the Unistar battery in the laboratory were both 100 % for the first 10 % of the cranks but thereafter reduced. The range of resistance was between 0.0016 Ω and 0.1735 Ω . In the 80 Hp engine, the SoH was 100 % for all the cranks. The resistance ranged between 0.0181 Ω and 0.0331 Ω and the cranking duration was 0.59 seconds. In the 115 Hp engine, both the SoH and SoC were 100 % and the car cranked in 0.56 s and due to increase in battery resistance the time rose to 0.72 s. The range of resistance for this battery when used in the 115 Hp engine was 0.0014 Ω – 0.0486 Ω . In the 250 Hp engine, it was between 0.2782 Ω and 0.2988 Ω with an average cranking time of 2 s which was high as compared to the lowest cranking time of 0.47 s on other occasions. Therefore, higher engine capacity and type of starter motor influence the power demands of the vehicle during engine cranking.

The moll k2 battery had a resistance between 0.0061 Ω and 0.0971 Ω for all the cranking events in the laboratory. When used in the 115 Hp engine, the battery resistance was between 0.0082 Ω and 0.0355 Ω and on all these occasions, the engine cranked successfully. The average cranking time for each crank was 0.96 seconds which was slightly higher compared to the average cranking time of a brand-new battery of 0.49 seconds. The battery cranked the 250 Hp engine successfully

on a few occasions with the car in a stationary position. The range of resistance was 0.0244Ω – 0.2059Ω and the average cranking time was 0.89 seconds.

The power output of a car engine is directly proportional to the engine capacity. Beside rpm, the output power of an engine depends on the number of valves, air-fuel ratio, compression ratio, air induction and efficiency among other factors. Hp and torque are always expressed at specific engine speeds and so the 250 Hp car can only attain the 250 Hp limit when the engine speed is 6000 rpm. The average rpm during cranking for the 5 cars was about 1000 rpm. The rated Hp of the 5 cars could not be realized during cranking since the cars needed to be in the first or second gear and under strain from either a load or steep road. There is however an exception for the turbo charged cars which can reach their peak Hp and torque at very low rpm. If an engine takes 120A at cranking, then when a 600 CCA battery is used, it will still draw 120A. Loose terminal connections cause high resistance. The cranking current is dependent on the engine size, circuit resistance, temperature, engine oil viscosity and the accessory loads. A four-cylinder engine may require as much cranking current as an eight-cylinder engine because it may need to crank faster to start. Optional electrical accessories, regenerative braking technology and advanced engine management systems, all place extra loads on the battery.

5.6 The BMS

The BMS was able to measure the voltage, current and temperature signals and compute the SoH of the batteries under test as programmed. During the BMS calibration period, the current sensor broke down and had to be replaced on four occasions since it was physically the most delicate component. Whenever the temperature sensor read $-127 \text{ }^\circ\text{C}$, the SoC of the battery appeared as 0% which on all such occasions wasn't true since the battery cranked the car engine successfully. From the data-sheet of the temperature sensor, the sensor would on some occasions erroneously read the temperature as $0 \text{ }^\circ\text{C}$ or $-127 \text{ }^\circ\text{C}$. The error on the temperature sensor can be corrected by resetting the sensor or programming the BMS to ignore the temperature readings of $0 \text{ }^\circ\text{C}$ or $-127 \text{ }^\circ\text{C}$. The temperature sensor was replaced twice but this problem still showed up on 0.1 % of the total number of cranking events carried out in this research.

At the initial stages of programming the BMS, the measured voltage and current values for each crank were displayed alongside the computed SoH. When the SoH was displayed without displaying and saving the V – I logs, the V - I logs recorded for each crank were higher. For this reason, the voltage and current logs for each crank neither displayed nor saved in the BMS but instead, only the computed SoH, cranking duration, temperature, SoC and voltage loss were displayed on the TFT thereby increasing the accuracy of the outcome. For the same reason, the V - I graphs for obtaining V_{loss} from the y-intercept value were not drawn for each cranking event but instead a regression formula was used to get those values.

From the results acquired, the cranking ability was specific to the type of application used. To detect dangerously low battery voltage levels in each application, the BMS needs additional software and hardware to compute the CCA of the batteries and the current drawn by the starter motor during cranking. An algorithm for finding the rate of charging and discharging of the battery in use needs to be found and thereafter compared with the current drawn by the starter to indicate the remaining number of cranks before the battery fails.

CHAPTER SIX

CONCLUSION AND RECOMMENDATIONS

6.1 Conclusions

This study was undertaken to fabricate a battery monitoring system based on the voltage loss associated with an engine cranking event and use it to evaluate the performance of 5 automotive starter batteries in the laboratory and in 5 different functional automobiles. Electronic sensors along with their schematic circuits for measuring the voltage, current and temperature were successfully designed and integrated in the BMS design. The BMS was used to assess the behavior of the changes in V and I signal of the LAB during engine cranking based on the developed algorithm to compute the SoH of the battery.

The results obtained from the analysis carried out by the BMS on the five SLI batteries show that the SoH of the batteries decreased with its usage. The Land Rover Varta battery and the Chloride Exide batteries were brand new and so they performed very well during the laboratory and field tests. As the battery charging and discharging cycles increase, the battery's resistance increases and consequently, the ability of the battery to crank the engine reduced. When the battery had a low SoH and SoC, the time taken for cranking increased from the average of 0.5 seconds to between 1- 2 seconds. Battery deterioration usually takes place in the background such that the user (the motorist in this research) may fail to detect its gradual degradation accurately.

This study found out that the SoH threshold value can be as low as 64.3 % for some cars and not just the recommended 80 % and this finding is corroborated by other researchers and corporate organizations as discussed in chapter five. A battery could have SoH that is below the required threshold for a car but when put in a different car which has lower power requirements, it worked very well. The Yuasa battery worked in the 250 Hp engine that draws 300A for a very short time as compared to the same battery installed in the 80 Hp engine that draws 120A during cranking in which it worked for a longer time. The lifetime of a battery also depends on the specific application to which it is put.

Whenever the batteries were used in the cars, they were charged by the car's alternator. The Unistar and moll m3 plus k2 battery showed a decline in charge acceptance because regardless of being

charged, the SoC could not rise to 100 %. The active materials in these batteries had been used up thereby affecting the charge retention of the batteries. The time taken to charge a battery should also be long enough to allow the battery to charge to full capacity for it to perform well and be in good condition. The Yuasa battery performed well when charged for a long, implying that a battery can be erroneously replaced whereas charging it correctly, by driving the car over longer distances, could have avoided the replacement.

This research also found out that a car starter battery can be fully charged thereby having a SoC of 100 % but the battery be unable to crank the engine successfully. The SoH, the ability of the battery to deliver the required power to an appliance when required, is therefore not directly proportional to the SoC but depends on the specifications of the application to which it is put. When a battery is failing, the voltage loss associated with the engine cranking event will be as high as 7.44 V as observed in some of the cranking events in this research.

With the BMS installed in the car, the motorist will not need to wait for the battery to fail completely before replacing it. Most battery monitors used in most of the present-day cars only shows the SoC, a parameter that cannot tell how healthy a battery is. The SoC and SoH monitoring using the developed BMS will ensure that loads in the car can be turned on and off appropriately to optimize battery utilization and eliminate failures from unintended discharge. The energy storage capability of the battery can be tracked as it decays over its lifetime using its SoH. Motorists can use the new BMS in their vehicles to monitor their battery performance, conserve energy, lower expenses on battery repairs and replacements and avoid the inconveniences caused by battery failures. Based on the results obtained from analysis of the performance of the BMS in the laboratory and in the field the BMS can be relied upon for qualitative analysis in monitoring the SLI battery from the moment it is installed in the car in a brand-new status to the time when it wears out. The reported methodology demonstrates that analysis of the cranking data from the BMS can be used as a means of quantifying the SoH of the SLI battery and informing the user on appropriate action to be taken when the need arises.

6.2 Recommendations

There is a gap between the laboratory-based tests and the real field application that needs to be addressed by future research. The performance of the BMS under operating conditions, such as vibration from bumpy roads and temperature extremes from snow, rain, fog or summer heat need to be studied for a longer period so that these external loads can be reflected in the battery monitoring systems algorithm for indicating the battery's available capacity.

The BMS should be installed in a car for a longer period, at least one year and the car used on a day to day basis to get a better capacity deterioration trend of the car starter battery which will in turn help to improve the efficiency and accuracy of the SoH indication algorithm.

The batteries were able to crank the car on some occasions where the SoH was below the recommended threshold of 80 % and so this threshold value needs to be reviewed.

REFERENCES

- Acton, Q. A. (2013). *Sulfur Compounds—Advances in Research and Application*. (2013) Edition. Scholarly Editions, Atlanta Georgia USA, 47.
- Andrea, D. (2010). *Battery Management Systems for Large Lithium Ion Battery Packs*. ARTECH HOUSE, Norwood MA 0262, USA, 16-18.
- Barbir, F. (2013). *PEM Fuel Cells: Theory and Practice*. MA 01803. Academic Press- imprint of Elsevier Inc, Netherlands, 425.
- Bayle, J. (2013). *C programming for Arduino learn how to program and use Arduino boards with a series of engaging examples, illustrating each core concept*. Packt Pub, . Birmingham England, 7.
- Bergveld, H. J., Kruijt W. S. and Notten P. H. L., (2013). *Battery Management Systems: Design by Modelling*. Springer Science & Business Media, Eindhoven Netherlands,197.
- Bertness, K. I. (2014). *USA Patent No. 8,674,654*.
- Brodd, R. J. (2013 edition). *Batteries for Sustainability: Selected Entries from the Encyclopedia of Sustainability Science and Technology*. Springer, New York USA,54,229.
- Buchmann, I. (2011). *Batteries in a Portable World: A Handbook on Rechargeable Batteries for Non-Engineers, Third Edition*. Cadex Electronics Inc, Bristish Columbia USA, 9.
- Buchmann, I. (2012). *Checking Battery Health while Charging*. Cadex Inc.
- Canbing, L., Yijia, C.,Yonghong, K. and Bin, Z. (2016). *Influences of Electric Vehicles on Power System and Key Technologies of Vehicle-to-Grid*. Springer, Beijing China, 1-2.
- Ceraolo, M., Huria, T., Pede, G. and Vellucci F. (2011). Lithium-ion starting-lighting-ignition batteries: Examining the feasibility. *Vehicle Power and Propulsion Conference (VPPC), 2011 IEEE* (p. 1). IEEE.
- Chen, C., Man, K. L., Ting, T.O., Chi-Un, L., Krilavicius, T., Jeong, T.T., Seon, J. K., Sheng-Uei, G., and Prudence, W. H. W. (2012). The 2012 IAENG International Conferance on Control and Automation, Electrical Engineering Special session: Design, Analysis and Tools for Integra . *Proceedings of the International Multi-conference of Engineers and Computer Scientists* (p. 823). Hong Kong China: IAENG.
- Clinton, C. Christianson, R. F. (1976). *USA Patent No. United States Patent 3,946,299*.
- David, L. and Reddy, T. B.. (2008). *Battery Basics. Battery Power and products Technology*, McGraw Hill Companies Inc, New York USA, 10-12.

- David, L. and Thomas, B. R. (2002). *Handbook of Batteries*. McGraw Hill, New York USA, 104-105.
- David, L. and Thomas B. R. (2011). *Lindens Handbook of Batteries 4th Edition*. McGraw Hill Companies Inc, New York USA, 619-621.
- David W. and Paul A. (2012). *Managing Temperature Effects in Nanoscale Adaptive Systems*, Springer New York, New York, 22.
- Dell, A.. and Strickland J. T. (2002). *USA Patent No. US 6,369,578 B1*.
- Denton, T. (2006). *Advanced automotive fault diagnosis second edition*. Elsevier BH, Burlington MA.
- Denton, T. (2011). *Automobile mechanical and electrical systems: automotive technology : vehicle maintenance and repair*. Elsevier/Butterworth-Heinemann Oxford England, Waltham, MA, 72.
- Denton, T. (2016). *Advanced Automotive Fault Diagnosis, 4th ed: Automotive Technology: Vehicle Maintenance and Repair*. 711 Third Avenue New York: Routledge, 204 - 210.
- Detchko, P. (2011). *Lead-acid batteries: science and technology ; a handbook of lead-acid battery technology and its influence on the product*. Elsevier, Amsterdam Netherlands, 5.
- Devore, J. L. (2009). *Probability and statistics for engineering and the sciences*. Belmont, Calif.: Brooks/Cole, Cengage Learning,463.
- Djamila, R. and Ernest, M. (2012). *Optimization of Photovoltaic Power Systems*. Verlag London limited London, 154.
- Ebby, R. L. (1979). *USA Patent No. United States Patent 4,180,770*.
- Emanuel, P., Herzal, Y., Israel, R., David, K. and Shlomo, R. (1988). *USA Patent No. 4,725,784*.
- Evans, B. (2011). *Beginning Arduino Programming*. Apress, Denver Colorado USA, 8.
- Florez, E.W. F., Brebbia C. A., Chejne F. and Mondragon F. (2015). *Energy and Sustainability VI*, WIT Press, Southampton SO40 7AA UK,243-247.
- Force, U. S. (2015). *Valve-Regulated Lead-Acid Batteries for Stationary Applications - Scholar's Choice Edition*. Scholar's Choice, San Diego CA USA, 29.
- Gerard C., Marolles, H., Gerard, G., Montrouge M. and Gerard G. M. (1972). *Paris, France Patent No. United States Patent 3,680,072*.
- Gilles, T. (2012). *Automotive Service: Inspection, Maintenance, Repair*. Cengage Learning, MA 02451 USA, 8,367.

- Halderman, J. D. (2014). *Automotive Engines: Theory and Servicing 8 edition*. Pearson, Boston USA, 87.
- Hans, F., Bergveld, H.J., Van, B., Johann, R. and Godefridus, C. M. (2003). *USA Patent No. US 6,515,453 B2*.
- Harmohan, S., Thirumalai, G.P., Richard, B.H., William, C. and Hovey, T. G. (2002). *USA Patent No. US 6,469,512 B2*.
- Hassan, K., Mohammad, A.K. and Maryam, M. (2006). ANN modeling of cold cranking test for sealed lead-acid batteries. *Journal of Power Sources*, **158(2)**, 936-943.
- Heyer, B. F.W. (1940). *USA Patent No. 2,225,051*.
- Hollebeak, B. (2011). *Class Room Manual for Automotive Electricity and Electronics Fifth Edition*. Delmar, Cengage Learning, Clifton Park NY 12065-2919 USA, 2-5, 471.
- Hollebeak, B. (2014). *Today's Technician: Automotive Electricity and Electronics, Classroom and Shop Manual Pack (6th ed.)*. Stamford CT, USA: Cengage Learning.
- Huggins, R. (2014). *Energy Storage 2010 edition*. Springer, New York USA, 245:
- Hui, W., Denys, Z., Deshang, K. and Yi, Cui. (2014). Improving battery safety by early detection of internal shorting with a bifunctional separator. *Nature Communications*, **5**, 5193.
- IEEE Power & Energy Society, Stationary Batteries Committee, Institute of Electrical and Electronics Engineers, IEEE-SA Standards Board. (2012). *IEEE guide for selection and use of battery monitoring equipment in stationary applications*. Institute of Electrical and Electronics Engineers, New York USA, 6-10.
- Jack, E., and Rob, T. (2014). *Automotive Technology: A Systems Approach*. Cengage Learning, NY USA, 542.
- James, L. and John, L. (2012). *Electric Vehicle Technology Explained second edition*. John Wiley and Sons, England, 30-31.
- Jha, A. R. (2012). *Next-Generation Batteries and Fuel Cells for Commercial, Military, and Space Applications*. CRC Press, Boca Rato FL USA, 10-11.
- Joey, J., Lei, Z. and Jiujun, Z. (2016). *Lead-Acid Battery Technologies: Fundamentals, Materials, and Applications*. CRC Press, Boca Raton Florida USA, 2-3.
- Juang, L. W. (2010). Online battery monitoring for state-of-charge and power capability prediction. University of Wisconsin Madison.

- Jurgen, G., Chris, K.D., Patrick, T.M., Zempaci, O., David, A. J.R. and Bruno, S. (2009). *Encyclopedia of Electrochemical Power Sources*. Elsevier, NX Amsterdam Netherlands,559
- Jurgen, G., Chris, K. D., Patrick, T. M., Zempachi, O., David, A.J.R. and Bruno, S. (2014). *Encyclopedia of Electrochemical Power Sources*. Elsevier, Amsterdam Netherlands, 729.
- Karden, E. (2017). Development trends for future automobiles and their demand on the battery. In E. Karden, *Lead-Acid batteries for Future Automobiles* (pp. 3-25).
- Koray, K., Yigit, C., Yakup, S.O. and Isik, C.(2005). A New Online State-of-Charge Estimation and Monitoring System for Lead-Acid batteries in Telecommunication Power Supplies. *IEEE TRANSACTIONS ON INDUSTRIAL ELECTRONICS*,**52**,5, 1316.
- Lonnie, C.G., Michael, C. and Mark, E. (2013). *USA Patent No. 8,437,908*.
- María, T., Penella, L.M., Gasulla, F. (2011). *Powering Autonomous Sensors*. Springer, Dordrecht Netherlands, 41-46.
- Matthias, S., Sergej, I., Niels, J., Raik, K., Simon, P., Riemschneider, K.R. and Jurgen, V. (2015). Vehicle Batteries with Wireless Cell Monitoring. 3-4. Germany, IEEE.
- Moseley T. Patrick, J. Garche, Karden E., David Rand. (2017). *Lead-Acid Batteries for Future Automobiles*. New York, USA: Elsevier Science.
- Muramatsu, K. (1987). *USA Patent No. 4,678,998*.
- Murugesan, V. M., Chandramohan, G., Senthil, K.M., Rudramourthy, R., Ashok, K.L., Suresh, K. R., Basha, D. and Vishnu, M.K. (2012). A Novel Approach To Develop ECU Based Automobile Starting System Using Lab View for Safe and Reliable Start. *ARPN Journal of Engineering and Applied Sciences*, **7**, 7, 868-869.
- Owen, C.D. and Gus, W. (2015). *Fundamentals of Medium/Heavy Duty Commercial Vehicle Systems*. Jones & Bartlett Publishers, Burlington MA 01803 USA, 378.
- Patrick T. Moseley, J. G. (2015). *Electrochemical Energy Storage for Renewable Sources and Grid Balancing*. Elsevier, Amsterdam Netherlands, 428-429.
- Pistoia, G. (2008). *Battery Operated Devices and Systems: From Portable Electronics to Industrial Products*. Elsevier Rome, 12-18.
- Pistoia, G. (2009). *Battery Operated Devices and Systems : From Portable Electronics to Industrial Products*. The Netherlands: Elsevier, 229.
- Patil, S.N., Sangmeshwar, S.K. and Prasad, R.C. (2011). Battery Monitoring System using Microcontroller. *International Journal of Computer Applications*, **28**, 1.

- Prengaman, R. D. (2017). Current-collectors for lead-acid batteries. In R. D. Prengaman, *Lead-Acid battery Technologies* (pp. 163-178). Oxford: CRC Press.
- Ronald E.W., Raymond, H.M., Sharon, L.M. and Keying, Y. (2004). *Probability & Statistics for Engineers & Scientists E I G H T H E D I T I O N*. Pearson Prentice Hall, Upper Saddle River N.I 07458 USA, 45.
- Sathiya, M., Leriche, J.B., Salager, E., Gourier, D., Tarascon, J.M. and Vezin, H. (2015). Electron paramagnetic resonance imaging for real-time monitoring of Li-ion batteries. *Nature Communications*, **72**, 6276.
- Sayed, M.R., Zongchang, L., Yan, C., and Jay, L. (2014). Review and recent advances in battery health monitoring and prognostics technologies for electric vehicle (EV) safety and mobility. *Journal of Power Sources*, **256**, 110-124.
- Schoch, M. Koningsman, J. Kizler, C. Schumucker, B. Kronenberg, M. Brenner, J. Schottle, M. Ruch. (2017). Monitoring Techniques for 12 V lead acid batteries in automobiles. In E. Schoch, *Lead-Acid Batteries for Future Automobiles* (pp. 415-442). Berlin German.
- Sheng, Xu., Yihui, Z., Jiung, C., Juhwan, L., Xian, H., Lin, J., Jonathan, A.F., Yewang, Su., Jessica, S., Huigang, Z., Huanyu, C., Bingwei, L., Cunjiang, Y., Chi, C., Tae-il, K., Taeseup, S., Kazuyo, S. and Sen, K.C. (2013). Stretchable batteries with self-similar serpentine interconnects and integrated wireless recharging systems. *Nature Communications*, **4**, 2.
- Sørensen, B. (2012). *Hydrogen and Fuel Cells: Emerging Technologies and Applications*. Academic Press-imprint of Elsevier Inc, MA 01803 USA, 140-363.
- Takao, K., Hiroaki, Y., Noriyoshi, S., Kotaro, W., Keinosuke, M., Kazunori, O., Gou, K., Hiroshi, N., Fumio, U., (1983). *USA Patent No. United States Patent 4,377,787*.
- Texas, I. (2012). *Battery Management Solutions*. Texas, US: TI.
- Thyagarajan, A., Raja, P. and Uma R. G. (2014). Battery Monitoring and Power Management for Automotive Systems. *American Journal of Energy Research*, **2**, 1-8.
- Valer, P., Henk, J.B., Dimitry, D., Paul, P.L.R. and Peter, H.L.N. (2010). *Battery Management Systems: Accurate State-of-Charge Indication for Battery-Powered Applications Volume 9, Softcover reprint of hardcover 1st ed. 2008 edition*. Springer, Eindhoven Netherlands, 187.
- Vepa, R. (2013). *Dynamic Modeling, Simulation and Control of Energy Generation*. Springer Science & Business Media, London, 325-327.

- Weng, C., Cui, Y., Sun, J. and Peng, H. (2013). On-board state of health monitoring of lithium-ion batteries using incremental capacity analysis with support vector regression. *Journal of Power Sources*, **235**, 36-44.
- Xiaodong, Z., Grube, R., Kwang, K.S., Mutasim, S. and Robert, C. (2009). Automotive battery state-of-health monitoring: a parity relation based approach. *Proceedings of the 7th IFAC Symposium on Fault Detection, Supervision and Safety of Technical Processes*. **42**, IFAC Proceedings Volumes, Barcelona Spain, 552-557.
- Yalian, Y., Xiaosong, H., Datong, Q. and Fangyuan, C. (2013). Arrhenius Equation-Based Cell-Health Assessment: Application to Thermal Energy Management Design of a HEV NiMH Battery Pack. *Energies*, **6**, 2709-2725
- Yevgen, B. and Jinrong Q. (2013). *Battery Power Management for Portable Devices*. Artech House, Norwood, 9.
- Yinjiao, X., Eden, W.M., Ma., K.L. and Tsui, M.P. (2011). Battery Management Systems in Electric and Hybrid Vehicles. *Energies*, **4**, 1840-1857.
- Zhang, X. (2012). "Battery State Of Health Monitoring System And Method" *Mason Ohio, USA Patent No. US 8,159,189 B2*.
- Zhongyue, Z., Jun, X., Chris, M., Binggang, C. and Zheng, C. (2014). Evaluation of Model Based State of Charge Estimation Methods for Lithium-Ion Batteries. *Energies*, **7**, 5065-5082.

Internet links

Autometer, Inc. (2016, July 10).<http://www.autometer.com/bva2100-es-8-stand-ac-14-printer-kit.html>. Retrieved from <http://www.autometer.com/>: <http://www.autometer.com/media/manual-2650-1724.pdf>

Autometer, Inc. (2016, July 10).<http://www.autometer.com/bva-350-technician-grade-intelligent-handheld-automotive-heavy-duty-truck-electrical-system-analyzer-for-6v-12-applications.html>. Retrieved from <http://www.autometer.com/>: <http://www.autometer.com/media/manual/2650-614X.pdf>

Bosch, Inc. (2016, July 10). <http://de-ww.bosch-automotive.com/en/products> . Retrieved from <http://www.bosch.com/en/com/home/index.php>:<http://de-ww.bosch-automotive.com/en/testing-equipment-products/battery-service-testing-equipment-products/bat-131/>

Bosch, Inc. (2016, July 10). <http://de-ww.bosch-automotive.com/en/products> Retrieved from <http://www.bosch.com/en/com/home/index.php>:http://de-ww.bosch-automotive.com/en/products_workshopworld/bat_301/

Bosch, Inc. (2016, July 10). <http://de-ww.bosch-automotive.com/en/products> (2016, August 3). Retrieved from <http://www.bosch.com/en/com/home/index.php>: http://de-ww.bosch-automotive.com/en/bat_110/bat110_bat_battery-service_testing-equipment_products_workshop

Bosch, R. (2015, 12). <http://www.boschdiagnostics.com>. Retrieved from <http://www.boschdiagnostics.com/pro/products/bat-110-battery-tester>.

Buchman, I. (2016, August 3). <http://www.cadex.com/en/products/>. Retrieved from <http://www.cadex.com/en/>: <http://www.cadex.com/en/products/spectro-ca-12-ga>

Delphi, Inc. (2016, August 3). Retrieved September, 3, 2016 from <http://www.argusanalyzers.com/forex.hu/images/pdf/ARGUS500.pdf>

Delphi, Inc. (2016, August 3). Retrieved September, 3, 2016 from <http://delphi.com/manufacturers/auto/http://delphi.com/docs/default-source/product-profile-pdfs/delphi-battery-monitoring-device.pdf?sfvrsn=4>

Maxim, I. (2016, June 30). <http://www.datasheetcatalog.com/maxim-dallassemiconductor/23/>. Retrieved from <https://www.maximintegrated.com/en.html>: http://www.datasheetcatalog.com/datasheets_pdf/D/S/1/8/DS18B20X.shtml

Microsystems, A. (2016, June 30). <http://www.allegromicro.com/>. Retrieved from <http://www.allegromicro.com/en/Products/Current-Sensor-ICs.aspx>: <http://www.allegromicro.com/en/Products/Current-Sensor-ICs/Fifty-To-Two-Hundred-Amp-Integrated-Conductor-Sensor-ICs.aspx>

Midtronics, Inc. (2016, 8 3). <http://midtronics.com/resources#manuals/>. Retrieved from <http://midtronics.com/>: <http://www.ja.midtronics.com/templates/midtronics-transportation-v2/catalogpdf/GRX3000-Brochure15.pdf>

Midtronics, Inc. (2016, 8 3). <http://www.ja.midtronics.com/shop/products-1/battery-and-electrical-system-diagnostics/exp-series-expandable-electrical-diagnostics/midtronics-exp-1000-handheld-electrical-system-tester>. (2016, 8 3). Retrieved from <http://www.midtronics.com/>: http://www.ja.midtronics.com/templates/midtronics_transportation_v2/catalogpdf/EXP1000_Brochure15.pdf

Projecta, Inc (2016, 8 3) www.projecta.com.au. (2016, 8 3). Retrieved from http://www.projecta.com.au/site/DefaultSite/filesystem/documents/BatteryMaintenance/BLT300_Instructions_Issue1.pdf

Projecta, Inc (2016, 8 3) www.projecta.com.au. (2016, 8 3). Retrieved from http://www.projecta.com.au/site/DefaultSite/filesystem/documents/BatteryMaintenance/BLT200_Instructions_Issue1.pdf

Semiconductors, F. (2014, September 11). <https://www.fairchildsemi.com/>. Retrieved from <https://www.fairchildsemi.com/products/power-management/voltage-regulators/positive-voltage-linear-regulators/>: <https://www.fairchildsemi.com/datasheets/LM/LM7805A.pdf>

Toshiba, Inc (2015, 10 5). www.toshiba.com/taec/news. Retrieved from http://www.toshiba.com/taec/news/press_releases/2012/assp_12_650.jsp.

Trojan, T. (2016, 10 5). www.trojanbattery.com/pdf/TrojanBattery. Retrieved from www.trojanbattery.com/pdf/TrojanBattery_UsersGuide.pdf

Yuasa, B. (2016, June 27). <http://www.yuasabatteries.com/>. Retrieved from http://www.yuasabatteries.com/pdfs/TechManual_2016.pdf: http://www.yuasabatteries.com/pdfs/Yuasa_Application_Guide_2016.pdf

APPENDICES

Appendix A: ELECTRONIC COMPONENTS DIAGRAMS AND THEIR SPECIFICATIONS

A-1 The Arduino microcontroller

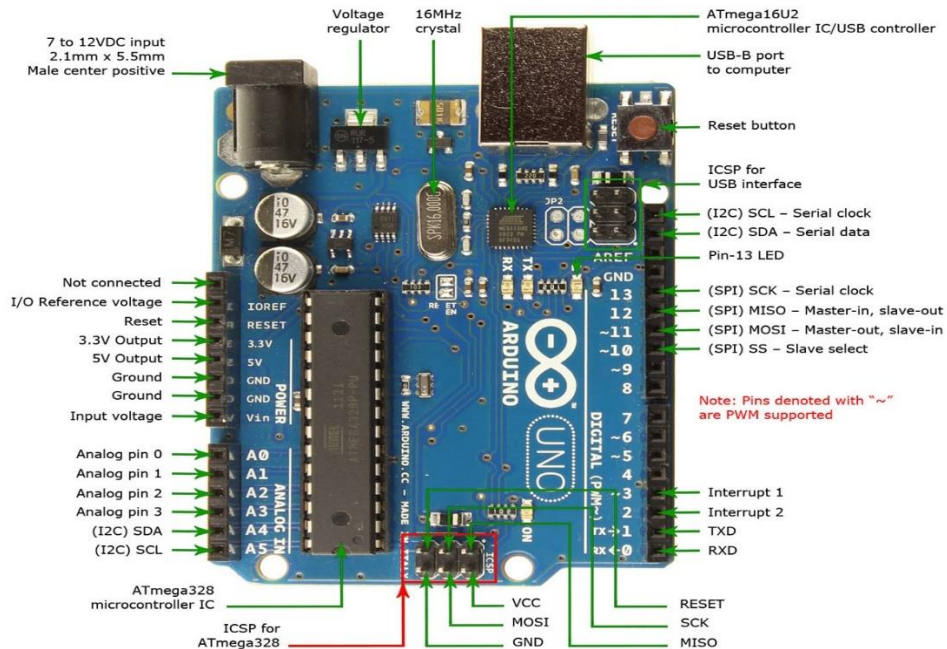


Figure A-1: The Arduino UNO R3 physical computing platform

The specifications of the microcontroller used are;

- i. Microcontroller ATmega 328
- ii. Operating Voltage 5 V
- iii. Input Voltage (recommended) 7V -12 V
- iv. Input Voltage (limits) 6V-20 V
- v. Digital I/O Pins 14
- vi. Analog Input Pins 6
- vii. DC Current per I/O Pin 40 mA
- viii. DC Current for 3.3 V Pin 50 mA
- ix. Flash Memory 32 KB of which 0.5 KB used by the bootloader
- x. SRAM 2 KB
- xi. EEPROM 1 KB
- xii. Clock Speed 16 MHz

A-2 The temperature sensor DS18B20



Figure A-2: The digital temperature sensor DS18B20

The specifications of the temperature sensor are (Wang Jingzhuo, Gong Chenglong, 2007)

- i. Unique 1-Wire® Interface Requires Only One Port Pin for Communication
- ii. Each Device has a Unique 64-Bit Serial Code Stored in an On-Board ROM
- iii. Multidrop Capability Simplifies Distributed Temperature-Sensing Applications
- iv. Requires No External Components
- v. Can Be Powered from Data Line; Power Supply Range is 3.0 V to 5.5 V
- vi. Measures Temperatures from -55 °C to +125 °C (-67°F to +257°F)
- vii. ±0.5°C Accuracy from -10 °C to +85 °C
- viii. Thermometer Resolution is User Selectable from 9 to 12 Bits
- ix. Converts Temperature to 12-Bit Digital Word in 750 ms (Max)

A-3 The current sensor integrated circuit ACS758XCB-200U

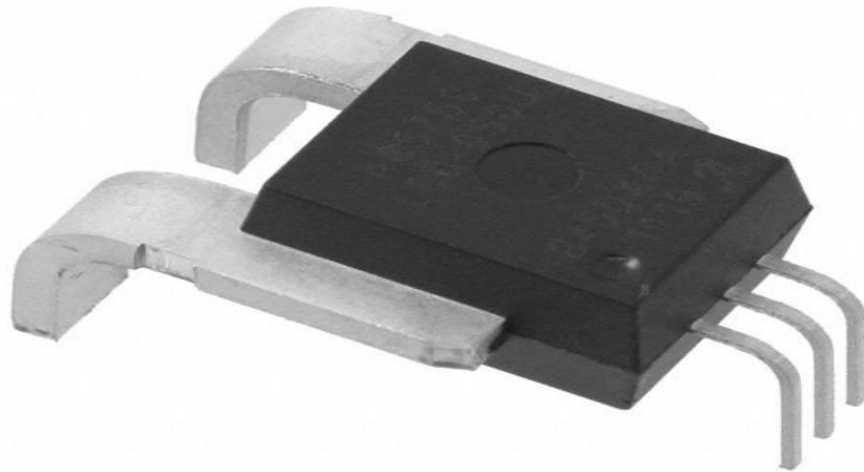


Figure A-3: The current sensor IC ACS755SCB-200U

The specifications of the current sensor are (Allegro, 2009);

- i. Integrated shield greatly reduces capacitive coupling from current conductor to die due to high dV/dt signals, and prevents offset drift in high-side, high voltage applications
- ii. Total output error improvement through gain and offset trim over temperature
- iii. Small package size, with easy mounting capability
- iv. Monolithic Hall IC for high reliability
- v. Ultra-low power loss: $100 \mu\Omega$ internal conductor resistance
- vi. Galvanic isolation allows use in economical, high-side current sensing in high voltage systems
- vii. AEC Q-100 qualified
- viii. 3.0 to 5.5 V, single supply operation
- ix. 120 kHz typical bandwidth
- x. μs output rise time in response to step input current
- xi. Output voltage proportional to AC or DC currents
- xii. Factory-trimmed for accuracy
- xiii. Extremely stable output offset voltage

- xiv. Nearly zero magnetic hysteresis
- xv. Industry-leading noise performance through proprietary amplifier and filter design techniques

A-4 The power regulator LM7805

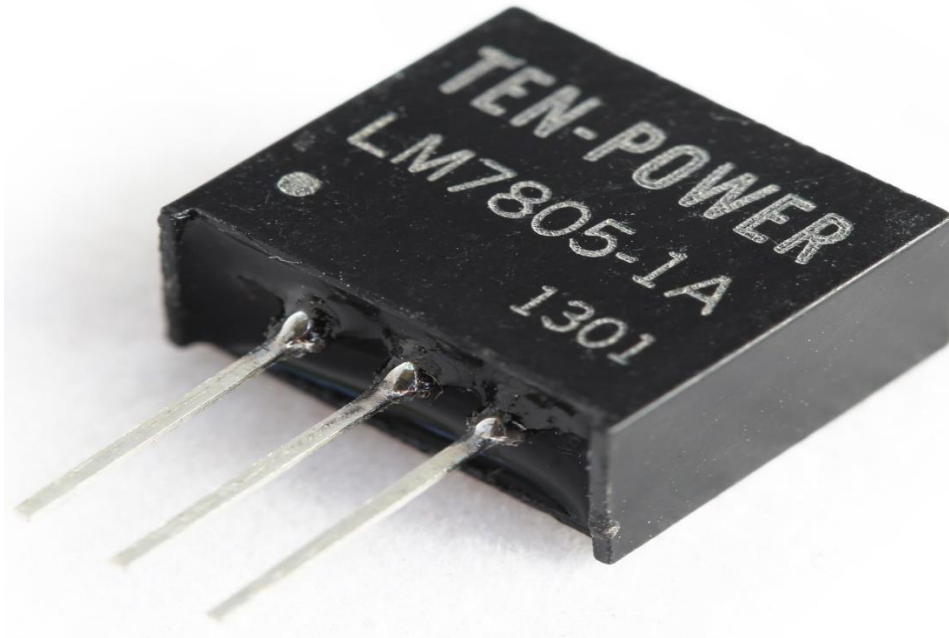


Figure A- 4: The LM7805 power regulator IC

Features of the LM7805 power regulator IC;

- i. Output Current up to 1A
- ii. Output Voltages of 5, 6, 8, 9, 10, 12, 15, 18, 24 V
- iii. Thermal Overload Protection
- iv. Short Circuit Protection
- v. Output Transistor Safe Operating Area Protection (Fairchild, 2001)

Appendix B: THE BMS CIRCUIT SCHEMATIC

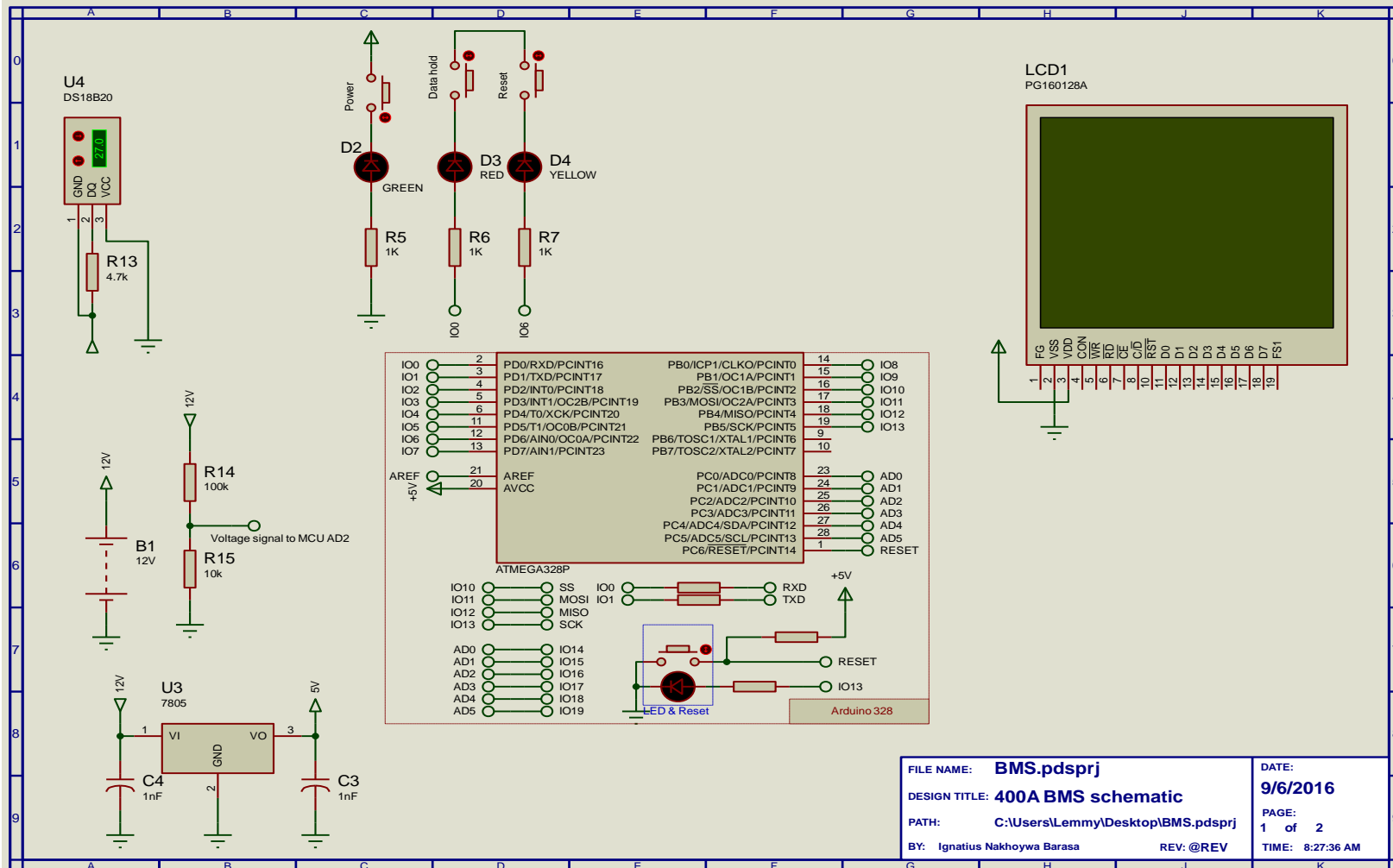


Figure B-1: The complete schematic circuit of the battery monitoring system generated using Proteuse Design Suite 8.1 sheet 1

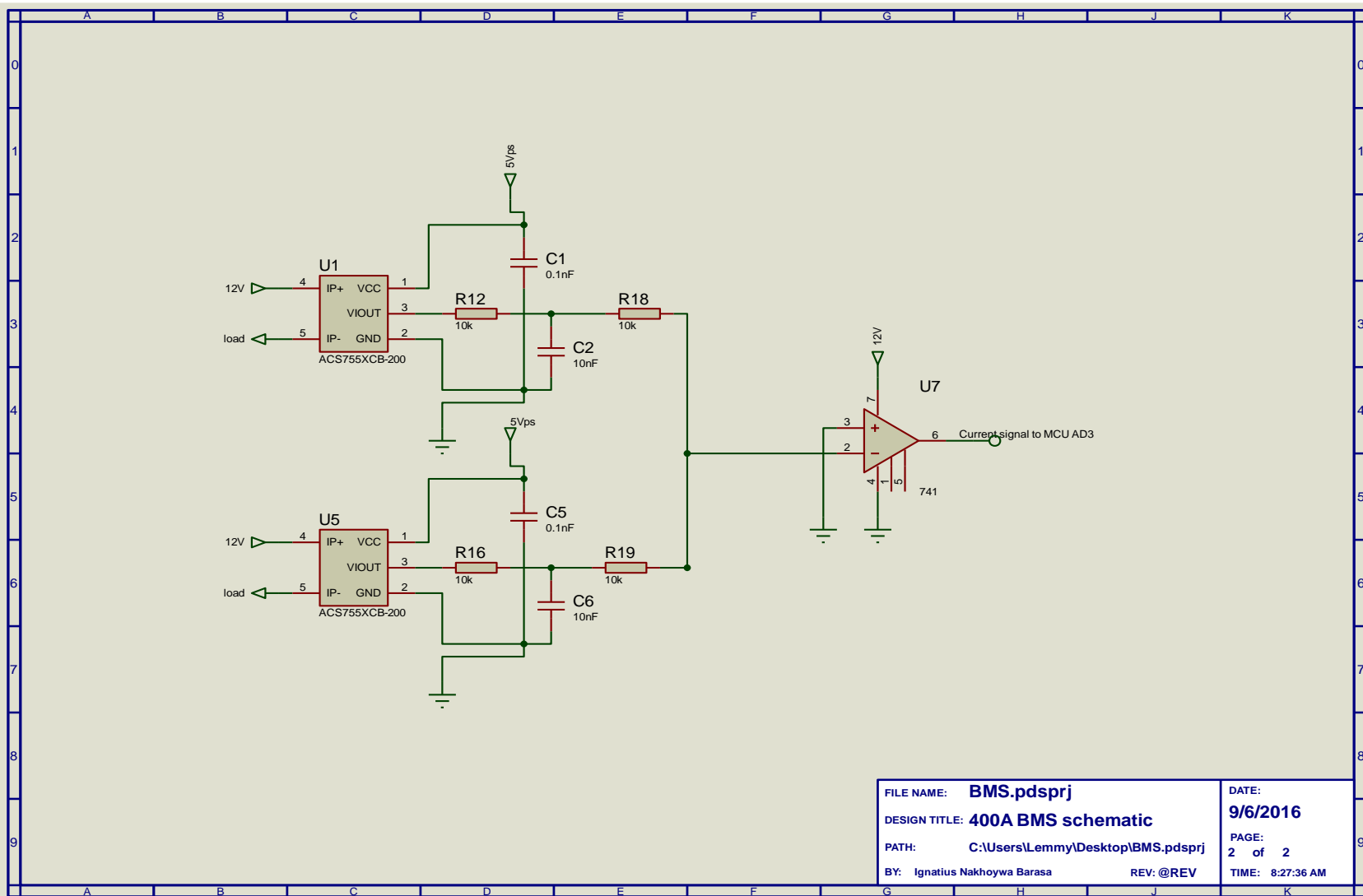


Figure B-2: The complete schematic circuit of the battery monitoring system generated using Proteuse Design Suite 8.1 sheet 2